Stony Brook University

ENSO modulation of the QBO, and QBO influence on tropical convection

A Dissertation presented

by

Wei Yuan

to

The Graduate School

in Partial Fulfillment of the

Requirements

for the Degree of

Doctor of Philosophy

in

Atmospheric Science

Stony Brook University

August 2015

Stony Brook University

The Graduate School

Wei Yuan

We, the dissertation committee for the above candidate for the

Doctor of Philosophy degree, hereby recommend

acceptance of this dissertation

Dr. Marvin A. Geller - Dissertation Advisor

Professor, SoMAS, Stony Brook University

Dr. Edmund K.M. Chang - Chairperson of Defense

Professor, SoMAS, Stony Brook University

Dr. Marat Khairoutdinov

Professor, SoMAS, Stony Brook University

Dr. Sultan Hameed

Professor, SoMAS, Stony Brook University

Dr. Karen H. Rosenlof

NOAA ESRL, Chemical Sciences Division, Boulder, Colorado

This dissertation is accepted by the Graduate School

Charles Taber

Dean of the Graduate School

Abstract of the Dissertation

ENSO modulation of the QBO, and QBO influence on tropical convection

by

Wei Yuan

Doctor of Philosophy

in

Atmospheric Science

Stony Brook University

2015

We look into the ENSO modulation of QBO amplitudes and periods using IGRA data, for the time from the 1950s to the 2010s (the whole period), and the separated time intervals before 1982 and after 1990. For the whole period and the time interval after 1990, the QBO has longer period and larger amplitude during La Niña than during El Niño. However, before 1982 there is no conclusive relationship between the QBO amplitude for the two ENSO phases, although the QBO period is still longer during La Niña. Since the period of the QBO is determined by the magnitude of the wave momentum flux driving the QBO, and the amplitude of the QBO is determined by the magnitude of the wave phase speeds that comprise the gravity wave spectrum. We then offer a possible explanation of how changes in deep convection might cause the ENSO-QBO relationship change before and after the 1980s, using OLR data.

We also use the cloud resolving model SAM to investigate the QBO influence on tropical deep convection. The downward penetration of the QBO temperature perturbation near the tropopause is crucial for the QBO modulation on the convection while the QBO wind shear has a very small effect. In the idealized Walker circulation experiments there is more precipitation in the area with the strongest precipitation during periods of QBO westerly phase. The idealized Walker circulation experiments with upper-level temperature perturbation reveals a potential mechanism for the QBO effects on the tropical circulation and associated convection. With a cold temperature anomaly near the tropopause, the tropopause height is lifted upward. The vertical extension of the raising branch of the Walker circulation also

increases in height, moving the peak of the vertical velocity profile [i.e. the level of the divergence] upward. The upward moving of the peak level of the w profile increases the gross moist stability. Thus, assuming the input of the moist static energy is approximately unchanged in the rising branch of the Walker cell, its precipitation will decrease, and the decrease precipitation is increased in the region outside the center of the Walker cell, as a result of this Walker circulation change.

Contents

List of Tables

List of Figures

Acknowledgements

I would like to express my special appreciation and thanks to my advisor Professor Dr. Marvin A. Geller, you have been a tremendous mentor for me. Thank you for encouraging my research and for helping me to grow as a researcher. Your advice on both research as well as on my life have been priceless. I would also like to thank professor Marat Khairoutdinov for his instruction on the modeling part of my research.

Thanks to my committee members, Professor Edmund Chang, Professor Marat Khairoutdinov, Professor Sultan Hameed and Dr. Karen Rosenlof for serving as my committee members. Thank you for your brilliant comments and suggestions.

Thanks to Peter Love, Tiehan Zhou, Ji Nie , Pu Lin and Jie Gong for inspiring discussions and suggestions while I was working on this dissertation. Thanks to Ping Liu, Jungmin Lee and Wei Zhang for helping me to run the cloud-resolving model.

Thanks to all my friends in SoMAS, a special thanks to my parents, husband and brother, for your love and support!

Chapter 1: Introduction

1.1 A Brief Introduction to the ENSO and the QBO

The El Niño/Southern Oscillation (ENSO) is a naturally occurring phenomenon across the equatorial Pacific Ocean, and it is the dominant mode of interannual variability in tropical climate. The period varies between 2 to 7 years, with a average period of around 4 years. It involves a periodic fluctuation in sea surface temperature (El Niño) and the air pressure of the overlying atmosphere (Southern Oscillation), see Bjerknes (1969). The ENSO cycle refers to the coherent and sometimes very strong year-to-year variations in sea-surface temperatures, convective rainfall, and surface air pressure (Phillip et al. 1987, Dai and Wigley 2000, Power et al. 2007). El Niño and La Niña are the two opposite extremes of the ENSO cycle. During the warm phase of the ENSO (El Niño), there is a warm SST anomaly in the central and eastern equatorial Pacific, while during the cold phase of ENSO (La Niña) there is a cold SST anomaly at these locations. ENSO is also associated with the large scale east-west Walker circulation over the Pacific. During El Niño events, the weakening of the Walker circulation generally brings drier conditions to the western Pacific region, and during La Niña events the Walker circulation is strong, and rainfall may be unusually high over Indonesia.

The quasi-biennial oscillation (QBO) is the low-frequency variability in the equatorial stratosphere, and it's the leading mode of the total variability of the tropical stratosphere (Reed et al. 1961, Veryard and Ebdon 1961,

Andrews et al. 1987). The main characteristic of the QBO is the oscillation of the zonal wind in the stratosphere. The zonal wind switches between easterly from westerly and propagates downward to the tropopause with a mean period of 28 to 29 months (Baldwin et al. 2001). The QBO can also be separated into two phases (easterly and westerly), and the QBO phases can be defined based on the zonal wind (Seo et al. 2013) or zonal wind shear (Zhou et al. 2001) at some stratospheric level, according to different purposes of studies. A widely used QBO stratospheric zonal wind data is the FUB (Free University of Berlin) QBO wind data, which includes zonal wind from seven levels in the stratosphere from three radiosonde stations, we use the FUB zonal wind data to define the QBO index in this dissertation.

1.2 The Wave Driving of the QBO

There are some previous studies trying to explain the cause of this QBO. Wallace and Holton (1968) demonstrated that a downward propagating momentum source was required to provide a reasonable explanation for the QBO. This was followed by the papers by Lindzen and Holton (1968) and Holton and Lindzen (1972), showing that the simultaneous presence of eastward and westward atmospheric waves could provide these alternating, downward propagating easterly and westerly momentum sources to explain the QBO.

Plumb (1982) showed a cartoon (Andrews et al. 1987, page 321) in which just two upward propagating atmospheric waves, one with a phase speed +c and another with a phase speed -c, could reproduce the essence of

the QBO. The physics of this cartoon is best discussed using Eliassen and Palm's Theorem 1 (Eliassen and Palm 1961, Lindzen, 1990)

$$\overline{p' w'} = -(u_0 - c)\rho_0 \overline{u' w'} \tag{1.1}$$

where p is atmospheric pressure, w is vertical velocity, u is zonal velocity, c is the wave's zonal phase velocity, and ρ is atmospheric density. The subscripts $(\,)_0$ denotes mean state variables, the superscript ( )' denotes wave variables, and the overbar denotes averaging over wave phase. The expression $\overline{p' w'}$ is the wave upward energy flux, and $\rho_0 \overline{u' w'}$ is the upward flux of gravity wave zonal momentum.

Equation 1.1 indicates that for upward propagating waves ($\overline{p' w'}$>0), the momentum flux ($\rho_0 \overline{u' w'}$) is positive (i. e., westerly) if the wave phase speed is greater than the mean zonal flow (i. e., $u_0 - c < 0$). Thus, in this case, if the waves are being dissipated, the mean zonal flow will be accelerated toward the wave phase speed c. In the same manner, if the wave phase speed is less than the mean zonal flow ($u_0 - c > 0$) and there is dissipation, the mean zonal flow will be decelerated toward the phase speed c. If the mean zonal flow is westerly the wave with the positive phase speed +c will be preferentially absorbed, since $u_0 - c$ is small for this wave, accelerating the mean flow toward +c, and the mean zonal flow maximum will descend until the shears near the surface become so great that this westerly shear zone is destroyed by diffusive processes in this simple model. In the meantime, the wave with negative phase speed freely propagates to higher altitudes, pro-

viding a easterly wind that descends with time. In this manner, alternating descending westerly and easterly shear zones are produced. The shear zones will descend more quickly with increasing wave momentum fluxes, producing an oscillation with shorter period. Also, if greater phase speed waves are present, the descending westerlies and easterlies will have greater magnitude, producing a QBO with higher amplitude. Thus, in this very simple picture, the QBO period depends on the magnitude of the wave momentum fluxes, and the QBO amplitude depends on the phase speed.

ENSO is associated with tropical convection, ENSO might modulate the QBO amplitude and period through its influence on the magnitudes of the wave momentum fluxes and the spectrum of wave speeds of the convection induced waves. More details will be discussed in chapter 2.

1.3 Previous Results of the ENSO and QBO Relationship

Previously, it was generally thought that the QBO and ENSO were uncorrelated, since the QBO and ENSO indices showed no significant correlation with one another (Xu 1992, Collimore et al. 2003, and Ho et al. 2009, Liess and Geller 2012). Liess and Geller (2012) calculated the correlation of the Niño3.4 SST anomaly index (`http://www.cpc.ncep.noaa.gov/data/indices/sstoi.indices`) and the FUB QBO 70 hPa zonal wind with 3 month lag (3 months is the approximated time for QBO signal to transport

downwardly from 70 hPa to the tropopause, Geller et al. 1997) between 1983 to 2004, the correlation coefficient is only 0.08. Ho et al. (2009) also found correlation coefficient as small as 0.08 for the QBO and ENSO summer mean indices during the period of 1976 to 2007. In Garfinkel and Hartmann (2007), the correlation coefficient of the CPC/NCEP Niño3 index and ERA-40 zonal wind at 50 hPa from September 1957 to January 2007 is even smaller (0.02), however, the correlation between the two indices starting in September 1957 up until August 1982 is -0.25, and the correlation from December 1990 to August 2007 is 0.26. They didn't provide any explanation for the nonstationary correlation relationship in their paper.

Taguchi (2010) looked into the ENSO-QBO relationship in another way, with reference to Wallace et al. (1993). In this paper, the author explored whether the QBO has ENSO-dependent variations in a statistical analysis of monthly equatorial stratosphere zonal wind data, using the monthly FUB QBO zonal wind data. The QBO is represented in a two-dimensional phase space, where the space trajectory is defined by the time series of the two leading modes of zonal wind variability. From the trajectories of the time series in the phase space, the distance from the origin and time rate of change in the argument, are used to represent the instantaneous amplitude and phase progression rate (period) of the QBO, respectively. The QBO amplitude and phase progression are examined in both the annual and ENSO cycles, and the results show that the QBO varies significantly in amplitude and period with the ENSO cycle. The QBO had more than about 10% larger amplitude during La Niña than during El Niño, with an average QBO period during El

Niño being about 25 months, whereas during La Niña it's about 32 months.

1.4 The QBO Modulation of the Tropical Tropopause

The QBO also exhibits a clear signature in temperature near the tropopause. Since the QBO is zonally symmetric, and the meridional and vertical motions accompanying the QBO are very small, the QBO mean zonal wind and temperature should satisfy the thermal wind relationship

$$\beta y \partial \bar{u}/\partial z = -RH^{-1}\partial \bar{T}/\partial y \tag{1.2}$$

In the equatorial β-plane, the distance from the Equator is relatively small the temperature gradient should satisfy

$$\partial \bar{T}/\partial y = 0 \tag{1.3}$$

at y = 0.

We can apply L'Hospital's rule to equation (1.2), the thermal wind relationship can be rewrite in the following form (equation 12.45 in Holton, 2004):

$$\partial \bar{u}/\partial z = -R(H\beta)^{-1}\partial^2 \bar{T}/\partial y^2 \tag{1.4}$$

where u is the zonal wind, T is temperature, z is log-pressure height, y is latitude, R is the gas constant for dry air, H is the nominal (constant) scale height used in the log-pressure coordinates, β is the latitudinal derivative of

the Coriolis parameter.

For QBO variations within a small meridional scale L from the Equator, thermal wind balance at the Equator is approximated as

$$\partial \bar{u}/\partial z \approx R(H\beta)^{-1}T/L^2 \tag{1.5}$$

During the QBO easterly phase, $\partial \bar{u}/\partial z$ is negative, accompanied with a negative temperature anomaly. This temperature anomaly is driven by an upward secondary motion in the stratosphere, and vise versa for the QBO westerly phase (see figure 1 in Plumb and Bell 1982). In this manner, the tropopause during the QBO easterly phase is higher and colder than during the QBO westerly phase, the temperature difference between QBO easterly and westerly phases can penetrate down a bit below the tropopause (Yuan et al. 2014).

This QBO modulation of the tropical tropopause has been noted previously by Randel et al. (2000) and by Zhou et al. (2001), and is consistent with the early work of Reid and Gage (1985). Zhou et al. (2001), using European Centre for Medium-Range Forecasting (ECMWF) reanalysis data, found that tropical CPT temperatures were about 0.5 °C colder during the easterly phase of the QBO than during its westerly phase. Using radiosonde data, Randel et al. (2000) found that their tropopause temperature variations were about a factor of two larger than those found by Zhou et al. (2001). This difference is understandable because interpolations using re-

analysis data are expected to smooth sharp features such as the CPT. Zhou et al. (2001), basing their analysis on only 15 years of ECMWF re-analysis data, tried to analyze QBO influences on the CPT independent of the ENSO effects. However, both Zhou et al. (2001) and Randel et al. (2000) were unaware of the ENSO influence on the QBO.

It has been established that the QBO influences extend downward to the tropopause and a bit below. Corresponding to the QBO modulation of the CPT temperature, it has been shown that there is a QBO modulation of water vapor mixing ratios in air entering the stratosphere through the cold, tropical tropopause region (Zhou et al. 2004, Liang et al. 2011).

1.5 The QBO Influence of the Tropical Convection

There have also suggestions that the QBO modulates tropical, deep convection (Collimore et al. 2003, Ho et al. 2009, Liess and Geller 2012), incidence of Atlantic hurricanes (Gray 1984a,b) and typhoon tracks (Ho et al. 2009).

Here, I'd like to introduce some previous results related to the tropical convection.

Gray (1984a) found that before 1982, tropical cyclone activity in the Atlantic was greater when the QBO was in its westerly phase or becoming

westerly, than when the QBO was in the easterly phase, and there were more intense Atlantic hurricanes occurring in the westerly QBO years.

Although the QBO signal is mainly in the stratosphere, some recent studies show significant effects of QBO on the troposphere, including the QBO modulations of tropical deep convection that have been found by Collimore et al. (2003), Ho et al. (2009), and Liess and Geller (2012), and possible links between the stratospheric QBO, troposphere QBO and SST in the tropics (Yasunari, 1989).

Collimore et al. (2003) checked the relationship between the height and amount of tropical deep convection and QBO with a 23-yr record of outgoing long wave radiation (OLR) and a corrected 17-yr record of the highly reflective cloud (HRC) index. They found that zonal means and maps of OLR and HRC carry a QBO signal, and the spatial patterns of the maps highlight the QBO signal of OLR and HRC in regions with high incidence of deep convection.

Ho et al. (2009) examined the possible influence of the QBO on tropical cyclone (TC) passages in the Western North Pacific, and they find that the number of TCs approaching the East China Sea is large during the westerly phase of the QBO; during the easterly phase, the number of TCs approaching the eastern shore of Japan is large.

Liess and Geller (2012) examine the relationship between QBO and the

distribution of tropical deep convection using ISCCP weather states and tropical precipitation to represent deep convection. Their results show that for deep convective clouds, relative differences in convective cloud cover between the QBO easterly and QBO westerly phases can be as large as 51%+/-7% of the annual average over isolated regions in the tropical West Pacific and 103%+/-35% over the East Pacific.

1.6 Possible Mechanisms for the QBO Modulation of Tropical Convection

In the previous section, I introduce some previous studies of the QBO influence on tropical convection. In those papers, the authors offered several possible mechanisms for the QBO modulation on the troposphere, based on characteristics of the QBO. I now give a brief summary of these mechanisms.

As mentioned in the introduction, the QBO is a quasi-periodic oscillation of the equatorial zonal wind in the stratosphere. The zonal winds switch between easterlies and westerlies with a mean period of about 28 months. According to the thermal wind relationship, there is an associated secondary meridional circulation and temperature anomalies associated with the QBO zonal wind oscillation (Plumb and Bell, 1982). During the QBO easterly phase, there is a positive vertical velocity anomaly in the tropical stratosphere, the opposite holds for the QBO westerly phase. This is called 'the secondary circulation', and it leads to a higher and colder tropopause during

the QBO easterly phase than during the QBO westerly phase.

No clearly established physical mechanism has yet been established for the QBO influence on tropospheric convection. In previous observational studies, however, the authors discussed the possible mechanisms.

One of the most discussed mechanisms involves the temperature anomalies and the associated tropopause height fluctuations between QBO E/W phases (Collimore et al. 2003; Liess and Geller 2012; Knaff 1993; Arpe and Leroy 2009). The temperature anomaly signal between QBO E/W phases is seen to penetrate into the upper troposphere (Yuan et al. 2014) and change the upper tropospheric static stability. Take the QBO easterly phase as an example, the upper tropospheric static stability decreases with a colder and higher tropopause, this should act to encourage convection near the tropopause with its associated latent heat release.

Vertical wind shear is another possible QBO influence. Higher QBO wind shear might shear off the tops of convection plumes and supress the convection (Gray et al., 1992a, b, Arpe and Leroy, 2009). Collimore et al. (2003) also mentioned the effect of cross-tropopause wind shear, but they thought that this should be a secondary mechanism. Near tropopause wind shear might also be related to formation of cirrus clouds (Gray et al., 1992b).

Another possible mechanism connecting the QBO with tropospheric convection involves QBO modulation of the large-scale circulations, like the

Hadley and Walker circulations. We should keep in mind that the center of action of QBO activity and troposphere convection are quite far apart in their altitudes. Gettelman et al. (2002) shows that a very small portion of convective events can reach the cold point tropopause height for both summer and winter (around 0.5%), if the QBO only interacts with this small fraction of overshooting convective plumes, then the time mean QBO modulation effects should be much smaller than the observational study results (for example, the Liess and Geller (2012) results on tropical convective clouds and precipitation and the Collimore et al. (2003) results on the OLR and high reflective clouds). Liess and Geller (2012) also showed a westward shift of the Hadley circulation and a stronger Walker circulation during the QBO easterly phase compared to the westerly phase. The QBO signal might be transferred downward to the height of the convective events, through the modulation of the large scale circulation. Nie and Sobel (2015) use the weak temperature gradient (WTG) approximation to parameterize the large scale vertical motions in a three-dimensional cloud resolving model study, and find robust tropical precipitation response to the QBO temperature anomaly.

Almost all these observational studies are checking the composite of some troposphere phenomena according to their definition of QBO phase. There is no systematic result about the troposphere response. In fact, sometimes the results are not consistent with each other for different time intervals. For example, Gray (1984a,b) and Camargo et al. (2010) both investigated the influence of the QBO on tropical cyclone activity, Gray (1984a) found a statistically significant relationship between the QBO and the North Atlantic

TC activity, however Camargo et al. (2010) showed that in the data after 1983, the relationship between the QBO and the North Atlantic TC activity can no longer be found.

There have been few modeling studies trying to understand the mechanisms for tropospheric convection response to the QBO. Also, there are some shortcomings of using GCMs studying the QBO influence on tropospheric convection. The simulation of the QBO in the GCM has been quite poor until recently. The GCM vertical resolution was usually not high enough to resolve the wave-mean flow interactions in the upper troposphere lower stratosphere (UTLS) region. Another questionable part is that there are many factors in the GCMs which might have effects on the tropical convection. SSTs, for example, are one of the dominant controlling factors on convection. Our results in chapter 2 show that the QBO and ENSO are not independent of each other. ENSO can modulate both QBO amplitudes and periods, so it's difficult to isolate QBO effects from the much larger ENSO effects on convection in both GCMs and observations. Another factor is the nature of the convective parameterizations, which are still rather crude, and might not respond properly to small changes in the UTLS region.

To summarize, the evidence for a QBO modulation of tropical deep convection has so far been based on statistical evidence in the previous publications, but such statistical evidence might be questioned on two bases. One is that the ENSO influence on tropical deep convection is so large that an incomplete removal of the ENSO signal would severely contaminate ev-

idence for a QBO signal. Furthermore, such statistical evidence provides no information on the physical basis for a QBO influence on tropical deep convection. This motivates us to utilize cloud-resolving modeling to examine the reality and physical basis for the QBO modulations of tropical deep convection, which have been found in previous studies.

1.7 Scientific Questions I Want to Answer

Motivated by the Taguchi (2010) paper, in which the author used the stratosphere zonal wind data only from three Western Pacific radiosonde stations and found out that QBO has longer period and larger amplitude during the time of La Niña than El Niño. We'd like to verify whether this relationship between the QBO and ENSO applies to all longitudes in the equatorial region? We also want to examine the ENSO-phase-dependent influence of the QBO on tropical cold point tropopause temperatures.

Garfinkel and Hartmann (2007) showed that while the correlation between the QBO and ENSO over the time 1957-2007 was very small, and not significant, over the early half of this overall time interval, before 1982 significant negative correlation was found and over the latter half, after year 1990, significant positive correlation was found. This motivates us to ask the following questions: whether Taguchi's (2010) results are equally valid over both the earlier and latter time intervals at the radiosonde stations all along the Equator? Is there any change between the ENSO-QBO relationship for the two time intervals before and after 1980s? And if the ENSO-QBO rela-

tionship changes with time, can we provide any interpretation?

If the ENSO-QBO relationship exists in the whole tropical region, then the ENSO and QBO will not be independent from each other, based on the previous papers showing the QBO influence on the tropical convection, and the fact that ENSO has a very stronger effect on tropical convection, I'd like to ask the question that whether the QBO influence on the tropical convection really exists? And what's the possible mechanism of the QBO influence on the lower tropospheric convection?

The questions about the ENSO-QBO relationship are discussed in chapter 2. Discussions about the QBO modulation of the tropical convection and the possible mechanism for the modulation are shown in chapter 3. The last chapter presents the conclusions and discussion.

Chapter 2 : ENSO Modulation of the QBO Amplitude and Period

Using the FUB QBO wind data, which is derived from three radiosonde stations in the Western Pacific region, Taguchi (2010) found that the characteristics of the stratospheric QBO varied significantly between ENSO phases, the QBO had more than 10% larger amplitude during La Niña than during El Niño and longer period, with an average QBO period during El Niño being about 25 months, whereas during La Niña it was about 32 months. Motived by this research paper, in this chapter we first try to verify whether the Taguchi (2010) relationship between QBO and ENSO applies to all longitudes.

A second motivation for this section is to examine the ENSO-phase-dependent influence of the QBO on tropical cold point tropopause (CPT) temperatures. This QBO modulation of the tropical tropopause has been noted previously by Randel et al. (2000) and by Zhou et al. (2001), and is consistent with the early work of Reid and Gage (1985). Zhou et al. (2001), using ECMWF (European Centre for Medium-Range Forecasting) reanalysis data, found that tropical CPT temperatures were about 0.5 °C colder during the easterly phase of the QBO than during its westerly phase, although Randel et al. (2000), using radiosonde data, found that their tropopause temperature variations were about a factor of two larger than those found by Zhou et al. (2001). This difference is understandable because interpolations using reanalysis data are expected to smooth sharp features such as the CPT. Zhou et al. (2001), basing their analysis on only 15 years of ECMWF re-analysis data, tried to analyze QBO influences on the CPT independent of the ENSO effects. Both they and Randel et al. (2000) were unaware of

the ENSO influence on the QBO, however. Here, we use more than 50 years of radiosonde data to re-examine the QBO modulation of CPT temperatures separately during the different ENSO phases.

Garfinkel and Hartmann (2007) found that although the QBO and ENSO were uncorrelated over the entire period 1957-2007, negative correlations were found over the early half of the whole period whereas positive correlations were found in the second half. This motivates us to ask the question whether Taguchi's (2010) results are equally valid over both the earlier and later time intervals at the radiosonde stations examined in Yuan et al. (2014), or is there any change between the ENSO-QBO relationships for the two time intervals.

In this chapter, I first introduce the data used for the calculations in section 2.1; the ENSO-QBO relationship and the related ENSO-phase-dependent influence of the QBO modulation on the tropical CPT temperature are shown in section 2.2; in section 2.3 I repeated the Taguchi (2010) analysis over both periods, and the results show that the ENSO-QBO relationship changes between the two time intervals, so in this section, I then offer a possible mechanism for the ENSO modulation on the QBO amplitude and period, and try to use this mechanism to explain the ENSO-QBO relationship change between the two time intervals.

2.1 Data

2.1.1 QBO Index and ENSO Index

The FUB QBO zonal wind data is used to define QBO easterly/westerly phases. The link to the data is: `http://www.geo.fu-berlin.de/met/ag/strat/produkte/qbo/qbo.dat` (Naujokat, 1986). It includes information mainly from three stations listed as follows:

Canton Island	2.46°S 171.43°W	Jan 1953-Sep 1967
Gan, Maldive Isl.	0.41°S 73.09°E	Sep 1967-Dec 1975
Singapore	1.22°N 103.55°E	Jan 1974-2015

The QBO phases are defined by the 50 hPa wind shear (Zhou et al. 2001), with a time lag of 6 months. The wind shear is defined as $U_{40hPa} - U_{70hPa}$. QBO westerly months are those months with positive lagged wind shear, and vise versa for QBO easterly months. The 6-month phase lag reflects the average time for the QBO shear to propagate downward to CPT levels.

The definition of positive/negative ENSO phase is according to the Oceanic Niño Index (ONI), which is based on sea surface temperature in the east-central tropical Pacific Ocean (Barnston et al., 1997). Information on the ONI can be found at (`http://www.cpc.ncep.noaa.gov/products/analysis_monitoring/ensostuff/ensoyears_1971-2000_climo.shtml`).

2.1.2 Radiosonde Data

IGRA/High-resolution Radiosonde Comparison

Since correctly determining the downward penetration of the QBO wind and temperature variations into the upper troposphere using radiosonde data requires high vertical resolution, the first choice would be to use HRES (US high vertical-resolution radiosonde) data (Gong et al., 2010), the 6 second HRES (`http://www.sparc.sunysb.edu/html/hres.html`) data are transmitted from the radiosonde in 6s increments corresponding to approximately 30m vertical resolution in the lower atmosphere. But those data are only readily available for a few stations in the tropics, and even there, the data is only available for 15 years, or less. An alternative is to use the Integrated Global Radiosonde Archive (IGRA, `https://www.ncdc.noaa.gov/data-access/weather-balloon/integrated-global-radiosonde-archive`, Durre et al. 2006), which are available for a number of tropical stations for more than 50 years, but those data have very limited vertical resolution.

Figure 1 shows a comparison of the QBO separation of the zonal wind and temperature structure using eleven years of HRES at Yap Island (9.48°N, 138.08°E) and also the same information derived using the IGRA data for the same period (1998-2008), using the methods described in Bell and Geller (2008). These data were composited with a 6-month lag according to the QBO wind shear at 50 hPa (Zhou et al., 2001). Note that the curves using the high vertical-resolution radiosonde data are almost indistinguishable from those constructed using the IGRA data. Quantitatively the IGRA tem-

peratures and winds differ from the high-resolution data by small amounts, the maximum temperature and wind difference are 0.65K and 1 m/s respectively. This then provides justification for our using the IGRA data to get information on QBO effects in the vicinity of tropopause levels. Also, we note that in figure 1, the QBO separation shows substantial tropospheric zonal wind differences, and this implies to us that a 11-year data set is not sufficiently long to properly separate QBO from ENSO influences. Results for Ponape and Koror (not shown) were very similar to what we found at Yap.

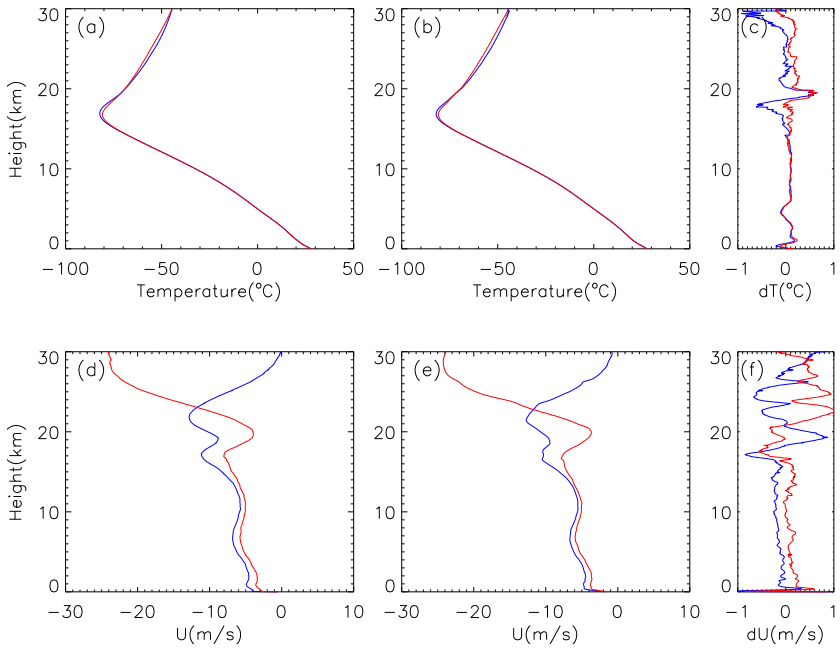

Figure 1: Comparison of composite QBO easterly (blue) and westerly (red) temperature profiles (top) and zonal wind profiles (bottom) using high vertical-resolution radiosonde data (left) and IGRA data (middle) for the years 1998-2008 at Yap Island (9.48°N, 138.08°E). The right column shows (c) the temperature and (f) zonal wind differences between HRES/IGRA: blue is during the QBO easterly phase whereas red is during the QBO westerly phase. The data were composited using a 6-month phase lag according to the wind shear at 50 hPa. The units of zonal wind and temperature are m/s and °C.

Ten IGRA radiosonde stations we used have data records ranging from just short of 4 decades to 6 decades, and lie within 10°of the Equator (see Table 1), and thus should allow for reasonable separation of QBO and ENSO effects. It should be noted that there are some other IGRA stations that also satisfy these criteria for data length and proximity to the Equator, but we have found significant missing and/or bad data at those other stations, so we restrict our analysis to data from those ten stations shown in table 1. It should be noted in figure 2 that there is still a concentration of stations in the Western Pacific, but there are three other stations in the tropical Atlantic and Indian Oceans. For our first goal we begin by repeating the analysis of Taguchi (2010) to determine whether the Taguchi (2010) results on El Niño/La Niña effects on the QBO period and amplitude apply at all longitudes. For this, we apply the Taguchi (2010) analysis at the 10 IGRA stations shown in figure 2.

Stations	Number	Latitude-longitude	Year-range
Seychelles	1	4.7S, 55.5E	1973-2011
Penang	2	5.3N,100.3E	1968-2011
Singapore	3	1.4N,104.0E	1955-2011
Koror	4	7.3N,134.5E	1951-2011
Yap	5	9.5N,138.1E	1951-2011
Chuuk	6	7.5N,151.9E	1951-2011
Ponape	7	7.0N,158.2E	1951-2011
Kwajalein	8	8.7N,167.7E	1952-2011
Majuro	9	7.1N,171.4E	1955-2011
Wideawake	10	8.0S,14.4W	1957-2009

Table 1: Locations and time ranges of data records of stations used in analysis

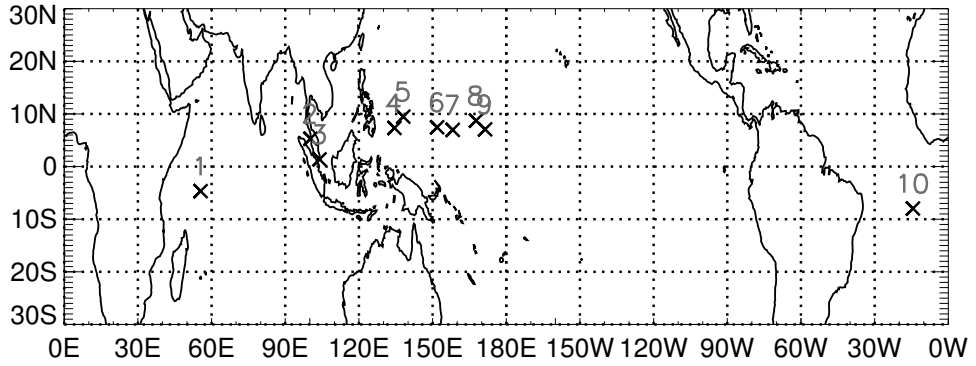

Figure 2: Location of IGRA stations analyzed for analysis of El Niño-La Niña effects on the QBO. The names, locations, and data length for each of these stations are shown in Table 1.

Monthly Mean Zonal Wind from IGRA

IGRA data include both mandatory and significant levels, the mandatory levels include these specified levels by World Meteorological Organization convention (surface, 1000, 925, 850, 700, 500, 400, 300, 250, 200, 150, 100, 70, 50, 30, 20, 10 hPa), and significant levels are defined as those levels where there is a significant change in the rate of change with height of the temperature or humidity. Bell and Geller (2008) have demonstrated that the IGRA data can give comparable detail on the tropopause temperature and stability structure, both in the extratropics and in the tropics. They did not show that those data retain high vertical-resolution information for the wind structure, however, so for us to justify the use of the IGRA data to correctly determine the QBO penetration into the upper troposphere, we first have to show that the high vertical-resolution and IGRA data give comparable information on the QBO structure.

Monthly Mean Temperature from IGRA

Monthly mean CPT (cold point tropopause) temperature monthly mean temperature at 100 hPa and 70 hPa are used in Chapter 2. To get CPT temperature, first we choose the soundings with records reaching up to 70 hPa or above, then define the CPT temperature as the coldest temperature of the sounding (and most of the time the report from the significant thermodynamic level). I only use months with 10 or more valid records to get monthly mean value.

The monthly mean 100 hPa and 70 hPa temperatures are calculated directly from all the valid 100 hPa and 70 hPa temperature records. Like CPT temperature, only months with 10 or more valid records are used.

2.1.3 Outgoing Longwave Radiation (OLR)

The monthly mean NOAA Interpolated Outgoing Longwave Radiation (OLR, Liebmann and Smith, 1996) is used to represent tropical deep convection. The time range of the data is from June 1974 to December 2013. These data are reported on a 2.5 degree latitude x 2.5 degree longitude global grid. I will only use the values in the tropical region in this dissertation. The link for the data is `http://www.esrl.noaa.gov/psd/data/gridded/data.interp_OLR.html`

2.2 ENSO Modulation of QBO Amplitude and Period: From 1950s to 2011

In this part, I present the methods and results for three distinct calculations. The first is the repetition of the calculations of Taguchi (2010), but for the 10 stations shown in figure 2; the second is the examination of the El Niño/La Niña influence on QBO modulation of CPT temperatures using the CPT temperatures directly from the IGRA soundings; and the third involves deriving zonal wind and temperature profiles so that we may determine the extent of the downward penetration of the QBO into the upper troposphere.

2.2.1 On the Zonal Symmetry of ENSO Influences on QBO Amplitudes and Periods

We repeated the calculations of Taguchi (2010), but here we analyzed the data individually from the 10 stations, shown in table 1 and figure 2, which are distributed in longitude and lie close to the Equator. For this, we used zonal wind data at 7 pressure levels (70, 50, 40, 30, 20, 15, and 10 hPa) from the 10 IGRA stations. For most of the stations, the data quality in the stratosphere in the early several years is relatively poor. First, we discard those months with 4 or more levels missing, for each station, which results in our discarding 5-20 years of the beginning from the data records (see table 2). After this, linear interpolation was used to fill in the missing wind data at levels where no wind data was reported. The wind data were deseasonalized and then smoothed using 5-month running averages. We then determined the two leading empirical orthogonal functions (EOF1 and EOF2), which correspond to the two phases of the QBO, plotted the time evolution of the time series for the coefficients of each of the EOFs (normalized by the standard deviation of the first principal component) in a phase-space where the coefficients for EOF1 are plotted on the abscissa and those for EOF2 on the ordinate. The QBO amplitude is then seen as the radius in the phase space trajectory (see equation (2) in Taguchi (2010)). The QBO periods are determined using the rate of rotation of the phase-space trajectories separately for El Niño and La Niña (see equation (3) in Taguchi (2010)). Readers can find more detailed information of the Taguchi method in Taguchi (2010). The definition of positive/negative ENSO phase is according to the Oceanic Niño

Index (ONI).

Figure 3 shows examples of (upper) the two EOFs for Majuro (7.1°N, 171.4°E), and (lower) the phase-space plots for Majuro and Wideawake (8.0°S, 14.4°W). At this station, EOF1 and EOF2 are two leading modes and they together account for almost all of the total variance (about 98%, 62.4% by EOF1 and 34.6% by EOF2). The EOFs plots for the other stations are similar with this one, so we don't show them here. In the two lower figures of figure 3, the points for months where the ENSO 3.4 index are positive (i.e., El Niño) are denoted by red plus signs, while the La Niña points are denoted by blue diamonds. The two phase-space plots shown in figure 3 are very similar, even though these two stations are separated by about 180°longitude. Note that, for both stations, the average norm of the blue points is greater than the red points, confirming that the QBO amplitude is larger during La Niña.

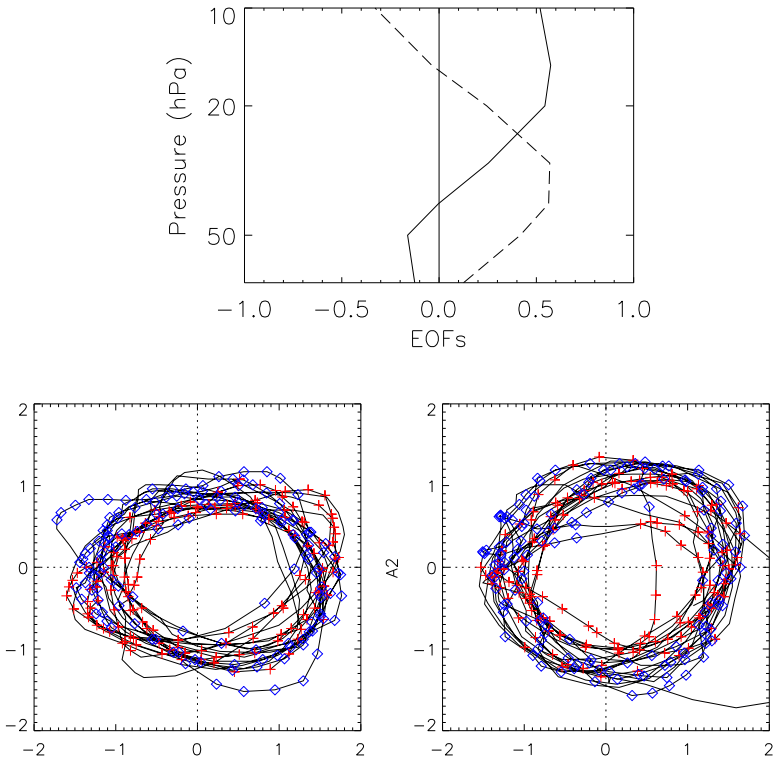

Figure 3: (Upper) Two leading EOFs at Majuro (7.1°N, 171.4°E). Each of the EOFs is normalized to be a unit vector. Solid line is for EOF1, and dashed line is for EOF2. (lower, left) Phase-space diagram at Majuro (7.1°N, 171.4°E) and (lower, right) phase-space diagram at Wideawake (8.0°S, 14.4°W). Both diagrams were constructed following the procedures of Taguchi (2010), where EOF1 and EOF2 were produced from monthly mean winds at that station in the lower stratosphere, and the time evolution is shown in the phase-space diagram, where the EOF2 coefficient is plotted vertically and labelled A2, and the EOF1 coefficient is plotted horizontally and labelled A1. The points for times of El Niño are plotted using red plus signs, and the La Niña points are plotted using blue diamonds. A1 and A2 are dimensionless.

The QBO relative amplitudes and rates of rotation in phase space for all ten stations are shown in table 2. Note that our mean QBO periods of 24.2 months for El Niño and 32.6 months for La Niña compare well with Taguchi's (2010) periods of 24.7 and 31.9 months. Applying the Student's t-test to QBO phase speeds and amplitudes, we find that they are almost all significantly different between times of El Niño and La Niña, at least at the 90% level. The only exception is the QBO phase speed at the Seychelles station, at which the data quality is relatively poorer than for the other stations.

Stations	Discarded years	EL PS	LA PS	EL AMP	LA AMP
Seychelles	4	14.9	11.2	1.16	1.24
Penang	0	14.4	11.9	1.1	1.2
Singapore	17	14.1	11.6	1.18	1.25
Koror	13	14.3	11.6	1.17	1.23
Yap	10	14.2	11.1	1.13	1.22
Chuuk	13	14.5	11.1	1.14	1.23
Ponape	13	14.5	11.3	1.17	1.23
Kwajalein	12	14.3	11	1.16	1.26
Majuro	9	14.3	11.3	1.17	1.24
Wideawake	4	14.2	11	1.17	1.3
Mean		25 months	31.8 months	1.15	1.24

Table 2: The QBO phase speeds (PS; unit is per month) and amplitudes (AMP; dimensionless) determined separately for El Niño and La Niña. 'Discarded years' is Length of discarded record from the beginning at each station. 'EL' means 'El Niño', 'LA' means La Niña.

Thus, we conclude, as anticipated, that the El Niño/La Niña dependence of QBO periods is approximately zonally symmetric and agrees very well with those quoted in Taguchi (2010), although our ratio of the QBO amplitudes are a bit less than he found.

2.2.2 On the El Niño/La Niña Influence on QBO CPT Temperature Variations

Both Randel et al. (2000) and Zhou et al. (2001) have analyzed the QBO influences on the altitude and temperature of the tropical tropopause. Those papers analyzed the QBO effects independent of El Niño and La Niña, since at that time, there was no appreciation of the ENSO modulation of the QBO. Because the QBO has greater amplitude and descends more slowly under La Niña conditions than during El Niño over the entire period analyzed, the vertical shear of the QBO zonal wind is greater under La Niña conditions than during El Niño. According to the thermal wind relationship shown in equation (1.4, 1.5), the QBO temperature modulations should be greater during La Niña than El Niño. Here, we ask the question to what extent this is seen at CPT levels?

To answer this question, we utilize the long IGRA data sets, and composite the coldest points on station soundings according to the wind shear at 50 hPa. This wind shear is computed using the zonal winds at 70 and 40 hPa, as was done by Zhou et al. (2001), but now separately for positive and negative Niño 3.4 SST (sea-surface temperatures) indices (i. e., mean

SST +/- ¼ standard deviation). Our results are shown in table 3. Note that the QBO easterly CPT temperatures are colder in all cases, and that these temperature differences are larger for La Niña than El Niño for all ten stations. The average temperature differences are, in general, larger than are shown in figure 7 of Zhou et al. (2001), and more consistent with the differences shown in figure 13a of Randel et al. (2000). This is to be expected since the interpolations of the ECMWF data will not properly resolve the sharp CPT feature, whereas radiosonde data used by Randel et al. (2000) and in this paper use no such interpolation. Applying the Student's t-test to these individual QBO differences indicates that they are almost all found to be significant, at least at the 90% level. From another point of view, from table 3 we can find that in all cases that the QBO modulations of CPT temperatures are greater during La Niña conditions, this feature is symmetric along the Equator, this fact can give much more statistical significance to our conclusion about the ENSO dependence of the QBO modulation.

Stations	Number	El Niño DT	La Niña DT	All DT
Seychelles	1	**0.69**	**2.12**	**1.49**
Penang	2	**0.69**	**1.24**	**1.02**
Singapore	3	**0.79**	**1.57**	**1.19**
Koror	4	**0.44**	**1.19**	**0.84**
Yap	5	**0.43**	**1.21**	**0.77**
Chuuk	6	0.38	**1.31**	**0.83**
Ponape	7	**0.55**	**1.28**	**0.88**
Kwajalein	8	**0.79**	**1.39**	**1.08**
Majuro	9	**0.58**	**1.07**	**0.84**
Wideawake	10	**0.56**	**0.85**	**0.79**

Table 3: The QBO westerly minus QBO easterly CPT temperature differences (DT; °C) determined for the 10 equatorial stations, using the CPT temperatures in the IGRA soundings. Bold underline represents 95% confidence using the Student's t-test; bold represents 90%; and regular font represents confidence below 90%.

Stations	Number	El Niño DT	La Niña DT	All DT
Seychelles	1	0.13	1.73	0.9
Penang	2	0.63	1.28	1.06
Singapore	3	0.79	1.23	1.02
Koror	4	0.39	0.99	0.75
Yap	5	0.21	0.88	0.59
Chuuk	6	0.33	1.13	0.71
Ponape	7	0.54	1.11	0.82
Kwajalein	8	0.74	1.08	1.00
Majuro	9	0.62	1.06	0.86
Wideawake	10	0.62	0.42	0.63

Table 4: The QBO westerly minus QBO easterly CPT temperature differences (DT; °C) determined for the 10 equatorial stations, using the CPT temperatures from the profiles derived from interpolations of the IGRA soundings.

The QBO CPT temperature differences are found to be much larger during La Niña than during El Niño. Compared with El Niño months, the temperature difference during La Niña can be 27% larger at Wideawake station, or even be over two times larger at the Seychelles and Chuuk stations. Zhou et al. (2004) showed that the winter dehydration region for air entering the stratosphere through the tropical tropopause is both larger in volume and colder when the QBO is in its easterly phase under La Niña conditions. Liang et al. (2011) have analyzed AIRS/MLS troposphere/stratosphere data for the period 2004-2010 and found that their values of the interannual variation of tropical mean stratospheric entry water vapor mixing ratios are very consistent with those suggested by Zhou et al. (2004). The results shown in table 3 show that this is even a larger effect than was indicated by Zhou et al. (2004) since the QBO temperature differences themselves are now shown to be larger during times of La Niña.

2.2.3 Wind and Temperature Profiles

To produce the wind and temperature profiles for the different QBO and ENSO phases, we use the spline-fitting methods suggested by Bell and Geller (2008) that were used to produce the IGRA results shown on the second column of figure 1. These results are shown in figure 4 for Ponape, as an example, where again we have composited the profiles with respect to QBO easterly and westerly phases according to the 50 hPa wind shear for all profiles, and for El Niño and La Niña separately.

By comparing the tropospheric zonal winds with those in figure 1, we see that we have been very successful in separating QBO influences from ENSO influences, since the winds under about 13 km are virtually identical for both easterly and westerly QBO phases. Secondly, consistent with the results of Zhou et al. (2001) and Randel et al. (2000), the CPT is colder under QBO easterly than during QBO westerly conditions, but now we see that this effect is much more marked under La Niña conditions. The ENSO dependence of the QBO modulation on CPT is shown more clearly in figure 5. Corresponding to figure 4, figure 5a and 5b shows the temperature differences and zonal wind differences at Ponape. It also shows that the El Niño temperature differences are smallest, followed by the all soundings differences, with the La Niña temperature differences being the largest. In figure 5b, the amplitude of zonal wind differences between QBO phases corresponds to the temperature differences according to the thermal wind relationship near the tropical tropopause region. Finally, we also see that the QBO temperature differences are consistent with the difference in the shears (figure 5c). Clearly, the wind shears are larger during La Niña than during El Niño conditions, which is consistent with the larger CPT temperature differences during La Niña. Note also that the temperature differences change sign as the sign of the wind shear changes.

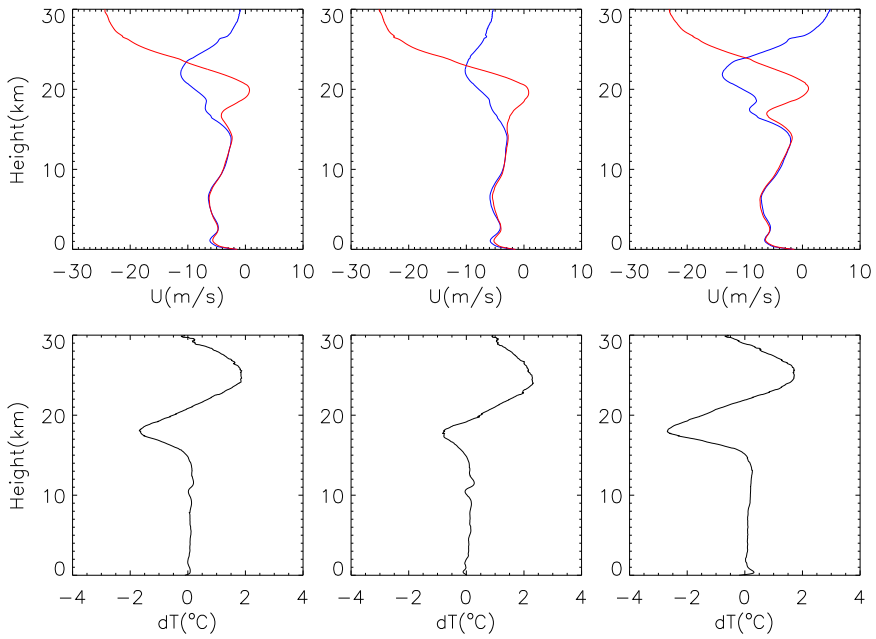

Figure 4: The QBO variations in (top) zonal wind and (bottom) temperature difference for (left) all ENSO phases, (center) El Niño, and (right) La Niña conditions for Ponape (7.0°N, 158.2°E): the differences are calculated by QBO easterly minus QBO westerly. The blue curves correspond to QBO easterly conditions, and the red curves to QBO westerly conditions. The data were composited using a 6-month phase lag according to the wind shear at 50 hPa. The units of zonal wind and temperature difference are m/s and °C.

We have produced figures analogous to figure 4 using the QBO criterion of Randel et al. (2000); that is to say, using the 50 hPa zonal wind with no phase lag, and we find very similar results, but the Zhou et al. (2001) wind shear criterion seems to produce slightly more consistent results, as indicated by generally smaller differences in tropospheric winds for the different QBO conditions.

It should be noted that the temperature differences in figure 5a are larger than in table 3. It should be expected that there would be some differences in the results using the CPT temperatures directly from the IGRA soundings versus obtaining these differences from the interpolated IGRA soundings due to various factors. First, not all soundings report CPT temperatures, so there is some difference between the soundings used in these two different computations. Also, for the soundings without recorded CPT temperature, the CPT temperature can only be interpolated from the records from nearby mandatory pressure levels, which are rather sparse near the CPT, so some differences are likely introduced by the interpolations. Table 4 shows the CPT temperatures derived from the interpolated profiles, since the values in table 4 are the largest CPT temperature difference from the temperature difference profile for all the station during each ENSO phase, so we don't apply any statistical significance test to table 4. In almost all cases, the QBO temperature differences are larger in table 4 than in table 3 for El Niño conditions, and they are all larger for La Niña conditions. The differences between the results shown in tables 3 and 4 are indicative of the uncertainties in these computations.

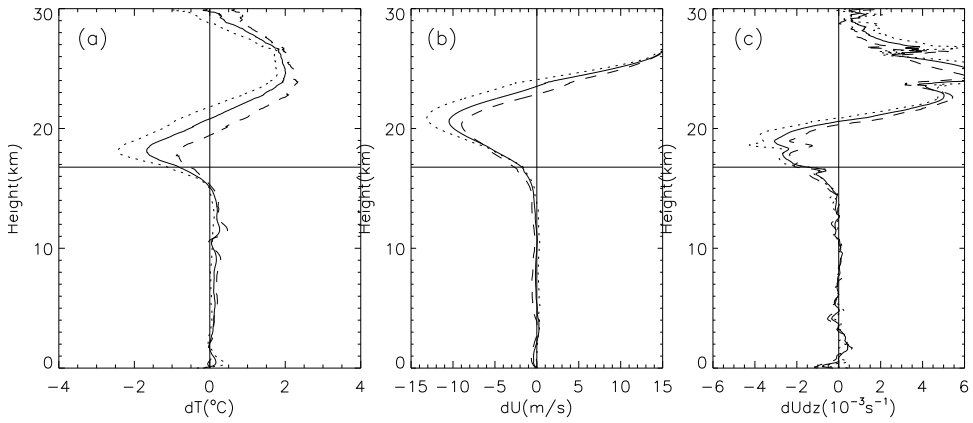

Figure 5: (a) Temperature differences and (b) zonal wind differences (QBO easterly phase minus QBO westerly phase) for Ponape, which correspond to the temperature and zonal wind profiles shown in Figure 2.4. (c) Vertical gradient of the zonal wind difference. Solid line represents the results from all ENSO phases; dashed line and dotted line represent El Niño and La Niña respectively. The horizontal line indicates the mean tropopause height, which is calculated from IGRA soundings. The units from left to right panel are °C, m/s and $10^{-3}s^{-1}$, respectively.

2.2.4 Summary and Discussion

In this section we have used IGRA data to verify the Taguchi (2010) results that the QBO has greater amplitude and longer period under La Niña conditions than under El Niño conditions for 10 near-equatorial stations, irrespective of longitude, over an approximate 60-year period, starting in the 1950s.

Because of the greater amplitude and slower descent rate of the QBO during La Niña conditions seen for the overall 60-year period of analysis, we anticipated that the QBO temperature signal should vary under different ENSO conditions, and we have verified that the QBO temperature signal is larger during La Niña conditions than during El Niño in the vicinity of CPT altitudes.

We have shown that analysis of IGRA wind and temperature profiles gives nearly identical results as similar analysis of high vertical-resolution radiosonde data for the same station over an 11-year period. Although 11 years does not seem to be sufficiently long to effectively separate QBO from ENSO influences, this gives us confidence that this separation can be carried out using IGRA data, which for many stations extend for more than 50 years, when the methodology of Bell and Geller (2008) is used to mimic high vertical-resolution data.

The results in this section strengthen further Zhou et al.'s (2004) as-

sertion, that maximum dehydration occurs in Northern Hemisphere winters when both La Niña and easterly QBO conditions exist. Zhou et al. (2004) reasoned that the coldest winter CPT temperatures exist over the Western Pacific Warm Pool under La Niña conditions, and CPT temperatures are cooler at all longitudes during QBO easterlies. These conditions when superposed produce the coldest conditions and greatest dehydration. In their argument, however, Zhou et al. (2004) did not take into account the ENSO influence on QBO strength. Our new results indicate an even stronger effect for the entire period analyzed, because QBO easterlies lead to cooler CPT temperatures under La Niña conditions than during El Niño. Given the changes observed in the ENSO/QBO relationship from the first half of this data record to the second half, however, further analysis is needed.

One application of the results shown in this section is the use of derived QBO westerly and QBO easterly wind and temperature profiles in cloud-resolving models, to see if we can obtain results consistent with those found by Collimore et al. (2003), Ho et al. (2009) and Liess and Geller (2012). That is to say, to check whether deep convection is enhanced in the Pacific Warm Pool region under QBO easterly conditions. This, in turn, would provide a QBO modulation in the latent heating forced teleconnection pattern.

Taguchi (2010) described two possibilities for explaining the ENSO influence of QBO periods. One is the influence of tropical upwelling. Previous work had indicated that tropical upwelling is stronger during El Niño, which

should act to make the QBO period longer, but this explanation seems to be working in the opposite direction to observations. Therefore, Taguchi (2010) concluded that this must be a consequence of the wave momentum fluxes being stronger during El Niño than during La Niña. Our hypotheis is that the more widespread convection during El Niño results in a greater zonally averaged gravity wave momentum flux, which in turn, gives a shorter QBO period. The greater QBO amplitude during La Niña over the entire period analyzed is probably due to more intense convection (as reflected in higher cloud tops) giving rise to a greater spread in the gravity-wave phase speeds excited. The fact that the ENSO influence on QBO amplitudes is less stable than the ENSO influence on QBO period is probably due to different variations in the ENSO modulation of convection intensity during the early and later portions of this 60-year period. I discuss more about this in the following section.

Most of the results shown so far in this chapter can be found in Yuan et al. (2014).

2.3 ENSO Modulation of QBO Amplitude and Period: Two Time Intervals

Taguchi (2010) found that during 1953-2008, the mean QBO period is about 31.9 months during La Niña conditions and about 24.7 months during El Niño conditions. He also found that the QBO amplitudes were more than 10% greater during La Niña conditions than during El Niño conditions. In the previous section I verified that these results were valid over 4~6 decades at all longitudes in the tropical region, by repeating the Taguchi (2010) analysis at 10 near equatorial radiosonde stations.

Garfinkel and Hartmann (2007) calculated the correlation coefficient between the Niño3 index and zonal wind at 50 hPa from September 1957 to January 2007. While the correlation coefficient for all 593 months is -0.02, the two indices were significantly negatively correlated from about 1953-1982 (r=-0.25) and significantly positively correlated from about 1990-2010 (r=+0.26). This prompts us to ask whether the Taguchi (2010) results are equally valid over both the earlier and later time intervals.

2.3.1 Correlation between ENSO Index and QBO Index

Garfinkel and Hartmann (2007) used the CPC/NCEP Niño3 index and the ERA-40 zonal wind at 50 hPa from September 1957 to January 2007 in their ENSO-QBO correlation coefficient calculation. Since we are using the FUB

wind data and ERSST.V3B index in this dissertation, my first step in this section is to test whether the changing ENSO-QBO correlation relationships between the two time intervals are still robust when both indices are slightly different and have longer records.

Figure 6 shows the variation of Niño3.4 index from three SST indices from CPC/NCEP, monthly ERSST.V3B index and two ONI (Oceanic Niño Index) indices. The horizontal axis is the year from 1950, The 'old ONI' index showed in the bottom panel is the ENSO index I used in the previous section (ending in 2012 February, so it's not long enough for the calculation in this section), the middle panel is the latest ONI index after CPC updated their strategy of calculating the ENSO index because of the significant warming trend in the Niño3.4 region since 1950 (check `http://www.cpc.ncep.noaa.gov/products/analysis_monitoring/ensostuff/ONI_change.shtml` for more details), the upper panel is the ERSST.V3B index. The new ONI index is calculated from the 3-month running mean of ERSST.v3b SST anomalies in the Niño 3.4 region (5°N-5°S, 120°-170°W), based on centered 30-year base periods updated every 5 years. Warm (red) and cold (blue) periods are based on a threshold of +/- 0.5°C for the ONI. For ERSST.V3B index, the El Niño months are defined as months with SST greater than the mean SST+¼ standard deviation. The La Niña months are those with SST less than the mean SST-¼ standard deviation.

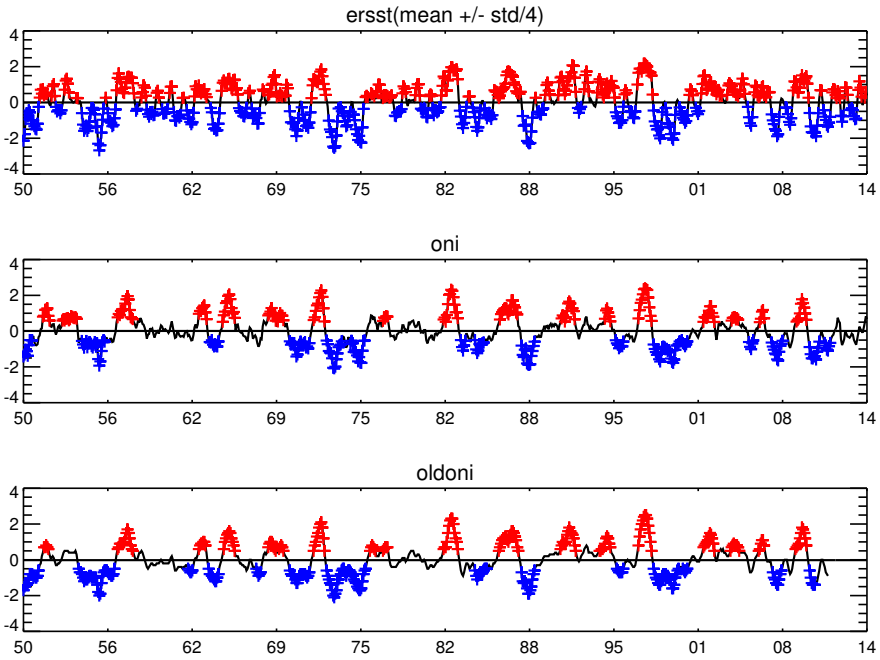

Figure 6: Comparison of the ERSST.V3B index, and two ONI, horizontal axis is the year from 1950. Bottom panel is the ONI index used in section 2.2, and it's not updated after February 2012, so it's not suitable for the calculation for this section. Red crosses indicate the El Niño months, blue crosses show the La Niña months.

The links of the ERSST.V3B index is `http://www.cpc.ncep.noaa.gov/data/indices/ersst3b.Nino.mth.81-10.ascii`; information of the two ONI indices can be found through this link: `http://www.cpc.ncep.noaa.gov/products/analysis_monitoring/ensostuff/ONI_change.shtml`.

The problem with dividing the IGRA sounding data into two time intervals is it decreases the length of record from around 50 years to around 25 years or less, for the first time period, the length can be even shorter because of the poor data quality in the early years. When I tried to use ONI to do the composite of QBO amplitude/period and the temperature, the months reaching the fixed threshold of +/- 0.5°C for the ONI are quite few for some stations in the first time period, which might cause great uncertainty in the results. So I choose to use the monthly ERSST.V3B index instead of the ONI index in this section, for which I can define the threshold more freely to include more months into the composite calculation.

Figure (7a) shows the Niño3.4 SST from the ERSST index (in black) and 50 hPa wind from the FUB wind data (in red), both detrended; and the Niño3.4 index is multiplied by 5 to get a clearer look. The vertical lines are marks of the year 1982 and 1990. Figure (7b) is the correlation between Niño3.4 SST index and FUB 50mb wind. The abscissa represents the beginning time of both indices, while the ordinate represents the ending time. The value at point (x_0, y_0) is the correlation coefficient between the two indices, both beginning at x_0 and ending at y_0. There is no time lag between the two indices, the length of each indices (y_0-x_0) should be at

least 20 years (240 months). The maximum negative correlation is between the indices of [1962-1982], the maximum positive correlation is between the indices of [1990-2010]. So in the following section, I choose 1982 and 1990 as the separating points, and define the years before 1982 as the first time period, and the years after 1990 as the second time period.

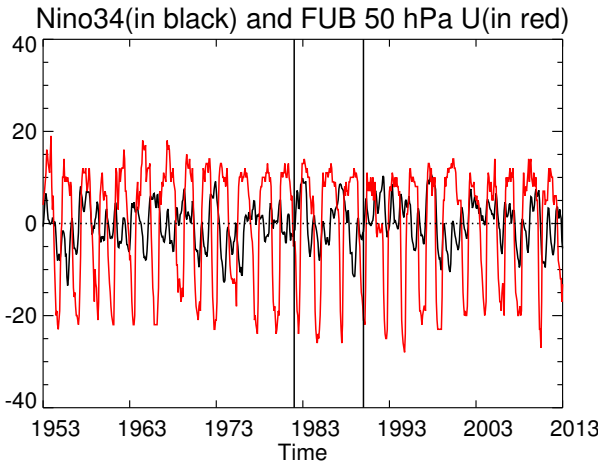

(a)

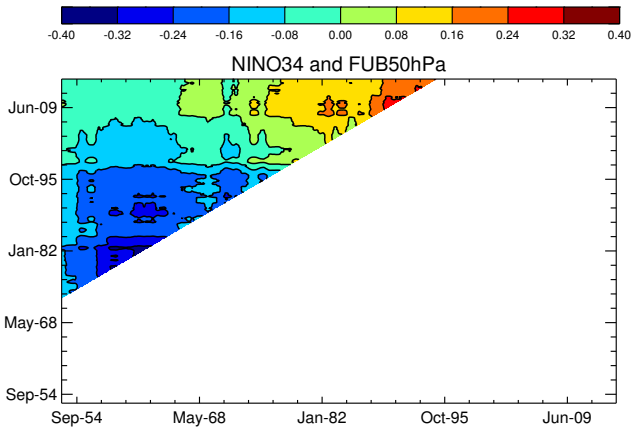

(b)

Figure 7: (A) Niño3.4 SST from ersst index (in black) and 50 hPa wind from FUB wind data (in red), both detrended; and the Niño3.4 index is multiplied by 5 to get a clearer look.The vertical lines are marks of the years 1982 and 1990. (B) correlation between the Niño3.4 SST index and FUB 50 hPa wind indices; the abscissa represents the beginning time of both indices, while the ordinate represents the ending time.

2.3.2 QBO Amplitude and Period before 1982 and after 1990 (IGRA Stations)

In this section, I apply the Taguchi (2010) method to the 7 levels stratosphere zonal wind to calculate the QBO period and amplitude during EL and LA months,before 1982 and after 1990. The same stations in the tropical region as listed in Table 1 are used here except Seychelles, at which station the availability of data in both the shorter component datasets were sufficiently decreased that the analyses were unreliable for this station.

There can be two approaches to apply the Taguchi (2010) method for the two time intervals calculation. One is first applying the EOF analysis to the all the zonal wind available, then use the same EOFs and PCs for the two time intervals, just choose the needed pieces of PCs to get the mean QBO amplitude and period. Another approach is applying the EOF analysis to the zonal wind record before 1982 and after 1990 separately, and then doing the composite of the related PCs to get QBO amplitude and period for the two time intervals. Because the data quality before 1982 is poor compared to the later years, and for some stations the zonal wind record available are very short (for example, only 11 years data(1972-1982) at Singapore are used in the calculation), doing EOF analysis to these short zonal wind data might bring large uncertainty to the results, so here I choose the first approach. I also try the second approach, the results (not shown) are similar to what I will show below. Student's t-test is used here for the statistical test, like in the whole time interval calculation.

Also, since the data quality become poorer with increasing altitude, especially in the early years of the IGRA data set, this is one of the reasons for the uncertainty in our calculations. As a test, I also apply the same method to the lower 5 levels of the monthly zonal wind, and it gives us similar results (not shown here) as the seven levels wind results.

Tables 5 and 6 show the QBO amplitudes and periods during EL and LA, for the time interval before 1982 and after 1990, from the calculation using the 7-level stratosphere wind records. For both time intervals, QBO periods are statistically significantly longer during La Niña than El Niño, both results, passing the 95% Student's t-test. As for the QBO amplitude, before 1982, for almost all stations, the QBO amplitudes are comparable between times of El Niño and La Niña. At some of the stations the mean QBO amplitude is even larger during El Niño, but these results can't pass the 90% Student's t-test, but for time periods after 1990, the QBO amplitudes during times of La Niña months are significantly larger than during El Niño

Stations	Begin	Ending	EL PS	LA PS	EL AMP	LA AMP
Penang	1968	1982	14.06	10.81	1.18	1.16
Singapore	1971	1982	14.78	10.6	1.16	1.16
Koror	1964	1982	14.48	10.59	1.16	1.16
Yap	1961	1982	14.5	10.7	1.17	1.15
Chuuk	1964	1982	14.51	10.29	1.20	1.21
Ponape	1964	1982	14.77	10.21	1.17	1.19
Kwajalein	1964	1982	14.52	10.55	1.17	1.21
Majuro	1964	1982	14.5	10.84	1.20	1.18
Wideawake	1961	1982	15.54	9.41	1.16	1.28
Mean			24.63 months	34.5 months	1.17	1.18

Table 5: The QBO phase speeds (PS; unit is degrees per month) and amplitudes (AMP; dimensionless) determined separately for El Niño and La Niña, for the time before 1982. 'EL' means 'El Niño', 'LA' means La Niña. Column 2 is the beginning year, column 3 is the ending year.

Stations	Begin	End	EL PS	LA PS	EL AMP	LA AMP
Penang	1990	2014	14.49	11.59	1.12	1.29
Singapore	1990	2014	14.47	11.59	1.21	1.35
Koror	1990	2014	14.50	11.69	1.15	1.35
Yap	1990	2014	14.34	11.54	1.08	1.31
Chuuk	1990	2014	14.60	11.38	1.09	1.31
Ponape	1990	2014	14.47	11.67	1.13	1.34
Kwajalein	1990	2014	14.45	11.83	1.13	1.30
Majuro	1990	2014	14.47	11.58	1.13	1.34
Wideawake	1990	2009	14.26	12.58	1.21	1.34
Mean			24.9 months	30.8 months	1.14	1.33

Table 6: Like Table 5, but for the time after 1990

2.3.3 Results of the CPT and 100 hPa Temperature

As I mentioned in section 2.2.2, according to the thermal wind relationship, larger QBO amplitudes should be accompanied by a larger QBO modulation of the near tropopause temperature. So here we applied the same method for table 3, checking the CPT temperature difference between the QBO E/W phases, for the time intervals before 1982 and after 1990. The years we used for the temperature calculation are the same as column 2 and 3 from table 5 and table 6.

In this part, besides the nine stations in table 5, I add a new station Howard (8.97°N, 79.55°W), located in the Caribbean to calculate the temperature for the period before 1982. The Howard station has nice data quality but its record ends at 1999, because of the short data length it's not used in Yuan et al. (2014), however it's good enough to reach our requirements for the temperature calculation for the first time interval. With the newly added station, all ten stations are still located within the tropical region (10°S to 10°N).

CPT

Like I did in the previous section, I utilize the IGRA data sets to get the monthly mean CPT temperature, and composite the coldest points for QBO E/W phases according to the wind shear at 50 hPa, and for the positive and negative ENSO phases (i. e., mean Niño 3.4 SST +/- ¼ standard deviation), before 1982 and after 1990. The results are shown in table 7 and table 8.

Since the CPT is colder during QBO easterly phases, the dT values shown in the tables are calculated from QBOW minus QBOE.

Stations	Number	El Niño dT	La Niña dT	All dT
Penang	1	**1.01**	0.14	**0.72**
Singapore	2	0.68	0.36	**0.71**
Koror	3	**1.3**	0.19	**0.75**
Yap	4	**1.19**	-0.32	0.49
Chuuk	5	**1.17**	0.05	**0.63**
Ponape	6	**1.27**	-0.06	**0.64**
Kwajalein	7	**1.19**	-0.33	0.57
Majuro	8	**1.25**	-0.26	**0.64**
Wideawake	9	**1.38**	0.27	**1.08**
Howard	10	**0.88**	0.55	**0.95**

Table 7: Like table 3, but for CPT temperature before 1982

Stations	Number	El Niño dT	La Niña dT	All dT
Penang	1	**0.89**	**1.47**	**1.2**
Singapore	2	**0.81**	**1.59**	**1.23**
Koror	3	0.38	**1.65**	**0.97**
Yap	4	0.41	**1.62**	**0.9**
Chuuk	5	0.38	**1.61**	**0.9**
Ponape	6	0.34	**1.62**	**0.91**
Kwajalein	7	**0.7**	**2.2**	**1.14**
Majuro	8	**0.56**	**1.64**	**0.93**
Wideawake	9	0.4	**1.16**	**0.67**

Table 8: Like table 3, but for CPT temperature after 1990

Table 7 shows the CPT temperature differences between QBO E/W phases (QBOW-QBOE) during El Niño, La Niña and all months. The temperature differences are larger for El Niño than La Niña for all the ten stations. The dT values for El Niño are almost all found to be significant, at least at the 90% level, except for one station Singapore, at which only 12 years of data can be used for the time interval before 1982 (see table 5), and this might be too short to get a statistically significant results. The dT values for La Niña can't pass the 90% significant level, which indicates that the mean CPT temperatures during QBOE and QBOW are quite close to each other for the La Niña months before 1982, and they are not significantly different between one another. This is understandable since the length of the overall dataset is twice that of the two component data sets, the statistical significance of these shorter data sets are decreased.

With shorter data record length for both first and second time intervals, we must be careful about the reliability of the monthly mean CPT temperatures, especially for the time before 1982. 100 hPa and 70 hPa are the closest mandatory levels below/above the tropopause in the tropical region in IGRA, the monthly mean 100 hPa and 70 hPa temperature can be calculated directly from all the valid 100 hPa and 70 hPa temperature records, while the CPT is determined by the criteria listed in section 2.1.2. If we plot the numbers of soundings which can be used to calculate the temperature at CPT/100 hPa/70 hPa for each month as a time series (not shown here), the numbers of soundings are significantly larger for the mandatory levels than for CPT before the 1970s. This situation improves for the later years with

overall improved data quality, so we expect the quality of monthly mean 100 hPa temperatures to better than the CPT temperatures, especially in the early years. As a test of the robustness of the CPT temperature results, here we also check the temperature difference between QBO E/W phases at 100 hPa, using the same method, to get table 7 and 8.

100 hPa and 70 hPa Monthly Mean Temperatures

The composite of 100 hPa and 70 hPa monthly mean temperatures show similar results. Generally speaking the 100 hPa is closer to the CPT than 70 hPa in all the stations we choose, so here we only list the results from 100 hPa monthly mean temperature in table 9 and 10. Like the CPT results, the dT values shown in these two tables are calculated from QBOW minus QBOE. For all the ten stations, the mean 100 hPa monthly temperature differences between QBO E/W phases are larger during El Niño than La Niña for the time interval before 1982, although some of the values can't pass the 90% significant level of Student's t-test. This relationship is reversed for the time period after 1990, with longer data length and improved data quality, the Student's t-test results for the second time interval give more siginificnace for La Niña compared with the first time interval.

From another point of view, as we discussed in connection with table 3, we find that that the feature of QBO modulations of CPT/100 hPa temperatures is symmetric along the Equator, the dT values are greater during El Niño conditions before 1982, while after 1990 they are greater during La Niña conditions. This fact can give much more statistical significance to

our conclusion about the ENSO dependence of the QBO modulation on the temperature near the tropopause.

Stations	Number	El Niño dT	La Niña dT	All dT
Penang	1	0.64	0.08	**0.59**
Singapore	2	0.68	-0.69	0.37
Koror	3	**0.81**	0.02	0.41
Yap	4	**0.71**	-0.25	0.21
Chuuk	5	**0.91**	-0.18	0.41
Ponape	6	**0.99**	-0.38	0.43
Kwajalein	7	**0.77**	-0.26	0.39
Majuro	8	**0.93**	-0.45	0.40
Wideawake	9	**0.81**	0.43	**0.65**
Howard	10	0.50	0.14	**0.48**

Table 9: Like table 3, but for the 100 hPa temperature before 1982

Stations	Number	El Niño dT	La Niña dT	All dT
Penang	1	**0.68**	**1.01**	**0.85**
Singapore	2	**0.75**	**1.39**	**1.05**
Koror	3	0.21	**1.11**	**0.65**
Yap	4	0.22	**1.23**	**0.58**
Chuuk	5	0.28	**1.17**	**0.64**
Ponape	6	0.25	**1.2**	**0.64**
Kwajalein	7	**0.59**	**1.85**	**0.91**
Majuro	8	0.38	**1.18**	**0.62**
Wideawake	9	**0.64**	0.45	**0.53**

Table 10: Like table 3, but for the 100 hPa temperature after 1990

2.3.4 Possible Mechanism for the Different ENSO Influences on the QBO during two time intervals

When we do the identical analysis as we did for the overall time period on the years before 1982 and the years after 1990 for the stations with adequate data during both intervals, we find our conclusions about the ENSO influence on the QBO period to be almost unchanged. The following table 11 is the summary of the ENSO-QBO amplitude and period relationship for the overall time period and the two shorter intervals, from Taguchi (2010), table 2, 5, and 6. For the nine remaining stations, the periods were consistently longer during La Niña (average period 24.7 months before 1982 and 34.5 months after 1990) than during El Niño (24.9 months before 1982 and 30.8 months after 1990), so the Taguchi (2010) results for QBO period are qualitatively valid for both time intervals. The ENSO influence on the QBO amplitudes has changed during these time intervals, however. In the years before 1982, we find the QBO amplitudes to be greater during El Niño, although this result is not statistically significant, but during the years after 1990, the QBO amplitudes are greater during La Niña, which agrees with the results of Taguchi (2010) and Yuan et al. (2014), for the overall period.

We then try to figure out why the ENSO modulation on QBO amplitudes changes before/after the 1980s, while the modulation on QBO periods is unchanged? We hypothesize that change of QBO amplitude and period relationship might be connected with the deep convection change during the two time intervals. The more widespread deep convection that occurs in

Period of analysis	QBO period EL	QBO period LA	QBO amplitude LA/EL
1953-2008	24.7 months	31.9 months	1.1
1950s-2010s	25 months	31.8 months	1.08
1950s-1982	24.7 months	34.5 months	1.01
1990-2010s	24.9 months	30.8 months	1.16

Table 11: QBO period and amplitude dependence on ENSO phase during various time intervals. The first row is from the Taguchi (2010) analysis. The second row is from the Yuan et al. (2014) analysis, and the last two rows are from the present analysis for the two time intervals.

connection with El Niño leads to greater zonally averaged gravity wave momentum fluxes, which, in turn, leads to more rapid descent of the QBO westerlies and easterlies, leading to shorter QBO periods during El Niño. Deeper convection occurs more during La Niña, this leads to a broader spectrum of gravity wave speeds, which, in turn, leads to greater QBO amplitudes. Furthermore, we hypothesize that the broader longitudinal extent of deep convection during El Niño than La Niña was a feature common to both the earlier period of the 1950s to the 1980s and the later period of 1990-2010s, but the greater amount of very deep convection during La Niña was more marked during the period 1990-2010 than during the earlier period of the 1950s to the 1980s.

Here, we use OLR as a proxy of tropical deep convection, spit into two time intervals (before/after 1984), check the strength and width of deep convection during EL Niño and La Niña separately. The reason we choose year 1984 as the separating point rather than 1982 is because the OLR data begins at 1974, so we want to keep at least 10 years of record for the first time period. According to Randel et al. (2001) and Zhang (1993), we define

super strong deep convection/strong deep convection/deep convection with OLR less than 210/220/230W/m^2.

In the following part, I will show some results from OLR data to support these hypotheses. However, we should keep in mind that since there are limited numbers of El Niños and La Niñas during the earlier and later time intervals, these observational results, by no means, prove that our hypotheses are correct. I am just trying to offer a reasonable interpretation here.

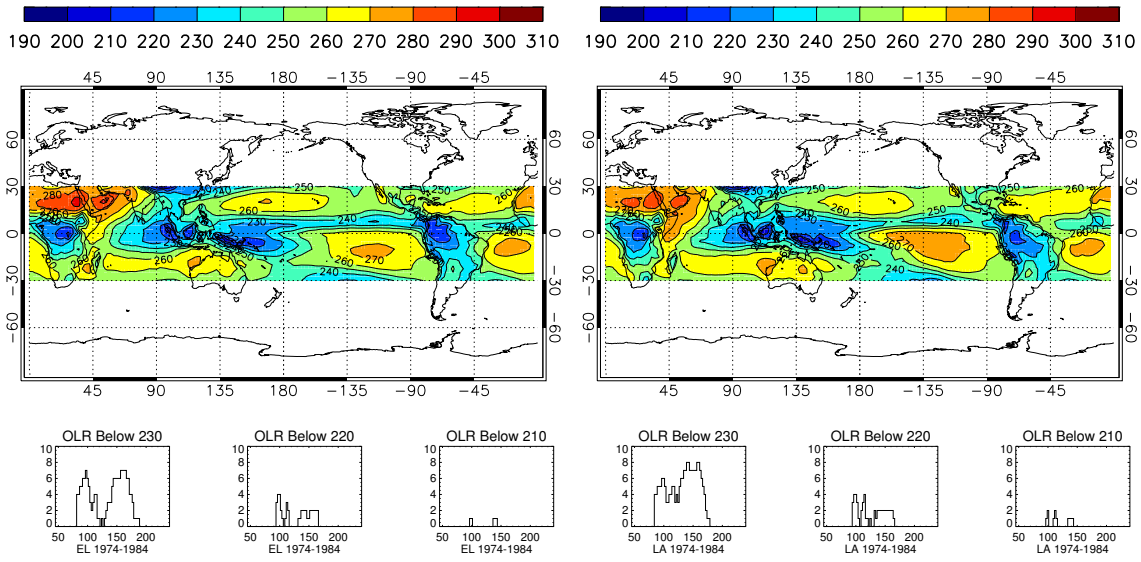

Figure 8: Top Left: OLR map between 30°S and 30°N for the average of El Niños for the period June, 1974 to May, 1984. Top Right: Same for La Niñas. Bottom Left: Number of grid points with OLR values below 210, 220, and 230W/m^2 between 10°S and 10°N in the map directly above for El Niño conditions during this period as a function of longitude between 50 and 250°E, i. e., over the equatorial Pacific. Bottom Right: Same for La Niña conditions.

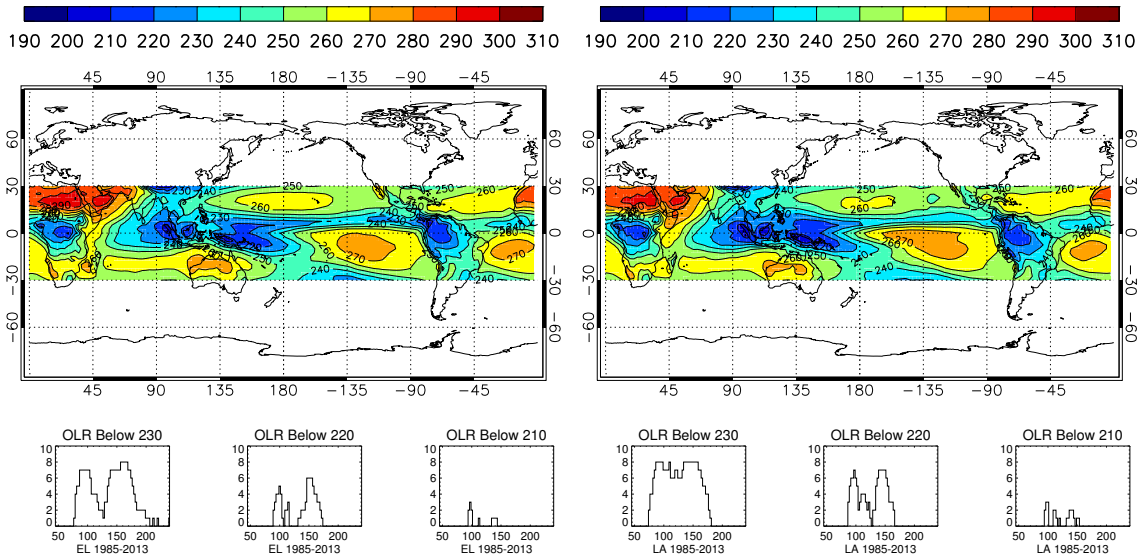

Figure 9: Same as figure 8, but for the period June,1984-December, 2013.

Figure 8 shows that, while the OLR values for deep (OLR $< 230W/m^2$) and deeper (OLR $< 220W/m^2$) convection have broader longitudinal extent during El Niño conditions, there is little difference in the intensity of the equatorial deep convection between El Niño and La Niña conditions in the period 1974-1984. In fact, there appear to be comparable amount of grid points with OLR values less than 220 W/m^2 (deeper convection) during times of El Niño and La Niña. The histograms in figure 8 show that, during the period of 1974-1984, there are 53 grid points with OLR less than $220W/m^2$ during La Niña, while the grid points number with OLR less than $220W/m^2$ during El Niño is 44.

On the other hand, while figure 9 shows a similar dependence of the longitudinal extent of deep convection on ENSO state as was seen in fig-

ure 8, there is much more deeper (OLR $< 220W/m^2$) and deepest (OLR $< 210W/m^2$) convection in the La Niña state than during El Niño in the period 1984-2013. In the histograms in figure 9, there are 25 (136) grid points with OLR less than $210W/m^2$ ($220W/m^2$) during La Niña, while the grid points numbers with OLR less than $210W/m^2$ ($220W/m^2$) during El Niño are 12 (87) respectively.

Beres (2004) has indicated that deeper convection should launch gravity wave spectra with wider spread in their phase velocities. To illustrate this, Geller et al. (2015) used the formulation of Beres (2004) to calculate the momentum flux launched by a convective heat source for two different horizontal scales of heating, σ_x = 3 km and 18 km, and for two different vertical scales of heating, h = 3 km and 8 km. This is shown in figure 10 (from Geller et al. 2015), which is analogous to the left-hand panel of figure 1 in Beres (2004). Note that in both the narrow convective heating case, σ_x = 3 km, and the broad convective heating case, σ_x = 18 km, not only do the momentum fluxes peak at higher gravity wave phase velocities for the larger depth of heating, but also much greater gravity wave momentum fluxes at higher phase speeds are seen for the case where the vertical extent of heating is larger.

Both this idealized simple calculation showing wave forcing of the QBO (Geller et al. 2015) and full modeling results of the QBO in a climate model (Zhou et al. 2015, Schirber 2015) demonstrate the following.

1. The period of the QBO is determined by the magnitude of the wave mo-

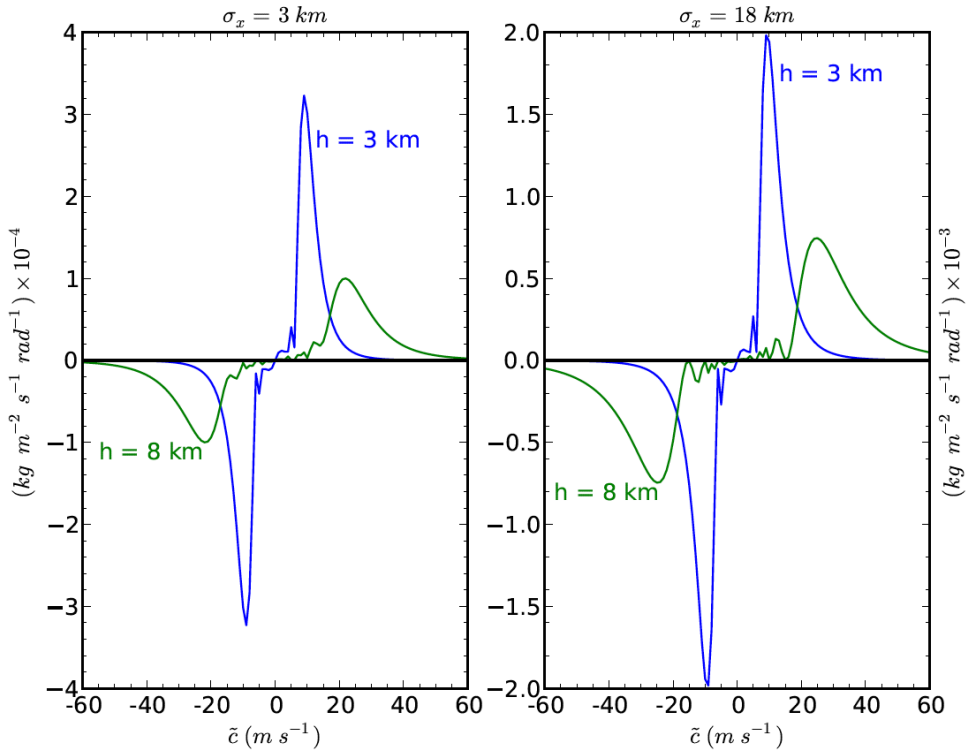

Figure 10: Momentum flux carried by thermally forced gravity waves in each azimuthal direction, for heat sources with frequency distributions given by equation (55) of Beres (2004) and horizontal scale σ_x = 3 km (left) and σ_x = 18 km (right) for a shallow heating depth, h=3 km (blue), and a deep heating depth, h=8 km (green). In all cases the integration limits in Beres (2004) equation (54) were taken to be $\nu_{min} = 0$ to $\nu_{max} = 2\pi/10$min. (after Geller et al. (2015))

mentum flux driving the QBO.

2. The amplitude of the QBO is determined by the magnitude of the wave phase speeds that comprise the gravity wave spectrum forcing the QBO.

In addition, modeling of the QBO in a climate model (Zhou et al. 2015) illustrates the following.

1. It is the parameterized gravity wave flux that determines the period and amplitude of the QBO even though it is the resolved wave fluxes that cause the QBO to penetrate low into the stratosphere, and even into the upper troposphere.

2. The QBO responds to the zonally averaged gravity wave momentum flux irrespective of how it is distributed in longitude.

These results suggest the following hypotheses to explain the Taguchi (2010) results.

1. During times of El Niño, deep convection is more widespread in longitude than during times of La Niña, leading to a larger zonally-average gravity wave momentum flux, which in turn produces faster descent of the QBO shear zones during El Niño than during La Niña, and this leads to longer QBO periods during times of La Niña than during times of El Niño.

2. During La Niña, there is more of the deeper and deepest convection than during El Niño. This leads to a broader gravity wave phase speed spectrum, and this produces larger amplitude QBOs during times of La Niña.

Analysis of observations suggest that, while the Taguchi (2010) results

of longer QBO periods during times of La Niña are robust both during the 1950s to the 1980s and 1990s to 2010s, the Taguchi (2010) results of larger QBO amplitudes during La Niña only hold after about 1990, and do not seem to hold in the period of the 1950s to the 1980s. We speculate that this is due to the broader longitudinal extent of deep convection during times of El Niño relative to times of La Niña during the entire period of the 1950s to 2010s, but the higher incidence of the deeper and deepest convection during times of La Niña only seems to be valid after about 1990. The observational evidence supporting this is certainly not definitive due to the small number of El Niños and La Niñas in the earlier and later time intervals analyzed, however. More work need to be done to either support or refute our hypotheses.

2.3.5 QBO Amplitude and Period before 1982 and after 1990 (FUB QBO wind data)

To check the robustness of the results shown in table 5 and 6, we apply the two-period EOF analysis to the FUB wind data. The results show that, the period of the QBO is longer during El Niño than La Niña for both time intervals, which agrees with the results in table 5 and 6. However, the amplitude calculated from the FUB wind data are larger during La Niña than El Niño months during both the earlier and latter time intervals. This result disagrees with the results in table 5 and 6.

The FUB wind data doesn't offer any temperature information, so we can't double check the QBO amplitude results with a similar temperature

relationship like in table 3. Here by looking into the construction of the FUB wind data, I will try to offer a possible explanation to the disagreement above. Naujokat(1986) combined the information from three stations (Canton Island, Gan and Singapore) to produce the FUB wind data, the stations are separated from each other in longitude. The first 22 years are from Canton Island (Jan 1957-Sep 1967, 171.43°W) and Gan (Sep 1967-Dec 1975, 73.09°E), the Singapore (103.55°E) data begins from January 1974. In the Naujokat (1986) paper, the author proved that the longitudinal differences in phase are small enough to be ignored, but she didn't discuss the longitudinal difference in amplitude and the possible influence that might bring into the calculation of the mean strength of the QBO. Hamilton et al. (2003) also examined the zonal asymmetries of the stratosphere zonal wind with a GCM simulation and limited radiosonde observation. In their results the zonal contrast in QBO amplitudes near 10 hPa at different longitudes exceeds 10%.

In other words, we can't rule out the influence caused by the zonal asymmetry of the QBO signal. If we want to explain the disagreement of ENSO-QBO amplitude relationships in this section and the previous section, we will need more information.

2.3.6 Another Statistical Test Method for the QBO Amplitude/Period and Temperature Results

Since not all the values in the previous tables pass the 95% or 90% significance level of Student's T-test, beside performing the previous Student's T-test, I have also tried another way to do the statistical test for the results of QBO amplitude/phase speed (table 2, 5, 6); CPT temperature (table 3, 7, 8) and 100hPa monthly mean temperature (table 9 and 10). All the variables, the time series of the QBO amplitude/period and the temperature are sorted into different groups, like El Niño/La Niña, or QBOE/QBOW.

Take a single station as an example, given two time series at this station, I calculate the mean values and SEMs (standard errors of the mean) of these two time series. I then plot the mean values +/- SEMs for all the ten stations in one figure. In the following figures, the horizontal axis indicates the stations as listed in table 1.

Let's start with the QBO phase speed results from table 2, 5, 6. I plot them in figure 11.

In figure 11, from the 1950s-2010s, in all the three panels, the two lines of the mean QBO phase speeds during El Niño/La Niña are clearly separated and have no overlap with each other. This indicates that the QBO phase speeds (periods) are significantly different during the time of El Niño and La Niña, with lower phase speeds (longer QBO periods) during times of La Niña.

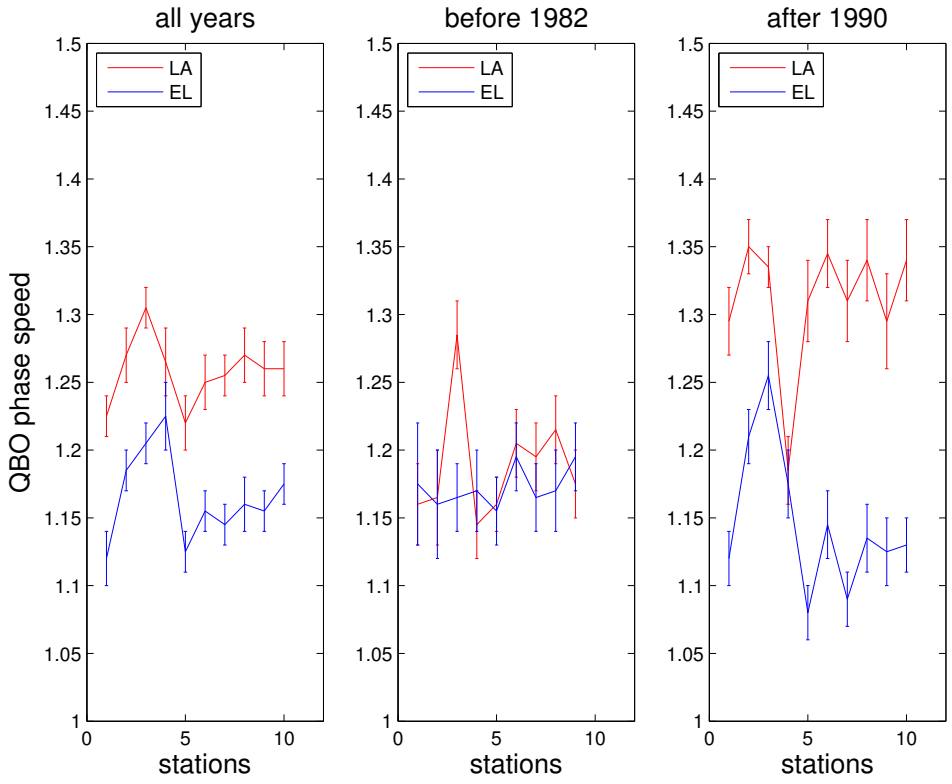

Figure 11: Mean QBO phase speeds for the 10 stations listed in table 1. (Left) all the years from the 1950s to 2010s, which were shown in table 2; (center) all the years before 1982, which are shown in table 5; (right) all the years after 1990, which are shown in table 6; blue is for the EL months, while red is for the LA months.

Figure 12 shows the QBO amplitude results for the 1950s-2010s, before 1982, and after 1990. In the left and right panels, there is one station with a little bit of overlap between the two lines during the time of El Niño and during the time of La Niña.

The QBO amplitude results before 1982 do not show similar El Niño/La Niña separation. There are overlaps for almost all stations, indicating there is no significant El Niño/La Niña difference in QBO amplitudes from the 1950s to the 1980s. This agrees with the Student's T-test results shown in table 5.

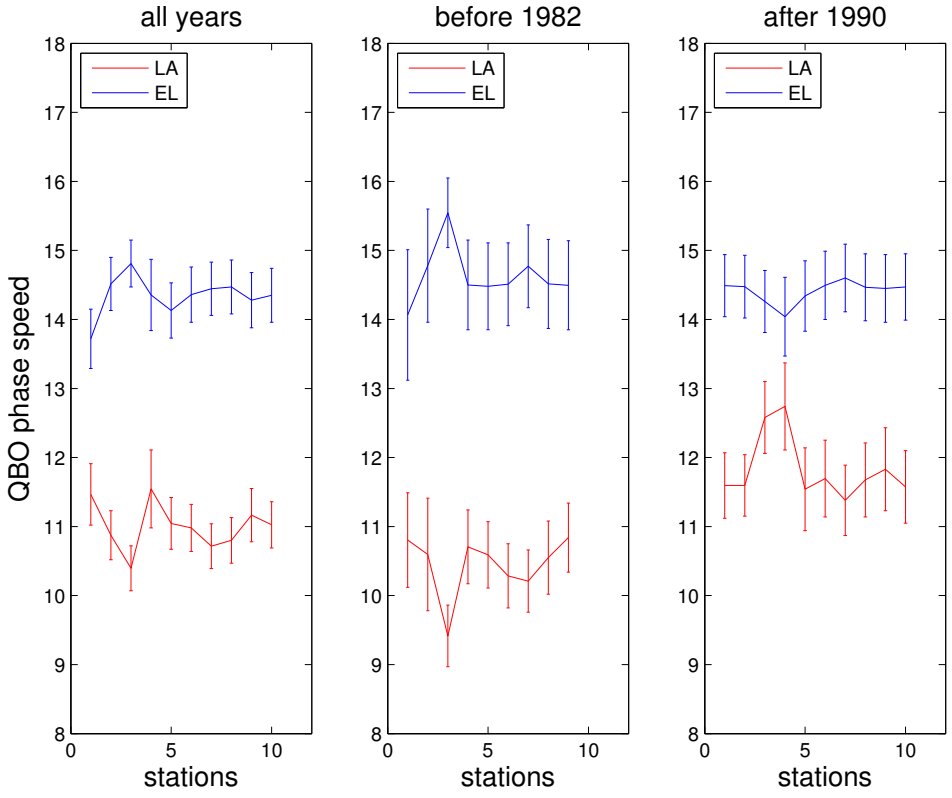

Figure 12: Similar with figure 11, but for the QBO amplitude.

Figure 13, 14, 15 show the mean values and the SEMs of the CPT temperature results, as listed in table 3, table 7 and table 8.

If we calculate the differences between the red and blue lines at each of the station in the figure 13-15, we will get the dT values in tables 3, 7, 8. Figure 13 shows that dTs are larger during the time of La Niña than El Niño for all years from the 1950s to the 1980s. There are no overlap between the two lines in both El Niño months and La Niña months, indicating that the EL/La Niña difference in the QBO modulation of the CPT temperature is significant for this overall period.

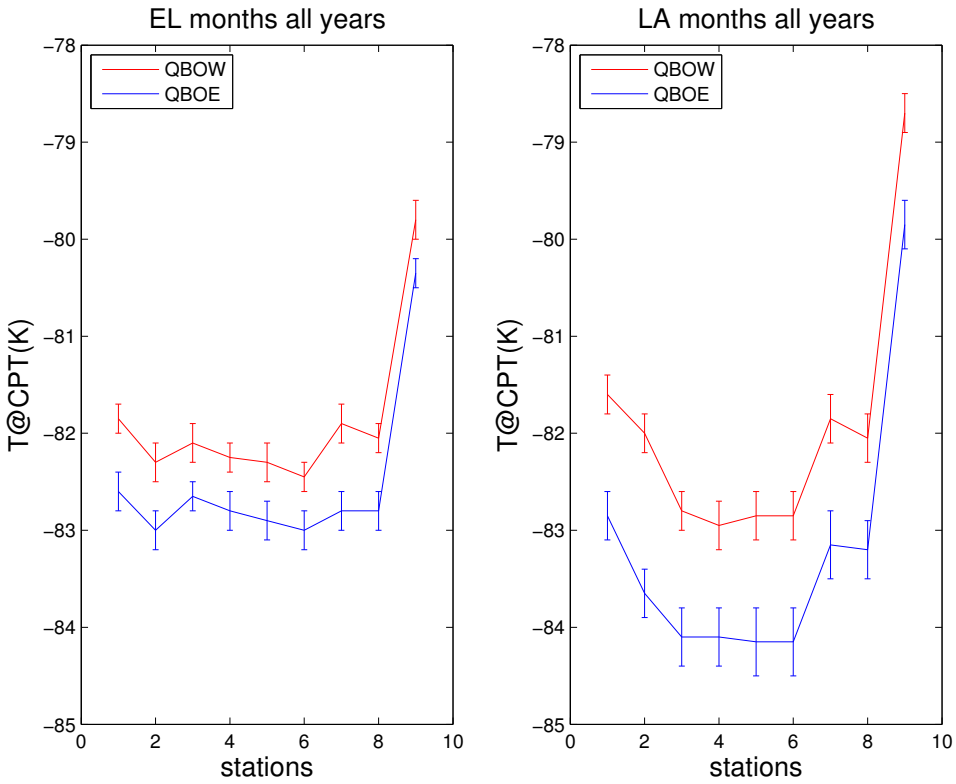

Figure 13: (Left) panel shows the mean CPT temperature for QBOW (red) and QBOE (blue) months during the time of El Niño between 1950s and 2010s, error bars indicate the SEMs of the CPT time series; (right) is the same as left panel but for the time of La Niña.

In figure 14, we can see that dTs are larger during the time of El Niño, and during times of La Niña, the CPT temperatures are not statistically significantly different between QBOE and QBOW phases.

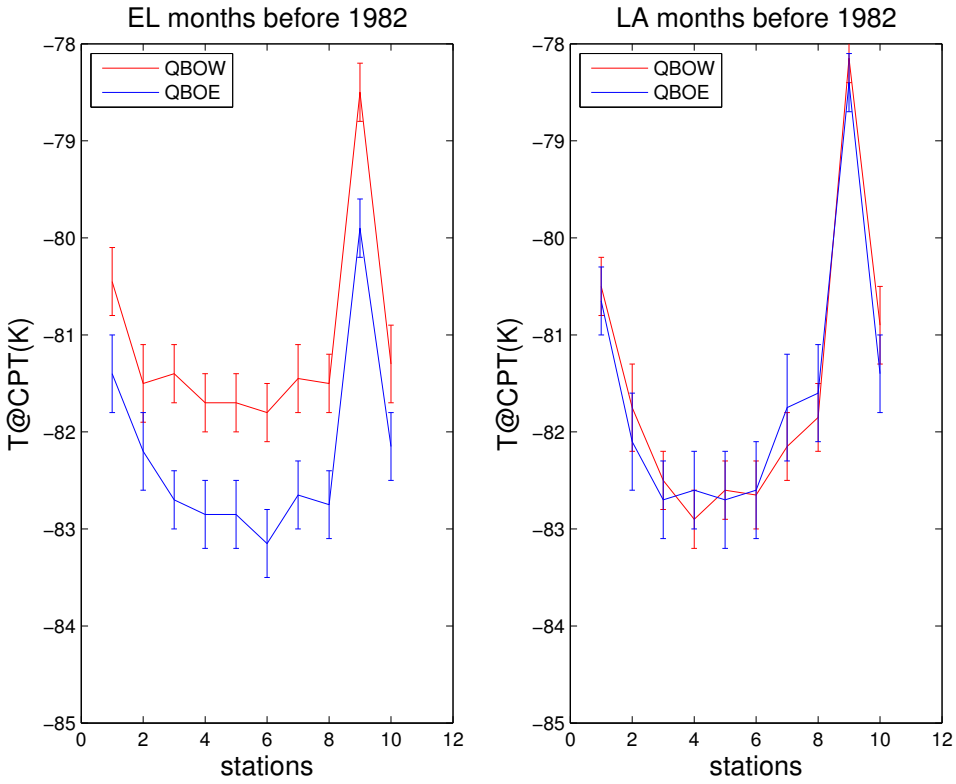

Figure 14: Same as figure 3 but for the time interval before 1982.

Figure 15 shows the CPT temperature results after 1990, dT values are larger during the time of La Niña. For the time of El Niño, there are overlaps at about half the stations, and this agrees with the results in table 8 pretty well.

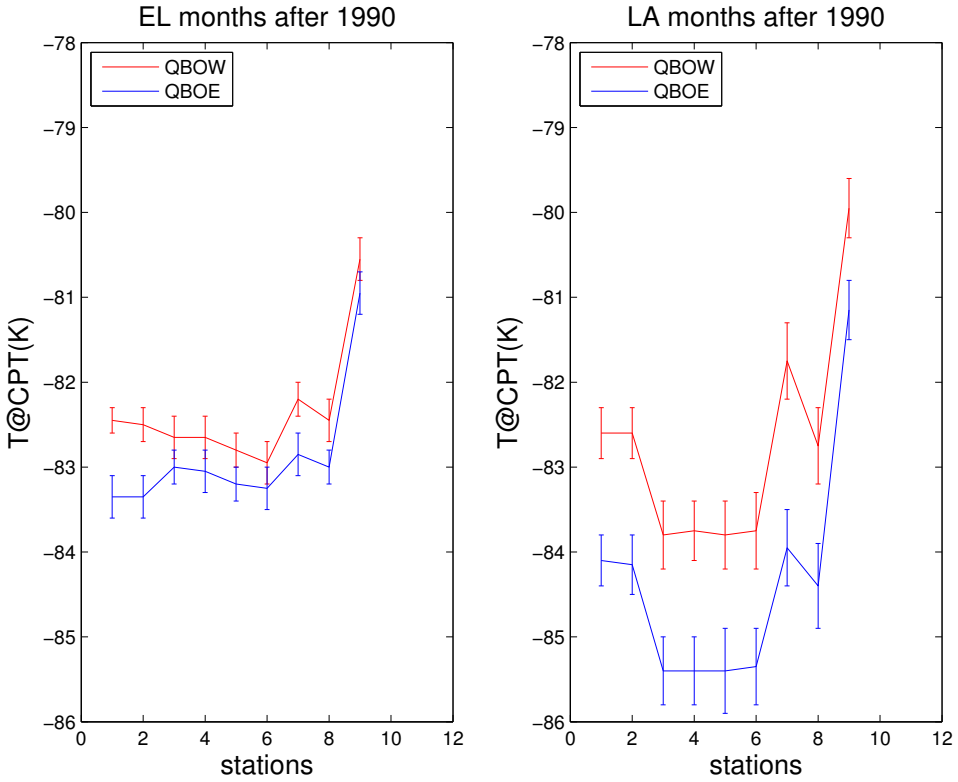

Figure 15: Same as figure 3 but for the time interval after 1990.

The following two figures (figure 16 and figure 17) show the results of the 100hPa monthly temperature shown in table 9 and table 10.

Before 1982, during the time of El Niño the 100hPa dT values are larger and there are less overlaps between the two lines; and this situation is reversed after 1990.

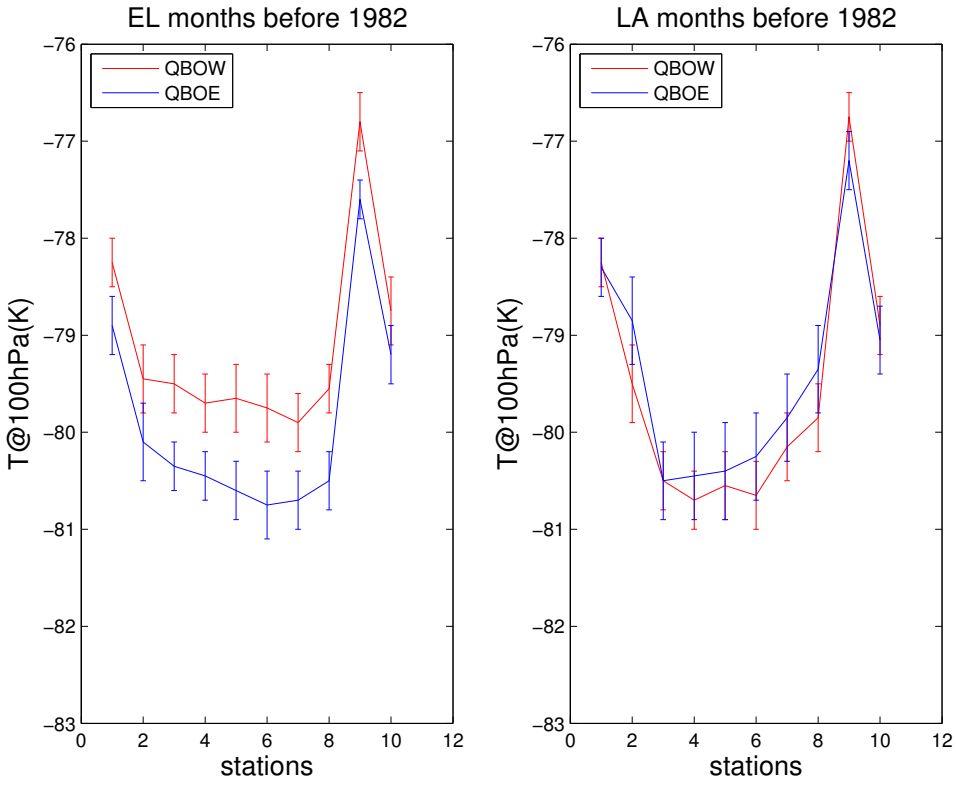

Figure 16: Same as figure 3 but for the 100hPa monthly mean temperature before 1982.

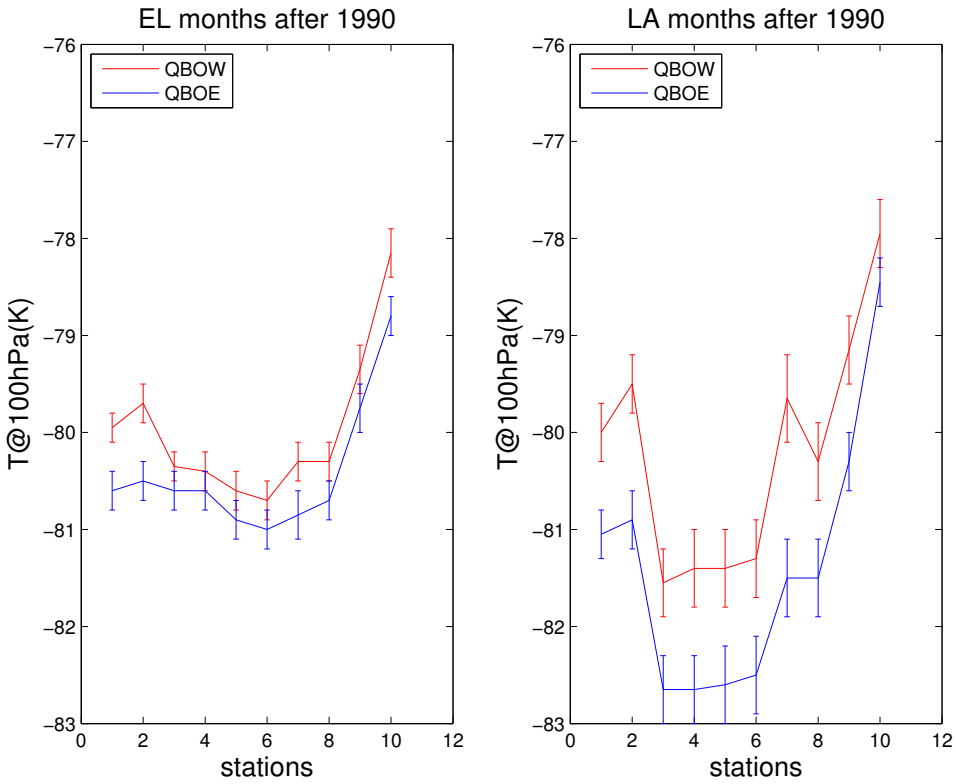

Figure 17: Same as figure 3 but for the 100hPa monthly mean temperature after 1990.

To conclude, with the mean and SEMs calculated for the QBO amplitude and period, CPT and 100hPa temperature differences, the results agree with the result in the tables, and the statistical test results agree with the Student's T-test results.

2.3.7 Summary and Discussion

In this section, motivated by the changing ENSO-QBO correlation relationship in Garfinkel and Hartmann (2007), I first calculate the correlation coefficient between the ERSST Niño3.4 index and the FUB wind data. Our calculation agrees with the Garfinkel and Hartmann (2007) results, which prompts us to apply the Taguchi (2010) method to the IGRA station stratosphere wind before 1982 and after 1990, to check whether the ENSO modulation on the QBO amplitude and period changes between the two time periods.

First, about the ENSO modulation on the QBO period, the QBO periods are both longer during La Niña than El Niño before 1982 and after 1990, which agrees with the Taguchi (2010) and Yuan et al. (2014) results.

The QBO amplitude relationships between El Niño and La Niña, however, are different between the two time intervals. For the later time interval, we still get larger QBO amplitudes during times of La Niña, as in Taguchi (2014) and Yuan et al. (2014). But for the time before 1982, the QBO amplitudes are comparable between the two ENSO phases.

I then check the CPT and 100 hPa temperature difference between QBO E/W during two ENSO phases to check the reliability of the QBO amplitude results. The temperature difference results support the QBO amplitude results with larger dT after 1990 while smaller dT during La Niña. This might imply that the QBO has larger amplitude during El Niño than La Niña.

In the final part, based on Geller et al. (2015) and Zhou et al. (2015), the period of the QBO is determined by the magnitude of the wave momentum flux driving the QBO, while the amplitude of the QBO is determined by the magnitude of the wave phase speeds that comprise the gravity wave spectrum forcing the QBO. We offer some hypothesis to explain the Taguchi (2010) results, that is, the more widespread convection during El Niño results in a greater zonally averaged gravity wave momentum flux, which in turn, gives a shorter QBO period. The greater QBO amplitude during La Niña over the entire period analyzed is likely due to the more intense convection giving rise to a greater spread in the excited gravity wave phase speeds. The fact that the ENSO influence on QBO amplitude is less stable than the ENSO influence on QBO period is likely due to different variations in the ENSO modulation of convection intensity during the early and later portions of this 60 year period. The results from the OLR data support these hypotheses.

Chapter 3: The QBO Influence on Tropical Convection : Cloud-Resolving Modeling Study

3.1 Introduction

Convective parameterizations in GCMs have difficulties in realistically representing convective processes (Derbyshire et al., 2004). Besides, it has been shown that the GCM results depend on the choice of the convective parameterization or the key parameters. All the proposed mechanisms of how the QBO modify deep convections are large-scale processes occuring in the convective time and space scale. Thus, a model that can realistically represent these convective processes is critical in this study. So in this chapter we investigate the responses of deep convection to the QBO with cloud resolving models. A cloud resolving model can explicitly resolve convective scale processes within a limited domain with relative high resolution (several km to several hundreds of meters). It has been proven to be a powerful tool for studying convection and its responses to environmental perturbations (Khairoutdinov and Randall 2003, Bretherton 2007, Wofsy and Kuang 2012).

Our strategy is first to try to find the troposphere response to the QBO in the CRM. And then, if there is robust QBO modulation, try to offer a possible mechanism. I will introduce the model setting and model results of the three-dimensional isolated convection cases section 3.2, and two-dimensional idealized Walker circulation model results will be discussed in section 3.3, the conclusion and discussion for the model results are in section 3.4.

3.2 Responses of the Convection to the QBO in an Isolated Deep Convection Case

3.2.1 Model Settings

Compared to the other modulation factors of tropical convection, like SST, and the large scale convergence or divergence of the water vapor, the QBO influence is expected to be quite modest. So while designing our experiments, we want to eliminate possible influences from other factors with strong effects on convection. So for the two cases in each group, we will keep all the other factors the same, the only difference between the cases will be QBO related.

I use a domain size of 128 km*128 km*32 km for the 3D cases. The horizontal grid spacing is 2 km. Periodic lateral boundary conditions are employed in both the X- and Y-directions. There are 76 vertical levels, with a variable vertical grid spacing of 75-500m up to about 20km and larger grid spacing above, the grid spacing between 11km and 20km are refined to 250m to better resolve the convective and radiative processes near the tropopause, following Blossey et al. (2010), the vertical grid spacing is shown in figure 18. The top 30% of the domain is set as a sponge layer to limit the gravity wave reflection from the model top (Khairoutdinov and Randall, 2003). The radiative scheme is the CAM 3.0 radiation parameterization. The Coriolis parameter is set to 0, since our study is focused on the tropical convection. SST is set as 301K for all the cases.

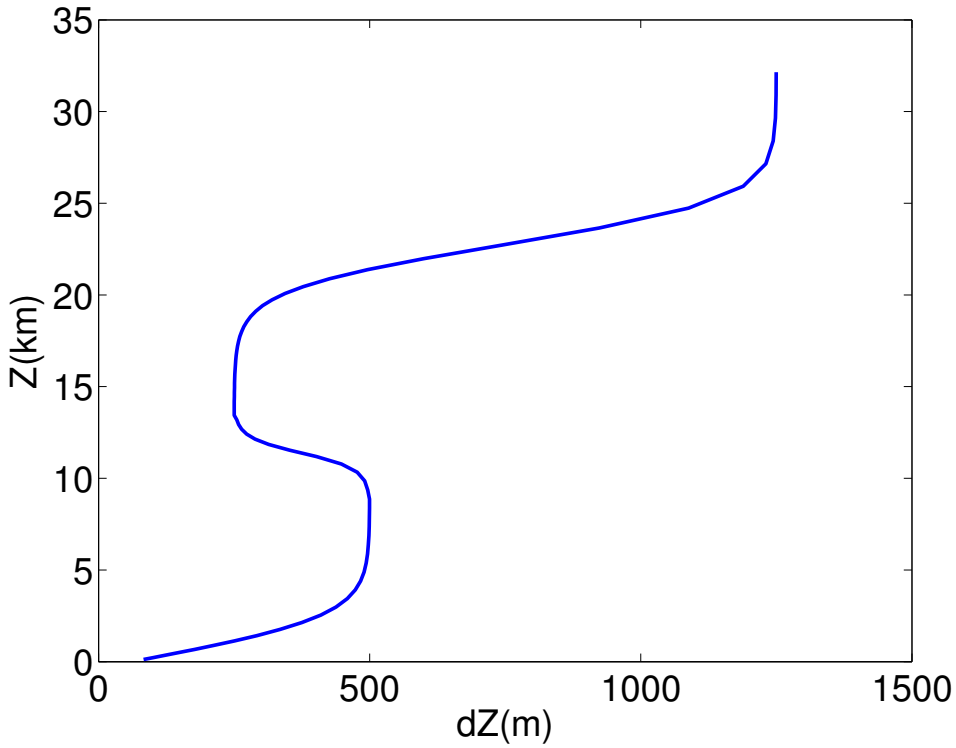

Figure 18: The vertical grid spacing for the 3D cases, the abscissa is the vertical grid spacing, varying from 75m at the bottom to 500m above 3km, then refined to 250m between 11km and 20km.

To start, I run the model to radiative-convective equilibrium (RCE) over a constant 301K SST, without any temperature or wind forcing, this case is used as the control (CTRL) case. The T_{rce} profile is shown as the black profiles in figure 19(a, b), the black horizontal lines in figure 19 indicate the tropopause height in the CTRL case, defined by the height with the coldest temperature. Comparing the T_{rce} profile with figure 1, we can see that this RCE case reproduces the tropical temperature profile very nicely, although the tropopause height from the CTRL case (slightly below 16 km) is slightly lower than in figure 1 (about 17km).

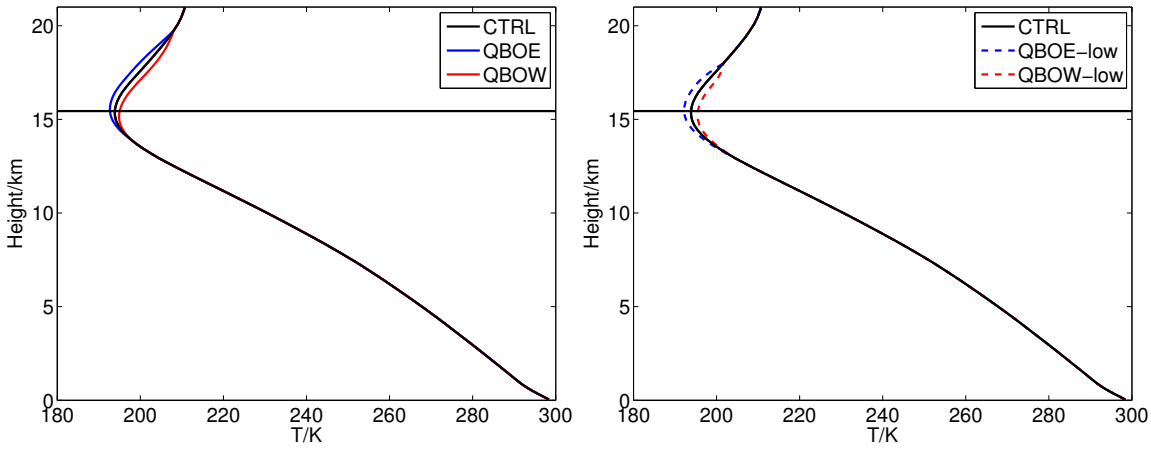

Figure 19: Absolute temperature profiles used as the reference temperature for the QBOE cases (blue line) and QBOW cases (red line). The profiles in (a) are for the case set 1, and the profiles in (b) are for case sets 2 and 3. The black profiles are the T_{rce} profile from the CTRL case. Black horizontal lines are the tropopause height from the CTRL case, defined by the height with the coldest temperature. The unit for temperature is K.

We then run three sets of cases to test the model responses to the QBO temperature and zonal wind signal, with the same grid setting as the CTRL case. Each set includes two cases, and the detailed information is listed in the following table.

1	dT @ QBOE	dT @ QBOW
2	dT_{low} @ QBOE	dT_{low} @ QBOW
3	dT_{low} w. U @ QBOE	dT_{low} w. U @ QBOW

Case set 1 is used to test the tropical convection response to the QBO temperature signal. For these two cases, we add (subtract) the temperature anomaly dT profile (solid line in figure 20a) from T_{rce} profile, to form the reference temperature profiles for QBOE and QBOW cases (blue and red lines in figure 19a). This creates a higher and colder tropopause during QBO easterly phase than QBO westerly phase. The temperature anomaly is located between 150 hPa and 55 hPa. The horizontal lines in figure 19 and 20a are the tropopause from the CTRL case, defined by the height with the coldest temperature, which is located at about 115 hPa. We choose these levels for the dT forcing to make sure the QBO temperature signal can penetrate into the upper troposphere, in order to mimic the QBO temperature signal downward penetration in figure 5a. The three profiles in figure 19a are identical below and above the dT levels.

Case set 2 is similar to case set 1, except the dT profile is moved downward to the height between 175 hPa and 70 hPa (see the dashed line in figure 20a), and the QBOE (QBOW) temperature profiles created with this lower

dT are plotted in figure 19b. The QBO temperature signal penetrates further into the troposphere compared to case set 1. This set of cases are use to test the sensitivity of the model outputs to the height of the dT forcing, or in other words, to the extend of the QBO downward penetration.

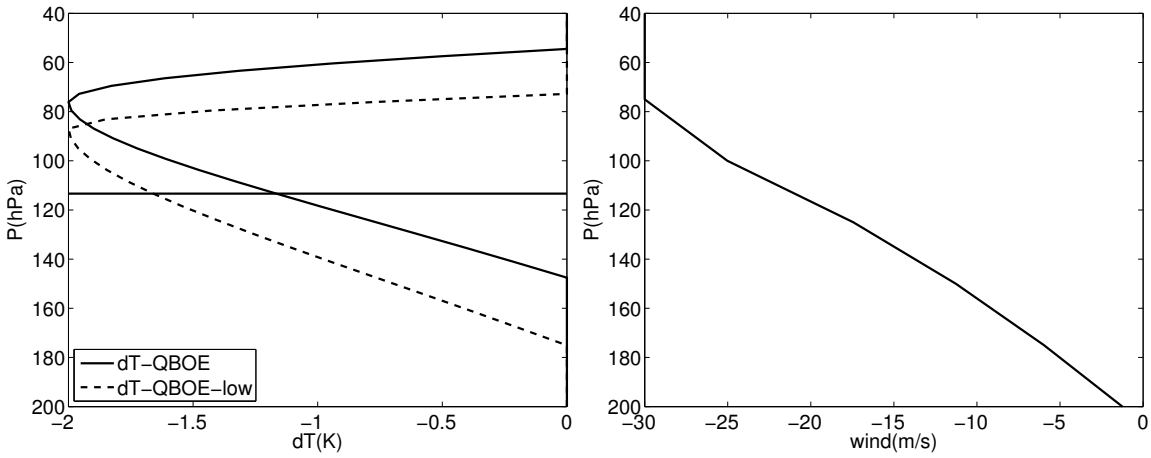

(a) (b)

Figure 20: (a) Black horizontal line is the cold-point tropopause height from the RCE case, defined by the height with the coldest temperature; The curved line is the temperature anomaly profile for QBO easterly phase, the maximum temperature anomaly is set as 2K; (b) Wind forcing for the QBO easterly phase, the unit is m/s. The wind forcing for QBO westerly phase has the same value but opposite sign.

In case set 3, we put both the lower dT forcing and the QBO zonal wind into the model. The profile of the negative zonal winds during QBOE is shown in figure 20b, the maximum zonal wind speed is set as 30m/s. For QBOW case the dT and zonal wind profiles have the same values with the QBOE case but with the opposite sign. We then compare the results of case sets 2 and 3, to check the effect of QBO zonal wind signal on the troposphere convection activities.

Note that the maximum value of dT is set as 2K, which makes the maximum CPT temperature difference between QBOE and QBOW cases to be 4K. This difference is larger than the observed QBO signal, in figure 5a the maximum CPT temperature difference is about 2-3K during the time of La Niña, the CPT temperature differences for the time of El Niño and all months mean are even smaller. And for the zonal wind anomaly shown in figure 20b, in the real atmosphere, the QBO wind signal doesn't penetrate too much below the tropopause, in the time-height contour figure of the FUB wind data, the wind speed is closed to zero near the 100 hPa pressure level (see `http://www.geo.fu-berlin.de/met/ag/strat/produkte/qbo/qbo_wind_pdf.pdf`). The height of our zonal wind forcing is set to be as low as around 200 hPa. However, since the QBO influence on the tropical convection is quite modest and we are doing idealized experiments here, we intentionally set the temperature forcing with a larger magnitude in order to get a robust model response.

Temperature is nudged to the reference profiles between 14 km and

20km with a time scale of 6 hours. We don't nudge the temperature below 14 km to prevent any artificial temperature adjustment caused by the nudging process, to make sure that any response below 14 km is only caused by the forcing we put into the near tropopause region. For case set 3, the zonal wind is put into the model as the large scale forcing.

A constant solar insolation of 408 W/m^2 is imposed at the top of the atmosphere, so there is no diurnal or seasonal cycle in the simulations. No prescribed radiation is applied in the simulation either. The time step is set as 15 seconds. Each case is run for 200 days. The last 150 days from the model output, which are statistically steady, are used in the following analysis.

3.2.2 The Effect of the Temperature Anomaly

This section shows the results from case set 1 and 2.

With the QBO temperature anomalies added between 150 hPa and 55 hPa in case set 1, that is between 14 km to 19km if converted to altitude, the mean precipitation of the last 150 days are almost identical for the QBO easterly and westerly cases. There are only some differences between the updraft cloud mass flux (MCUP, shown in figure 21a) and cloud fraction (CLD, shown in figure 21b) at the upper part of the troposphere. There is almost no difference of the updraft cloud mass flux or cloud fraction below 10km.

With the colder tropopause during the QBO easterly phase, the updraft cloud mass flux is larger between the height of 10km to about 13 km, and the cirrus cloud fraction is increased compared with the QBO westerly phase. These two increases from the QBO westerly phase to QBO easterly phase agree with the discussion about the QBO modulation on the static stability near the tropopause, the colder and higher QBO easterly tropopause encourages the local upward motion and formation of local cirrus clouds. However, there is almost no response of the deep convection cloud and precipitation. In another word, the near tropopause temperature anomaly can't be transferred downward to affect the lower convection.

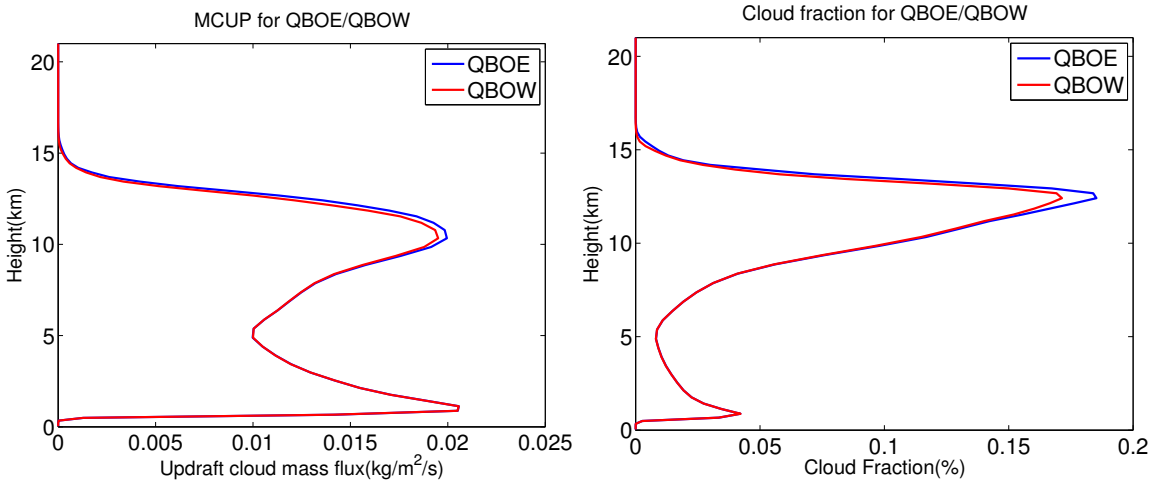

(a) (b)

Figure 21: (a) updraft cloud mass flux for QBOE/W, the unit is $kg/m^2/s$; (b) Cloud fraction for QBOE/W. Blue line is for QBO easterly phase, red line is for QBO westerly phase.

The results of case set 1 don't give robust response of the tropical convection, one possible reason is that the distance between the QBO signal

from above and the convection from below is too large to reach one another. In this case, the tropopause height is around 15.5km, while the height of maximum cloud fraction is about 13km. It's difficult for the convection below to feel the influence from above. I then run the two cases in case set 2, move the temperature anomalies downward for about 1km to the height between 175 hPa and 70 hPa (13km to 18 km), and check the sensitivity the results to this change of forcing height, the results from these two cases are shown in figure 22.

In figure 22, the differences of the updraft cloud mass flux and cloud fraction between two cases both increase compared with figure 21, however, there is still no robust response in the lower convection and precipitation. Here we have already put the bottom of the dT forcing at 13km, which is around the same height of the maximum cloud fraction, and 2.5km below the tropopause height. With this extreme situation of the QBO temperature signal penetration, the QBO temperature still can't influence convection in the lower part of the troposphere.

With lower temperature forcing, the high cloud fraction and updraft cloud mass flux response is stronger, although there is still no robust response in the lower troposphere and the precipitation. If we compare the results of the two cases with different height of the temperature forcing, the lower the temperature forcing is, the stronger the model response is, the penetration extent of the QBO signal is important for the QBO influence on the troposphere. These two sets of cases at least confirm one thing that is discussed in

the previous research papers, that is, the tropical deep convection should be strong enough to contact with the upper QBO, that might explain why the QBO influence is always in the region of the strongest convection (Collimore et al., 2003). However if we only consider the QBO influence on the static stability in this isolated point of view, the lower tropical deep convection can't feel the QBO modulation effect. There should be other mechanism doing the job, if any effect exists.

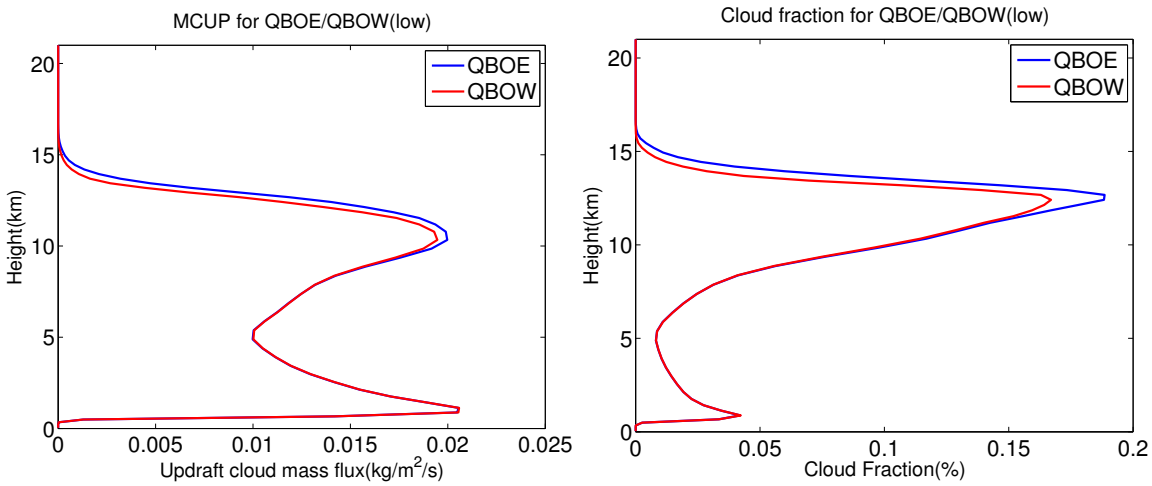

(a) (b)

Figure 22: Same as figure 21, but with a lower temperature forcing.

3.2.3 The Effect of the Wind Anomaly

To test to the effect of the zonal wind shear, I run a third set of cases, adding the easterly (westerly) wind shear to the previous set of cases with negative (positive) temperature anomaly at the lower levels, run the two cases for 200 days, and then compare the model results with or without the wind shear

during QBO easterly and westerly phases, respectively. I have done the comparison for both QBO phases, but I'd like to only show the results from the QBO westerly phase here in figure 23, the results for both QBO phases are quite similar to each other. Figure 23a shows that, compared to the case without wind shear, the mean updraft cloud mass flux is almost unchanged at all levels.

The zonal wind shear, however, can increase the high cloud fraction near the tropopause, there is no cloud fraction difference from the lower part of the troposphere. The mean precipitations are still the same for the cases with or without wind shear added. It seems that the only effect of the wind shear is to blow at the high cirrus clouds and enlarge the covering area of the high cloud. There is no dynamic effect transferred downward to the lower troposphere.

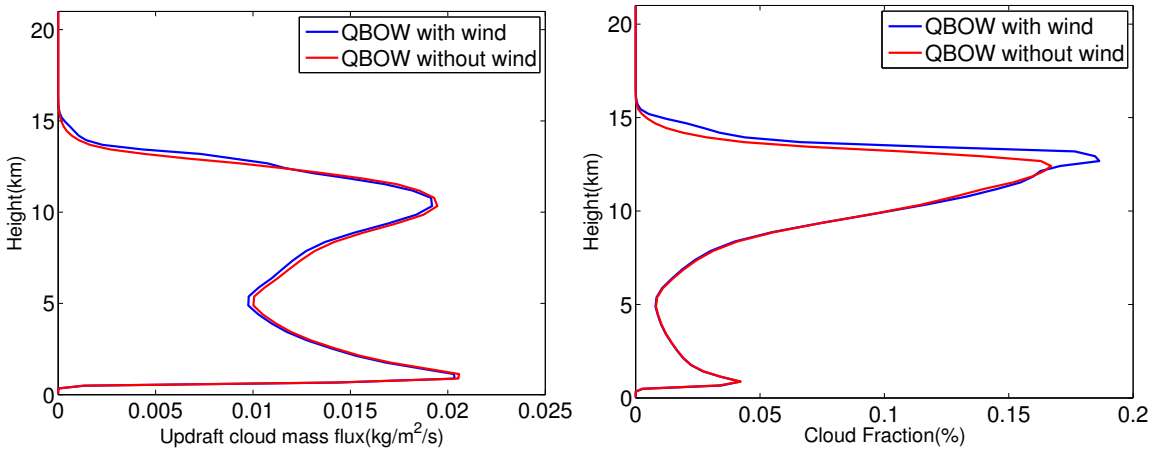

Figure 23: (a) Upward cloud mass flux for QBO westerly phase with the lower temperature forcing, with or without wind shear, the unit is $kg/m^2/s$; (b) Cloud fraction for QBO westerly phase with the lower temperature forcing, with or without wind shear. Blue line is for the case with wind shear, red line is for the case without wind shear.

3.2.4 Summary and Discussion

The tropopause height in the CTRL case is about 115 hPa, the lower temperature forcing case is an extreme situation of the QBO temperature downward penetration. Even in this set of cases, almost no precipitation difference can be found between the QBO E/W cases, the only differences are still the high cloud fraction and the related updraft cloud mass flux near the height where the temperature forcing is added. If only considering the modification to the stability near the tropopause, the QBO signal of the tropopause temperature and tropopause height will only cause the response of the cirrus cloud fraction. The QBO signal can't be transferred downward with this three-dimensional isolated convection case design. There is no positive feedback process working as an amplifier to transfer the QBO temperature signal to lower level if we only look into the problem from a single point. The large scale circulation might be critical between the QBO and the troposphere convection, as mentioned in Liess and Geller (2012).

Adding wind shear to the stratosphere region can only increase the cloud fraction of cirrus clouds in our model framework. The QBO temperature and wind shear anomaly can both cause effects on the high cirrus clouds, the radiative effect might give a response in the tropical convection, but this can't be done with this 3D framework.

If we review the design of these three sets of cases, there is a fundamental weakness that it artificially separates local convection and large-scale

motions, which are strongly coupled in the tropics due to the weakness of rotation constraints (Emanuel et al. 1994). Viewing the large-scale motion simply as results of the convection and neglecting their interactions may result in far too weak convective responses to the QBO perturbations. Consider an isolated convective column that is either in radiative-convective equilibrium (RCE) or with prescribed large-scale vertical motion, its precipitation is directly linked with vertically integrated cooling of the column. With a QBO-associated perturbation applied on the isolated column, for example, an OLR anomaly of 5 W/m^2 (Collimore et al. 2003) or a cooling anomaly of 0.5 K/day from 100 hPa to the top of the atmosphere (Reid and Gage 1985, these assumed numbers are larger than observational estimations to be on the safe side), the corresponding precipitation anomaly is only 0.15 mm/day, one order of magnitude smaller than observations (Liess and Geller 2012). Only considering this kind of localized influence from the tropopause temperature on the troposphere convection through the modulation of the static stability is not enough to explain the suggested QBO influence on troposphere convection. Other factors like the large-scale Walker and Hadley circulations might be important in the communication processes between the QBO and the lower troposphere.

If we compare our isolated convection case results with the Nie and Sobel (2015) results using the WTG approximation, they use the WTG method to represent the large scale circulation in their frame. In their method, however, the forced vertical velocity is calculated from the temperature anomaly to represent the real large scale circulation in their model. In the follow-

ing part of the dissertation, I will use the SAM model in a two-dimensional domain, first using a very simple SST distribution to set up a Walker-like circulation, and then shows the response of the 2D model to a QBO-like temperature (heating) forcing. We will also compare the results of our 3D cases, 2D cases and the WTG cases of Nie and Sobel (2015) in the following section.

3.3 Responses of Convection to the QBO in an Idealized Walker Circulation

In this section, we explore the idea that the QBO influences tropical deep convection mainly through modifying the tropical large-scale circulation. Given the fact that few studies have been done in this direction, we shall start from a simple and idealized case that is transparent to understand: the Walker circulation.

Neglecting air-sea coupling, the Walker circulation can be thought as driven by SST gradients. The rising branch is usually located in the high SST region, associated with vigorous and deep convection. The deep convection and the large-scale Walker circulation are strongly coupled. In the previous section, the deep convection is isolated from the large-scale environment. The simulation results show the responses of isolated convection to the QBO are small. However, when coupled with the large-scale circulation, the responses of convection to the QBO may be amplified by potential feedbacks, as will

be shown in the subsequent sections.

3.3.1 Model Settings for the Idealized Walker Circulation Experiments

There are 64 vertical levels, the vertical grid spacing increases from 75m near the surface to 500m above 3km. The model has a rigid lid at above 28 km, and a wave-absorbing layer is also used at the upper 30% of the domain to damp gravity waves, like in the 3D cases. Horizontal resolution is 2 km, I run the model with 2048, 4096 and 8192 grid points for the following cases. A Smagorinsky-type scheme is used to represent the effect of subgrid scale turbulence. The surface fluxes of sensible heat, latent heat, and momentum are computed using Monin-Obukhov similarity theory. Surface zonal wind is set to be 5 m/s to make sure the surface sensible heat flux is proportional to the SST (Kuang 2012). Note that the 5m/s surface zonal wind is only used for the surface fluxes calculation, it doesn't involve with the model zonal wind output. Periodic lateral boundary conditions are employed. We run each case for 300 days, and use the last 200 days in our following analysis.

An idealized radiative cooling rate of 1.3 K/day is imposed in the troposphere with Newtonian damping in the stratosphere (Pauluis and Garner 2006, Wofsy and Kuang 2012), rather than using an explicit radiative transfer calculation. The radiative cooling rate is defined in this way:

$$\frac{\partial T}{\partial t} = \begin{cases} -1.3K/day & \text{for} \quad \text{T>207.5K} \\ (200K - T)/5day & \text{elsewhere} \end{cases} \tag{3.6}$$

We choose this simplified radiative cooling scheme because when a very similar model was used to do comprehensive simulations of the Walker cell (Bretherton 2007, Wofsy and Kuang 2012), the results had highly variable, nonlinear behavior with the full radiative transfer calculation. For the problem we are trying to look into here, the QBO influence on the tropical convection can be quite modest, so we'd like to start with the most simple model setup, trying to eliminate any unnecessary uncertainty. Except the cases I am going to show in the following sections, I did try a set of cases with realistic radiative scheme, in those cases the model needed more than 2000 days to get a relatively steady case, and the results are still too noisy to distinguish between the model response of the QBO-like forcing and the potential model noise. The results with the simplified radiative scheme, however, are much cleaner, so in this dissertation I will just show the results of the simplified case.

A sinusoidal SST distribution is applied to the bottom of the domain with the form:

$$SST(x) = SST_0 - dSST * cos(2\pi x/A) \tag{3.7}$$

A is the domain width. SST_0 is set to 300K, and I choose dSST as 2K/4K/6K in the following cases. Maximum SST is in the midpoint of the domain. This

sinusoidal SST distribution will drive a Walker Cell like circulation. Figure 24 shows the (a) sinusoidal SST distribution with a 4096 km domain, SST_0 is 300K, dSST is set as 6K; (b) the streamfunction of the large scale Walker cell driven by this SST distribution, the unit of the stream function being kg/s; and (c) the time mean precipitation distribution after the case reaches RCE, with no temperature forcing added, we call this the 'CTRL' case. The streamfunction figure shows that this setup produces an overturning, Walker cell-like circulation, with ascent over the highest SST and descent over the colder SST on both sides. The precipitation mainly occurs in the 1000km area in the center of the domain, where the SST is the highest.

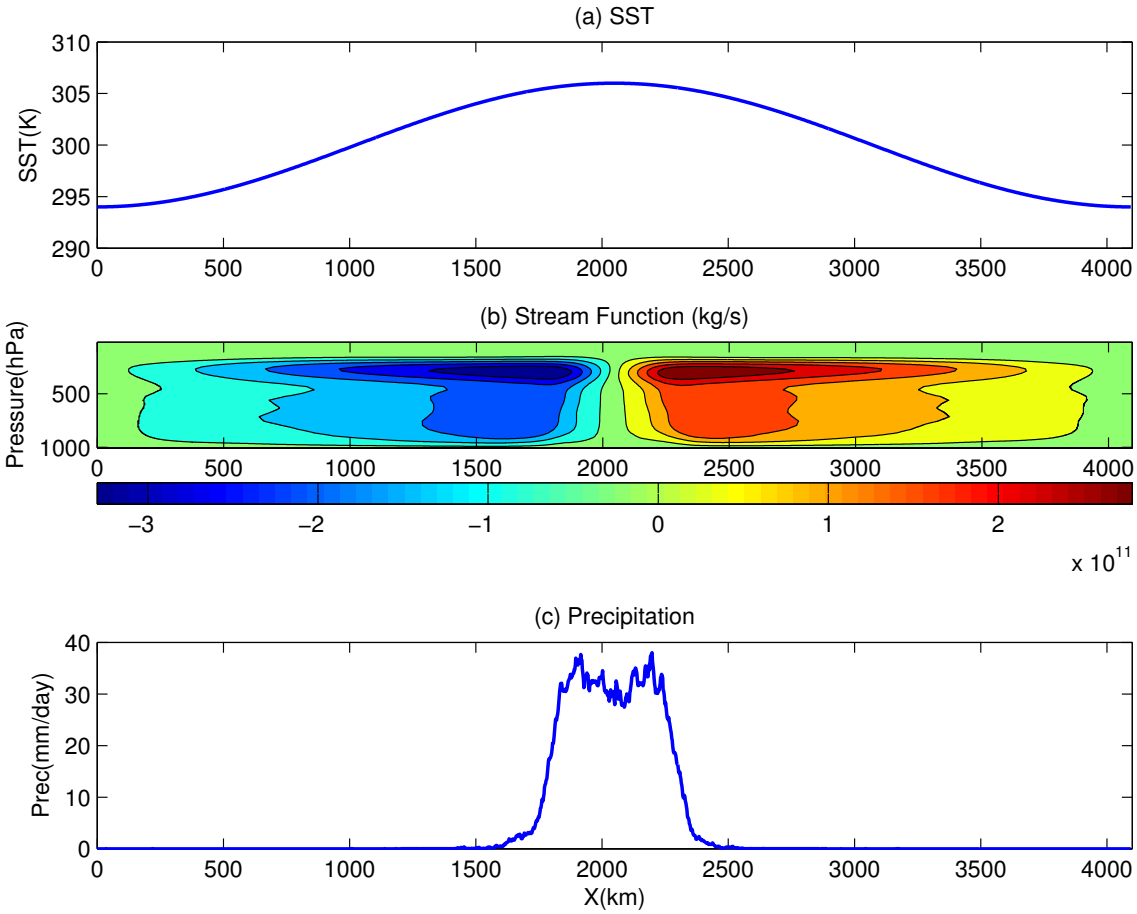

Figure 24: (a) Sinusoidal SST distribution with a 4096 km domain, SST_0 is equal to 300K, and dSST is equal to 6K; (b) the streamfunction of the large scale Walker cell driven by this SST distribution, the unit of the stream function is kg/s; and (c) the time mean precipitation distribution, the unit for precipitation is mm/day. The precipitation and streamfunction are calculated after the CTRL case reaches RCE. There is no temperature forcing added in this case.

3.3.2 the Walker Circulation and Convection Responses to the Temperature Forcing near the Tropopause

Based on the two-dimensional control case, as the mean vertical velocity of an anelastic model with cyclic boundary conditions is zero, I add an additional heating (cooling) rate profile dT/dt near the tropopause levels, to mimic the downward (upward) secondary circulation during QBOW (QBOE) case and to represent the warmer (colder) tropopause during the QBO westerly (easterly) phase (see figure 25). Other model settings are the same as in the control case. These temperature forcings are the only forcing added to the model. I will simply use QBOW (QBOE) case to refer to the experiments with warm (cold) anomalies in the following part of the dissertation.

The way we put the temperature forcing into the 2D model is different from the 3D cases. Instead of nudging the domain mean temperature to some reference temperature profile, we put in a profile of heating rate anomaly instead. A reason why we use a heating rate anomaly is that later in this chapter we will test the sensitivity of the convection response to the forcing height. This is easier by adding a fixed heating rate anomaly profile at different levels. Also, I want to clarify is that this method of adding the temperature forcing, although it will produce a higher and colder tropopause during the QBO easterly phase, the mechanism is not exactly the same as occurs during the QBO in the real atmosphere. In the real atmosphere, the temperature differences between the QBOE and QBOW phases are created by the secondary meridional circulation that must accompany the zonal wind

shears, and here, in our 2D model, since the domain mean vertical velocity is always zero, there is no accompanying domain mean vertical velocity that leads to the QBOE and QBOW temperature differences..

These heating (cooling) forcing profiles are added symmetrically to all the grid points along the horizontal direction since the QBO is symmetric along the Equator. As expected, we get a higher and colder tropopause for the QBOE case (figure 26). The maximum value of the dT/dt is set as 0.4K/day, in order to get a reasonable tropopause temperature difference between the QBOE and QBOW cases. Take figure 26a as an example, when the heating (cooling) rate forcing is centered at 150 hPa, the temperature difference near the tropopause is about 3K between the QBOE and QBOW cases, which is slightly larger but still comparable to the temperature difference profile between the two QBO phases shown in figure 5.

Figure 25 shows three different levels where we add the heating forcing. The blue dashed line represents the tropopause height from the CTRL case. All three heating forcing profiles have some part (or the whole profile for the blue one centered in 200 hPa) below the tropopause height, to represent the downward penetration of the QBO temperature signal. The model sensitivity to the height of heating forcing is discussed in a following section of this chapter. Here I'd like to start with the model results with the heating forcing centered at 150 hPa (red line in figure 25).

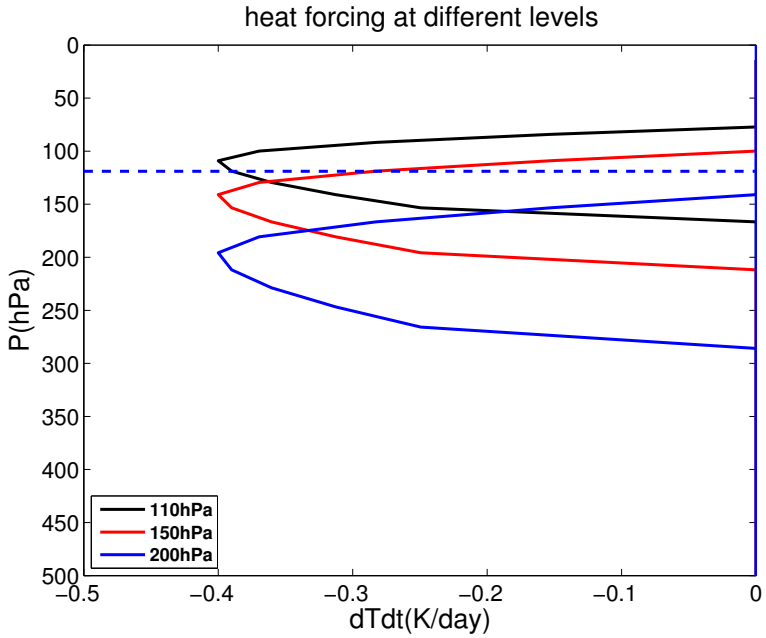

Figure 25: Heating rate dT/dt added in the model as the heating forcing at different levels, the unit is K/day. Solid black/red/blue lines are the heating rate forcing dT/dt profiles with the maxima at 110/150/200 hPa. The horizontal blue dash line is the tropopause from the control case with 4096 km domain size and dSST=6K.

Figure 26a shows the domain mean temperature difference between the QBOE and QBOW cases (black), and the normalized heating forcing for the QBOE case (red). The heating forcing is the same one as the red profile in figure 25. The heating forcing profile is normalized according to the maximum value of the temperature difference. Figure 26b are the domain mean temperature profiles for QBOE (blue) and QBOW (red) cases. Figure 26a and 26b both indicate that QBOE case has a higher and colder tropopause than the QBOW case, and the magnitude of the temperature difference is about 3K, which is a reasonable value compared with the observational sounding results.

The temperature responses in figure 26a can penetrate down into the lower part of the troposphere, this is quite different from the three-dimensional results, in which the temperature responses are confined near the tropopause region. Thus, it is likely that the two-dimensional model can better enable the interactions between the higher and lower part of the model.

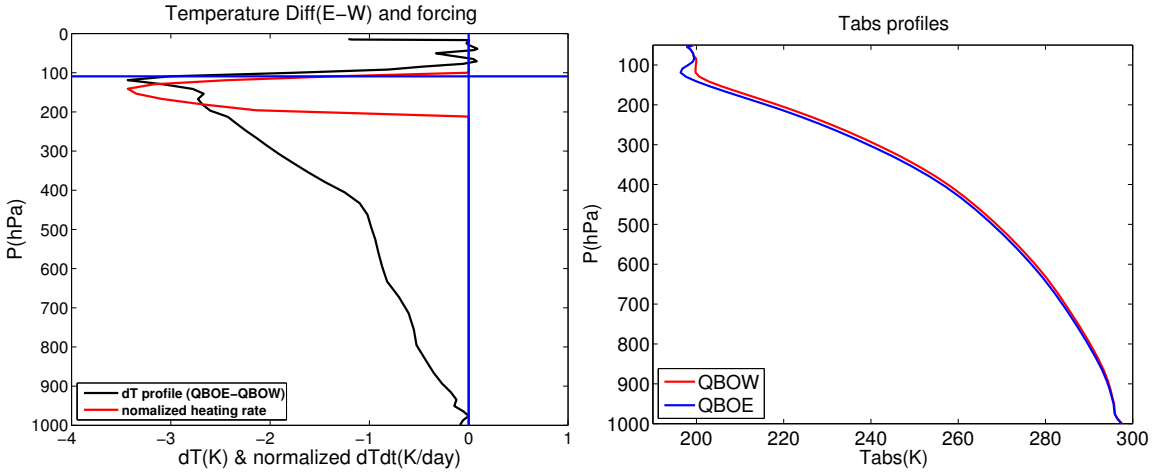

(a) (b)

Figure 26: (a) Domain mean temperature difference between the QBOE and QBOW cases (black), and the normalized heating forcing for the QBOE case (red). The heating forcing profile is normalized according to the desired maximum temperature difference; (b) Domain mean temperature profiles for QBOE (blue) and QBOW (red) phases.

We then compare the mean precipitation distribution along the horizontal direction for the QBOE/QBOW/CTRL cases, shown in figure 27a. The greatest precipitation differences occur in the center of the domain, where the SST is the largest and the precipitation itself is the strongest. In the center of the domain, the precipitation is strongest with positive heating forcing added (QBOW case), while the case with negative heating forcing (QBOE case) has the smallest precipitation. The precipitation band is broader in the QBOE case than QBOW case, and the QBOE case has larger precipitation than the QBOW case on the two sides outside of the strongest precipitation area. Figure 27b shows the cloud fraction distribution for the three cases, which are quite similar to the precipitation distribution.

Note that for the three precipitation distributions in figure 27a, if we calculate the domain average precipitation, the QBOE case with negative heating forcing has the largest domain average precipitation, following by the control case with no heating forcing, and then the QBOW case with positive heating forcing. The domain average precipitations are very close to each other for the three cases, however. These results agree with the three-dimensional cases results, that is, the negative heating forcing will increase the domain mean precipitation, albeit very slightly.

In other words, although the QBO easterly phase-like heating forcing slightly increases the domain mean precipitation, the more robust feature of the two-dimensional model output is that, the heating forcing added near the tropopause height can clearly redistribute the precipitation along the hori-

zontal direction, and the QBO westerly-like heating forcing will increase the precipitation in the location with the highest SST and largest precipitation.

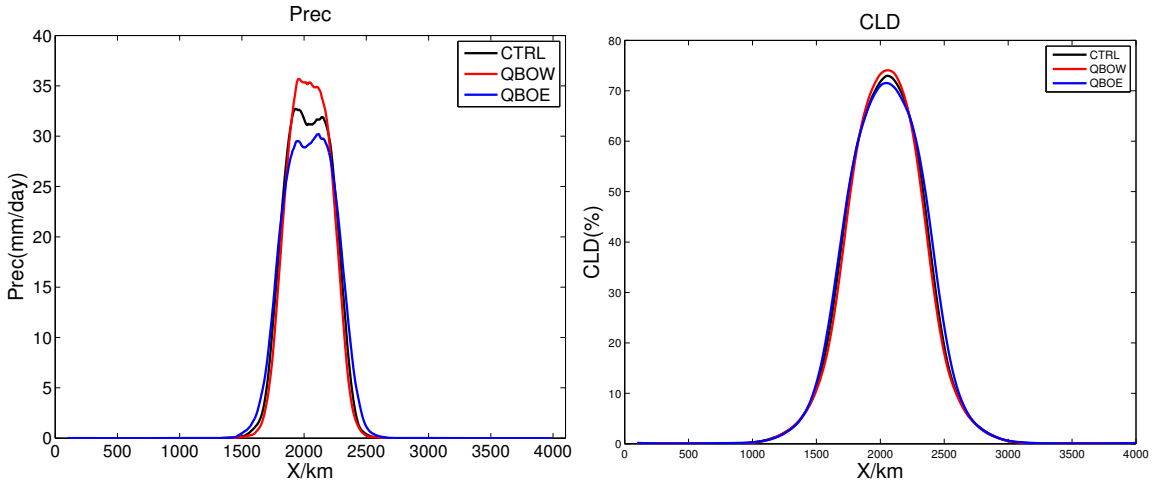

(a) (b)

Figure 27: Distribution of (a) precipitation and (b) cloud fraction in the 4096 km domain, with heating forcing centered at 150 hPa, and dSST=6K. Blue/red/black line shows the result with cold/warm/no heating forcing, respectively. The unit of precipitation is mm/day, and cloud fraction unit is %.

Compared to the three-dimensional cases in which there are no precipitation responses to the QBO signal, the two-dimensional cases show clear QBO modulation on the precipitation. In order to understand the physical process in the precipitation redistribution, I look into the streamfunction maps and the vertical velocity profiles of the QBOE and QBOW case outputs, shown in figure 28 and 29.

In figure 28, (a) is the streamfunction of the QBOE case, and (b) is the difference of the streamfunctions between the QBOE and QBOW cases

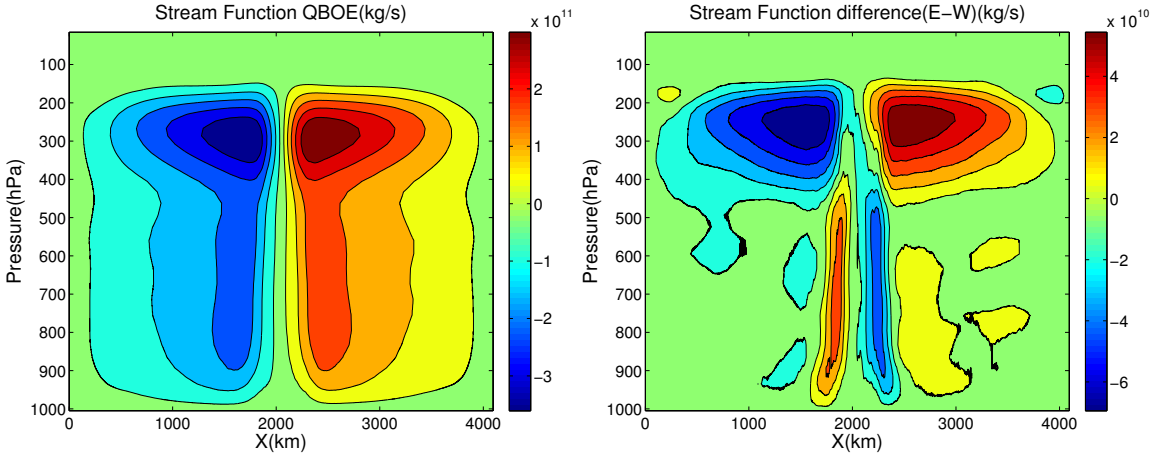

(a) (b)

Figure 28: (a) Time mean streamfunction for the QBOE case, and (b) the streamfunction difference between the QBOE and QBOW cases. Both within the 4096 km domain, and both for the cases with dSST=6K, and the heating forcing centered at 150 hPa. The units are kg/s.

(QBOE-QBOW). With cold forcing added near the tropopause, the outflow near 250 hPa increases about 20% in the QBOE case compared to the QBOW case. The outflow changes are also found from changes of the mean zonal wind (not shown here). However, in the QBOE case, the streamfunction decreases from the surface to about 500 hPa at the central region of the domain, indicating that the upward motion in the center slows down in the lower and middle troposphere.

This slowing down of the upward motion in the QBOE case is also seen in figure 29. Here, I choose a region of 200km width in the center of the domain, and plot the mean vertical velocity w profiles of the QBOE and QBOW cases. Figure 29b is the normalized w profiles of those plotted in figure 29a. From the prospective of the Moist Static Energy (MSE) budget

(Sobel 2007, see more detailed analyses in the following subsequence section). The precipitation is closely related to the 'top-heaviness' of w. As seen from figure 29b, during the QBOE phases, the w profile is more 'top-heavy'. To be more quantitative, we define a top-heaviness (TH) index as the difference between the normalized w in the upper troposphere (the w maximum level, about 300 hPa) and lower troposphere (700 hPa):

$$TH = w_0@300hPa/w_0@700hPa \tag{3.8}$$

TH is greater for the QBOE case (6.1) then for the QBOW case (4.7), consistent with what we see from figure 29.

Here, I'd like to discuss a little bit more about the mean rising branch vertical velocity response to the temperature forcing. The upper limit of the heating forcing profile is at about 100 hPa, the maximum value of the profile is located at 150 hPa level, and the tropopause pressure is 110 hPa (see figure 25). Figure 29c shows the mean vertical velocity difference between QBOW and QBOE (QBOW-QBOE) with this temperature forcing added to the model. The w difference between the QBOW and QBOE cases is negative from 120 hPa to 300 hPa, this negative w difference agrees with the arguments in Gray (1992a, b), which is, warmer temperature anomaly near tropopause during the QBO westerly phase inhibits the convection development, this mechanism is also suggested by previous papers (Collimore et al. 2003, Liess and Geller 2012). However, the w difference between QBOW and QBOE becomes positive below the 300 hPa level, and we expect that

the positive precipitation response (QBOW-QBOE) in the center (figure 27) might be strongly related to the vertical velocity anomaly in these lower levels.

Until now, the idealized Walker circulation results has shown that a negative heating forcing lifts the tropopause height, increases the outflow strength of the Walker cell near the tropopause, and moves the peak level of the w_0 profile upward to be more 'top-heavy'. In the following section, we will try to connect the top-heaviness of the w_0 profile and the precipitation, through a simple MSE budget analysis. This analysis will address the question of how the modest shift of w_0 profile can leads to the sizable precipitation anomalies.

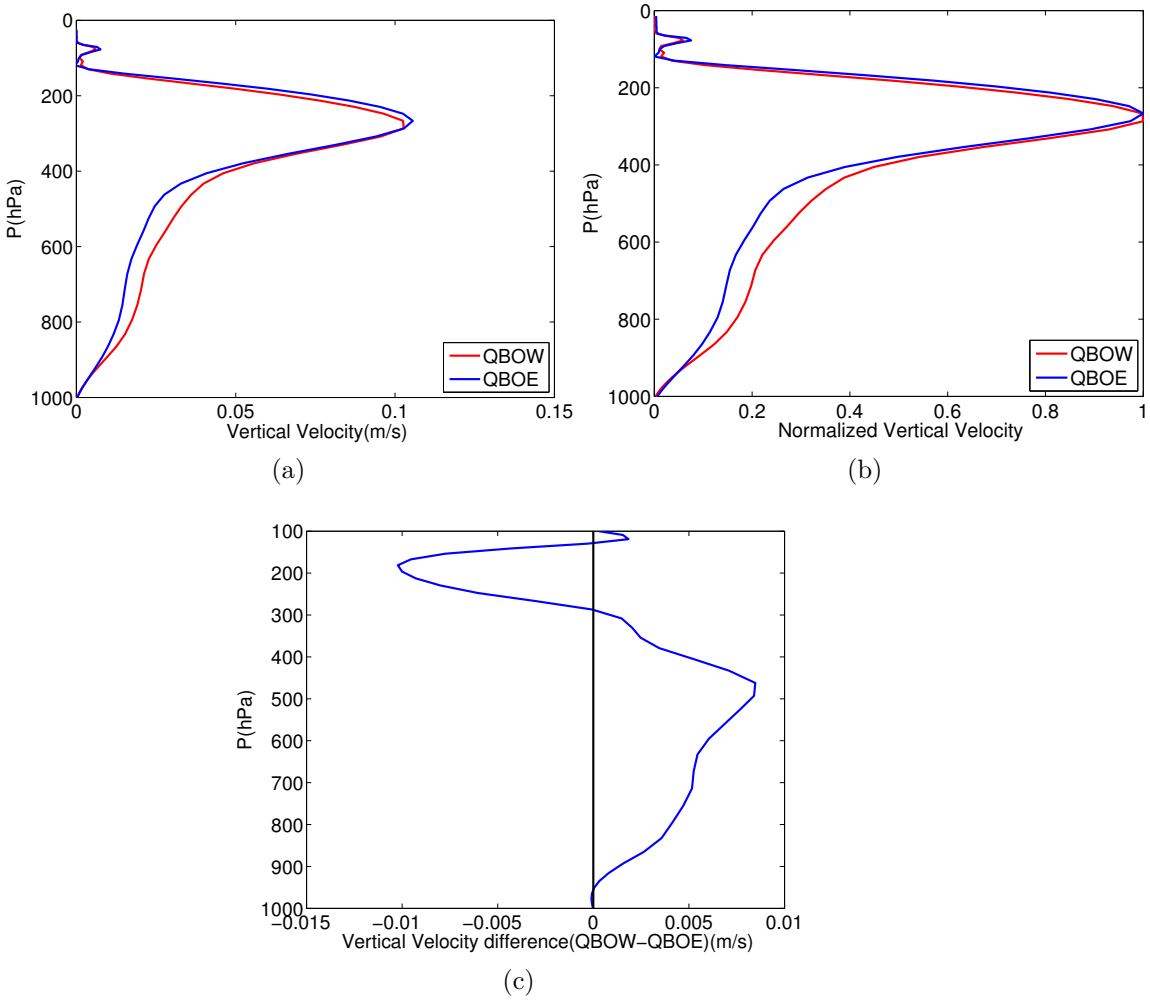

Figure 29: (a) Mean vertical velocity in the center 200km of the domain; (b) normalized vertical velocity for the two profiles in figure (a); (c) the difference between the two profiles in figure (a). The blue lines in figure (a) and (b) are for the QBOE cases, while the red lines are for QBOW cases.

3.3.3 the Moist Static Energy Budget Analyses

It has been shown that the MSE budget analysis is a useful framework to gain insights into precipitation distributions and its variations (Neelin and Held 1987, Sobel 2003, Nie and Sobel 2015, and many others). Here, I apply this diagnosis framework to the responses of precipitation of the idealized Walker circulation to the QBO-like temperature forcing. Of particular interest are the positive precipitation anomalies in the center region of the domain (Figure 30), because it is the vigorous deep convection region that feels the perturbations in the upper troposphere-lower stratosphere the most. The negative precipitation anomalies at the flanks are likely an indirect response of the Walker circulation changes in the central region, by continuity.

The vertical integrated dry static energy (DSE, $s = C_pT + gz$, where C_p is the specific heat of dry air, and g is gravitational acceleration) equation in a steady state can be written as

$$\langle w\frac{\partial s}{\partial z}\rangle + \langle u\frac{\partial s}{\partial x}\rangle = H + P + R. \tag{3.9}$$

where H is the surface sensible heat flux, P is the surface precipitation, and R is the vertically integrated radiative heating. The mass-weighted vertical integral from the surface to the top of atmosphere of a physical field * is denoted as the brackets $\langle * \rangle$. In the above equation, the left hand side (LHS) terms are vertical and horizontal advection of s, respectively. Note that the idealized Walker circulation experiments here are in a 2D setting in the x and z directions. The right hand side (RHS) terms are the source and sink

terms of s.

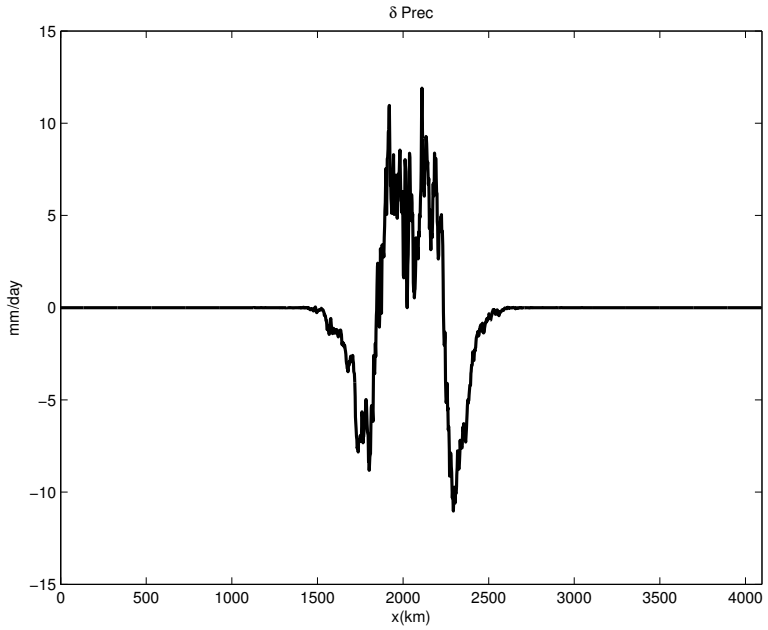

Figure 30: The distribution of precipitation anomalies (QBOW-QBOE) in the x direction.

In a similar way, the vertically integrated moist static energy (MSE, $h = s + Lq$, L being the latent heat of vaporization) equation can be written as

$$\langle w\frac{\partial h}{\partial z}\rangle + \langle u\frac{\partial h}{\partial x}\rangle = H + E + R, \tag{3.10}$$

where E is the surface latent heat flux.

Defining the gross moist stability (GMS) as:

$$M = \frac{\langle w\frac{\partial h}{\partial z}\rangle + \langle u\frac{\partial h}{\partial x}\rangle}{\langle w\frac{\partial s}{\partial z}\rangle + \langle u\frac{\partial s}{\partial x}\rangle}, \tag{3.11}$$

We obtain a diagnostic equation for precipitation P, from equation 3.9-3.11,

$$P = \frac{1}{M}(H + E + R) - H - R. \tag{3.12}$$

M is a dimensionless number, representing the efficiency of the column moist static energy export by the large-scale flow. In Raymond et al. (2009), M is defined in the form of the divergence of s and h. Here I choose the advective form because, as will be shown later, the changes of M in response to the QBO-like temperature forcing is mostly due to changes of the vertical advection component.

I have calculated each term of the budget equation 3.9 and 3.10 for both the QBOE and QBOW phases. Figure 31 shows each term of equation 3.9 in the QBOE, the budget for MSE is shown in figure 32.

Starting from the DSE budget equation, the close match between the sum of the LHS and RHS terms of equation 3.9 indicates the DSE budget is well closed (figure 31a). The vertical adiabatic heating is the dominant term in the LHS (figure 31b). The horizontal temperature advection is remarkably small, because the weak temperature gradient is very weak in this equatorial channel. On the RHS, there is a radiative cooling independent of x specified by the experiment design. The precipitation term, representing the convective latent heat release, is the dominant term on the RHS in precipitating area. The budget analysis for the QBOW phase has very similar results, thus are not shown here.

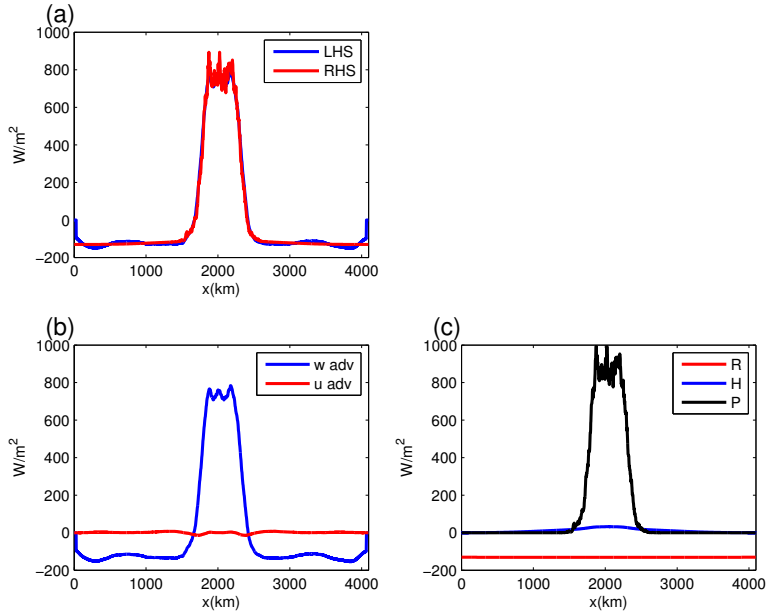

Figure 31: The DSE budget terms in equation 3.9. (a) The sum of the LHS and RHS terms of equation 3.9. (b) The breakdown of the LHS terms. (c) The breakdown of the RHS terms.

The LHS and RHS for the MSE budget equation are shown in figure 32a. The latent heat flux and radiative cooling are important in the RHS, while the sensible heat flux is negligible (figure 32c). The vertical and horizontal advection terms have comparable magnitude for the MSE budget (figure 32b). This is because, although the temperature gradient is weak, there is a strong moisture gradient toward the center of domain associated with the Walker circulation. The horizontal advection term has a local minimum in the center (figure 32b), because the low level inflow of the Walker circulation is weaker toward the center region. Right in the center of the domain, u is zero, thus the horizontal advection is zero. The vertical advection of MSE is strongest in the center, another manifestation of the raising branch of the Walker circulation.

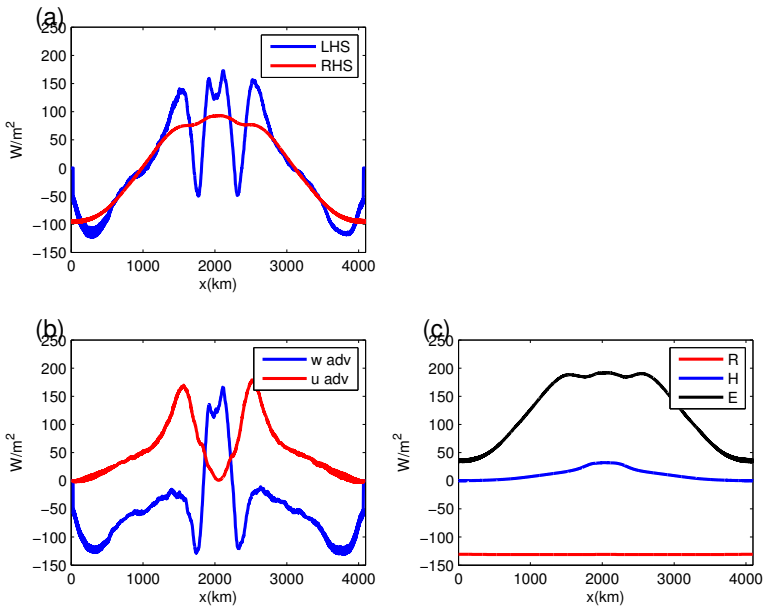

Figure 32: Same as figure 31, but for the MSE budget equation 3.10

The LHS and RHS of equation 3.10 follow each other in general, however, sizable imbalance between them exists in the central region. This imbalance is seen to be due to the covariation between the MSE vertical gradient and vertical motion.

The MSE vertical advection term shown in figure 32 is calculated using the time-averaged (denoted by an overline in the following equations) w and h in the steady state.

The exact vertical advection term should be

$$\overline{\langle w\frac{\partial h}{\partial z}\rangle} = \langle \overline{w}\frac{\partial \overline{h}}{\partial z}\rangle + \overline{\langle w'\frac{\partial h'}{\partial z}\rangle}. \tag{3.13}$$

The covariance term $\overline{\langle w'\frac{\partial h'}{\partial z}\rangle}$ is neglected in equation 3.9. However, as seen in figure 33, w and h have strong variations in time, and they tend to correlate with each other. Note that the time resolution of the data shown in figure 33 is 5 days (the model output frequency). The variation is expected to be even stronger in shorter time scales. Also note that q has largest variance in the flank of the central region (1500km to 1700km and 2300km to 2500km). That may explain the large variations in the MSE budget (figure 32a).

I have checked that even if I calculate the $\overline{\langle w\frac{\partial h}{\partial z}\rangle}$ term with the 5 days time resolution data, the results are improved, but still not enough to close the budget.

I believe that to have a precise calculation of $\overline{\langle w\frac{\partial h}{\partial z}\rangle}$ a time resolution of several hours, the convection overturning time scale, is required.

Given the current limitation, to take the covariance term into consideration, I approximate equation 3.13 as

$$\overline{\langle w\frac{\partial h}{\partial z}\rangle} = \alpha\langle\overline{w}\frac{\partial\overline{h}}{\partial z}\rangle. \tag{3.14}$$

α is a constant, diagnosed as about 0.45.

In other words, it is assumed that the covariation term $\overline{\langle w'\frac{\partial h'}{\partial z}\rangle}$ is proportional to the total term.

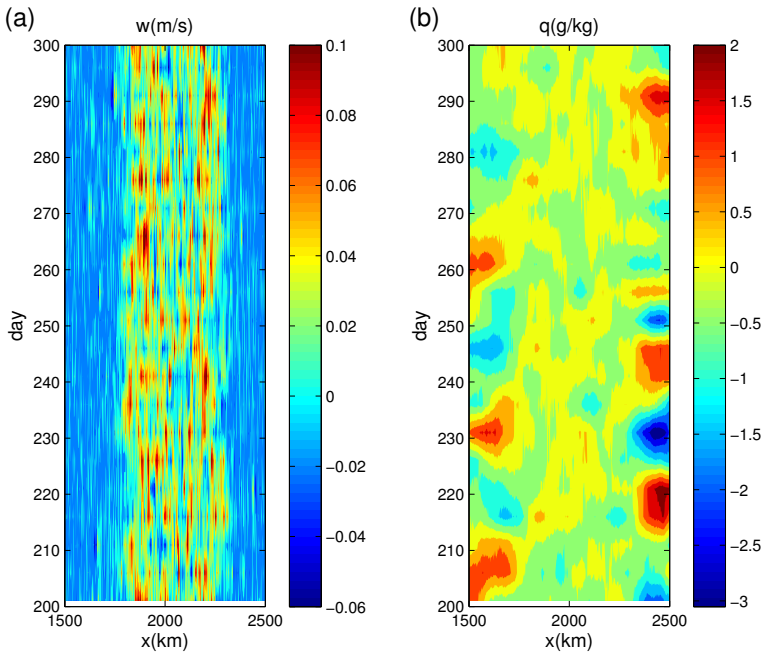

Figure 33: The Hovmöller diagram of (a) vertical velocity w on 500 hPa and (b) water vapor q at 850 hPa for the control case. Note a 1000 km window in the center of the x-domain is shown here.

In the following analyses, I shall focus only on the center region, where the horizontal advection term in both the DSE and MSE budget is negligible. Neglecting the horizontal advection and the sensible heat flux terms, and combining with equation 3.14, equation 3.12 becomes

$$P = \frac{1}{M}(E + R) - R, \tag{3.15}$$

where

$$M = \frac{\langle w \frac{\partial s}{\partial z} \rangle}{\alpha \langle w \frac{\partial h}{\partial z} \rangle}. \tag{3.16}$$

This definition of M is the same as in Sobel (2007), except for the coefficient α. Note that M depends only on the shape of w (i.e. the top-heaviness of w), but does not depend on the strength of w.

One can linearize equation 3.15 around a reference state of the QBO neutral phase, and write down the perturbation precipitation as the following,

$$\delta P = (M^{-1} - 1)(\delta R + \delta E + \delta F) + \delta(M^{-1})(E + R). \tag{3.17}$$

The first term on the right hand side is the component of δP due to anomalies of the sum of radiative cooling, latent heat flux, and the imposed temperature forcing (δF). The second term on the right hand side is the component of δP due to changes in gross moist stability M.

The term of equation 3.17 are calculated averaged over a region of 200km width in the center of the domain. δ is defined as QBOW minus

QBOE. Each term is shown in table 12.

Note that consistent with previous studies (e. g., Sobel 2007), a more top-heavy w profile in the QBOE has a greater M. Pluging them into equation 3.17, the RHS-1 term gives a precipitation anomaly of 3 mm/day, and the RHS-2 term gives a precipitation anomaly of 2.8 mm/day. The precipitation anomalies implied from the MSE budget analyses is 5.8 mm/day, which is very close to the results directly from the model outputs (5.2 mm/day).

The above MSE budget analysis suggests that the changes in the 'top-heaviness' of w can explain about half of the precipitation anomalies. The other half is due to the change of the MSE source (radiation, latent heat flux, and the imposed forcing). Now, I would like to simply explain the contribution of each MSE source term. First, note that since M is smaller than 1, $M^{-1} - 1$ is positive in equation 3.17. In the QBOE phase, there is a cold temperature anomaly (figure 26b) near the tropopause. Note that the radiative scheme is relaxed toward 200K below 207.5K, so the cold anomaly in the QBOE phase leads to a radiative heating anomaly. Thus, the contribution from R (QBOW-QBOE) is negative (table 12). The contribution from E is negative too, and it seems to be consistent with the precipitation responses. With a fixed 5m/s surface wind and the fixed SST distribution, the change of latent heat flux can only be due to the change of the surface layer relative humidity. In the QBOW phase, there is more precipitation in the convective region, leading to greater surface layer relative humidity, and thus smaller latent heat flux. The contribution from F is positive by experiment design.

The heating forcing in the QBOW is a positive anomalous MSE source.

δR	δE	δF	M(QBOW)	M(QBOE)
-4.7 W/m^2	-7 W/m^2	18.6 W/m^2	0.064	0.071

Table 12: Terms of the precipitation anomaly budget equation in equation 3.17.

Now, with the previous discussion about the idealized Walker circulation results and the MSE analyses, I'd like to give a brief summary of a potential mechanism of the QBO modulation on the convection.

The idealized Walker circulation experiments with upper-level temperature (heating) perturbations reveal a potential mechanism for the QBO effects on the tropical circulation and associated convection. With a cold temperature anomaly near the tropopause, the tropopause height is lifted upward. The vertical extension of the rising branch of the Walker circulation also increases in height, moving the peak of the vertical velocity profile [i.e. the level of the divergence] upward. The upward displacement of the peak level of the vertical velocity profile increases the gross moist stability. Thus, assuming that the input of the moist static energy is approximately unchanged in the rising branch of the Walker cell, its precipitation will decrease, and the decreased precipitation is largely redistributed in the region outside the center of the Walker cell, as a result of this Walker circulation change.

3.3.4 Sensitivity to the Height of the Forcing

As we have shown in the isolated convection cases, the model response is sensitive to the height of the temperature anomaly. The updraft cloud mass flux difference and the cloud fraction difference of the high clouds between the QBOE and QBOW cases are greater when the QBO signal penetrated down further into the troposphere.

Here we also do a sensitivity test of the idealized Walker circulation cases to the height of the forcing. The parameters of the three sets of cases (including the domain size; the height of the maximum heating rate anomaly and the dSST value) are listed in table 13. For first sets of cases, the domain size is set as 4096 km, and the dSST is fixed to be 6K. The second set of cases has been done in the previous section. Here we move the dT/dt profile upward to 110 hPa and downward to 200 hPa, and run the two new sets of case sets in the same manner. The locations of the heating forcing profiles are shown in figure 25.

For the center 200km of the domain, we calculate the ratio of the precipitation change between the two cases with respect to the mean precipitation P_{ratio}, and the top-heaviness for the normalized vertical velocity profile, and list the results in table 13.

$$P_{ratio} = 2 * \frac{P_{QBOW} - P_{QBOE}}{P_{QBOW} + P_{QBOE}} \tag{3.18}$$

The P_{ratio} for the first set of cases is only 1.3%. In these two cases, only a small portion (less than half in height) of the heating forcing is added below the tropopause level (see figure 25). In our other test cases with the heating forcing moved upward with even less forcing below the tropopause (not shown), the precipitation response is even smaller. So we can draw similar conclusions as in the 3D cases that it's crucial for the QBO signal to penetrate to a certain level below the tropopause, before it communicates

with the large-scale circulation and the tropical convection. Given a QBO signal confined in the stratosphere, it will be very difficult for the modulation of convection to occur.

As the heating forcing is moved downward from the level of 110 hPa to the level of 200 hPa, the ratio of the precipitation difference (QBOW-QBOE) to the mean precipitation increases from 1.3% to 40% in the center of the domain. This indicates that the tropical convection response to the QBO-like temperature forcing becomes stronger with a lower QBO temperature signal penetration.

Note that 40% P_{ratio} of the precipitation changes seems to be a too large response compared with the commonly known QBO modulation scale, this is because the cases with forcing at 200 hPa level are extreme cases for the QBO temperature penetration, with the tropopause located near 115 hPa in these model results, it is difficult for the QBO signal to penetrate 100 hPa downward.

TH_e is always larger than TH_w for each set of the cases, the conclusion that warmer (colder) temperatures near the tropopause level can decrease (increase) the 'top-heaviness' of the w_0 profile and encourage (discourage) precipitation in the center of the domain holds for all the cases. If we compare the TH_es of all the QBOE cases, the top-heaviness increases when the heating forcing is moved downward, and this is accompanied with a decreasing precipitation in the rising branch. For TH_ws, the direction of the

TH_w change is opposite, TH_w decreases with lower heating forcing, while the precipitation in the domain center increases. In other words, both the encouragement (discouragement) effects of the QBOW (QBOE) heating forcing on the rising branch precipitation become greater when the QBO signal penetrates further downward.

Domain size	dSST	height of forcing	$P_{ratio}(\%)$	TH_e	TH_w
4096 km	6K	110 hPa	1.3	5.4	5.0
4096 km	6K	150 hPa	18.7	6.1	4.7
4096 km	6K	200 hPa	40	6.4	3.7

Table 13: Parameters for the sensitivity cases to the forcing height, and P_{ratio} and the THs calculated from the model outputs. The unit for P_{ratio} is %, TH is unitless.

3.3.5 Sensitivity to dSST

We then test the sensitivity of the model to the dSST. For these cases, the domain size is set to 4096 km, and the heating rate anomaly is put at the 150 hPa level. We then run the cases with dSST = 2K, 4K and 6K. The results are listed in table 14. With larger dSST within the same domain, the Walker circulation becomes stronger and precipitation becomes larger (not shown), which agrees with Wang and Sobel (2011). The P_{ratio} also increases with the dSST. For each set of the cases, the 'top-heaviness' is larger during QBOW than during QBOE.

3.3.6 Sensitivity to the Model Domain

We then test the model sensitivity to the horizontal domain size. In these cases, the dSST is 6K and the heating rate anomaly is put at the 150 hPa

domain size	dSST	height of forcing	$P_{ratio}(\%)$	TH_e	TH_w
4096 km	2K	150 hPa	6.4	6.6	4.5
4096 km	4K	150 hPa	8.8	6.1	5.3
4096 km	6K	150 hPa	18.7	6.1	4.7

Table 14: Same as table 13, but for the sensitivity cases to the dSST.

level. The domain sizes change from 4096 km, 8192 km and 16348 km. With the same heating forcing, the relative precipitation change decreases with increasing domain size and decreasing Walker circulation strength. The results are listed in table 15. For these cases, we still get larger TH_e than TH_w with all three different domain sizes.

Table 14 and 15 both prove that the relative precipitation change is related to the strength of the Walker circulation. With stronger tropical convection and an enhanced large scale Walker circulation, it is easier to feel the modulation resulting from the QBO from above.

domain size	dSST	height of forcing	$P_{ratio}(\%)$	TH_e	TH_w
4096 km	6K	150 hPa	18.7	6.1	4.7
8192 km	6K	150 hPa	12.7	6.1	4.5
16384 km	6K	150 hPa	12.9	3.6	3.1

Table 15: Same as table 13, but for the sensitivity cases to the horizontal domain size.

3.4 Conclusions and Discussion

In this chapter, we use a cloud resolving model to investigate a possible mechanism for the QBO modulation on tropical convection and precipitation. We run cases with both a three-dimensional isolated convection model and an

idealized two-dimensional Walker circulation.

The possible mechanisms can be briefly separated into three categories: the QBO modulation through the temperature and static stability anomaly near the tropopause; through the different zonal wind shear in the tropopause region; and through the modulation of the large-scale Walker circulation. The influences from each possible mechanism are listed as follows.

Let's start from the influence from the zonal wind shear, from our model results the only effect of the zonal wind shear is to increase the high cloud fraction, and there is no thermodynamic effect from the zonal wind shear.

The second possible mechanism is the QBO temperature signal near the tropopause and the related static stability anomaly. In the isolated convection cases, the near tropopause temperature anomaly can modify the amount of the high cirrus cloud. The cirrus cloud fraction is larger when the CPT temperature is lower during the time of QBOE and vise versa for the time of QBOW, but this effect can't be effectively transferred to lower levels. However, when the temperature (heating) anomaly is added to the idealized Walker circulation cases, which allow the large-scale circulation development, the results show robust convection and precipitation difference between the QBOE and QBOW situations.

Perhaps one should not be surprised by the weak precipitation responses to the QBO perturbations in the simulations of isolated convection. As the

convective heating (thus precipitation) is largely determined to be whatever needed to balance the adiabatic cooling associated with vertical motion, imposing a prescribed and fixed vertical motion does not allow a strong signal in precipitation responses. To gain a better understanding of the possible responses of deep convective precipitation to the QBO, one needs to take the deep convection and the associated large-scale vertical motion and their interaction into consideration. In other words, it is better to examine the QBO influences on deep convection in the context of a large-scale circulation system. In the tropics, perhaps the simplest, however, the most important circulation is the Walker Circulation.

In the rest of this section, I examined the responses of an idealized Walker Circulation to the QBO-like heating/cooling in the upper troposphere lower stratosphere. Comparing the QBOW to the QBOE, there is a positive precipitation anomaly at the peak mean precipitation region, and negative precipitation anomalies at the flanks of the peak mean precipitation region. The Walker circulation diverges at a higher altitude in the QBOE phase. Using the MSE budget analyses for the rising branches of the Walker circulation, we proposed a possible mechanism to explain the precipitation and the Walker circulation responses. With a cold temperature anomaly near the tropopause, the tropopause height is lifted upward. The vertical extension of the rising branch of the Walker circulation also increases in height, moving the peak of the vertical velocity profile upward. The upward moving of the peak level of the vertical profile increases the gross moist stability. Thus, in the rising branch of the Walker cell, when the input of the moist static

energy is approximately unchanged, its precipitation will decrease, and the decrease precipitation is redistributed at the flanks of the Walker cell.

The proposed mechanism is an extension of the results of Nie and Sobel (2015). They used cloud-resolving simulations in a small domain with parameterized large-scale vertical motion. Here, we explicitly resolve both the convection and the large-scale circulation, provides an independent and, perhaps, stronger arguments for the QBO influences on deep convection.

In the last section of this chapter, we test the idealized Walker circulation model sensitivity to the height of the near-tropopause temperature (heating) forcing, the SST perturbation amplitude and the horizontal domain size. The results show that the QBO modulation on the troposphere convection and precipitation requires the QBO signal to get down low enough below the tropopause. And the model responses to the temperature (heating) forcing are greater when the QBO signal penetrates further down or the tropical convection becomes stronger. This agrees with the observational results that the QBO modulation is robust at the location where the convection is the strongest (Collimore et al. 2003, Giorgetta et al. 1999).

Chapter 4: Conclusions

We are trying to answer the following questions in this dissertation. First, We'd like to verify whether the Taguchi (2010) relationship between the QBO and ENSO applies to all longitudes in the equatorial region? Also, we want to quantify the ENSO influence on the QBO modulation of the tropical cold point tropopause temperatures? The second question is motivated by the Garfinkel and Hartmann (2007). With the changing correlation between the ENSO and the QBO before and after the 1980s, we inquire whether Taguchi's (2010) results are equally valid over both the time intervals at radiosonde stations along the Equator? Is there any change between the ENSO modulation of the QBO amplitude and period for the two time intervals? Also if the ENSO-QBO relationship changes with time, what is the possible mechanism? Given that ENSO and the QBO are not independent from each other, and the fact that ENSO is a very strong effect that can influencing the tropical convection, I'd like to ask the question that whether the QBO influence on the tropical convection, which had been shown in several previous observational studies, really exists? And what credible mechanisms for the QBO influencing lower troposphere convection?

4.1 The ENSO Modulation of the QBO and the Possible Mechanism

In chapter 2, we first apply the Taguchi's (2010) method to the IGRA data at 10 near-equatorial stations, over an approximate 60-year period starting in the 1950s, and verify that the ENSO modulation of the QBO amplitude

and period in the Taguchi (2010) paper holds for the 10 equatorial stations for the entire 60-year period. Because of the greater amplitude and slower descent rate of the QBO during La Niña conditions for the overall 60-year period of analysis, we anticipated that the QBO temperature signal should vary under different ENSO conditions, and we have verified that the QBO temperature signal is larger during La Niña conditions than during El Niño in the vicinity of CPT altitudes for the entire period analyzed.

Motivated by the changing ENSO-QBO correlation relationship shown in Garfinkel and Hartmann (2007), I calculate the correlation between ERSST Niño 3.4 SST index and the FUB wind data over a longer time and get the similar results to those of Garfinkel and Hartmann (2007), the correlation between the two indices is negative during the first half and becomes positive in the second half, the maximum negative and positive correlation coefficients occur for the time interval before 1982 and after 1990, respectively. This prompts us to apply the Taguchi (2010) method to the IGRA station stratospheric wind for these two time intervals separately, and check whether the ENSO modulation on the QBO amplitude and period changes between the two time periods. The CPT temperature differences between QBO E/W phases during two ENSO phases are also examined here, both to check the reliability of the QBO amplitude results as well as to obtain those results on their own. Due to the concern that CPT temperature time series, when divided into two halves, might cause larger uncertainty of the results with the shorter length and poorer data quality, especially for the first interval, we also examine the 100 hPa temperature differences using the same methodol-

ogy as used for the CPT temperature differences.

And the results are as follows:

First, about the ENSO modulation on the QBO period, the QBO periods are longer both during La Niña than El Niño for the time intervals before 1982 and after 1990. In other words, compared with the Taguchi (2010) and Yuan et al. (2014), the ENSO-QBO period relationship remains unchanged with the shorter time series, before and after the 1980s.

Second, the QBO amplitude relationships between El Niño and La Niña are different in the two time intervals. For the second time interval, we still get larger QBO amplitude during the time of La Niña, like in the overall 60-year study, but for the time before 1982, the ENSO differences in QBO amplitudes are not conclusive between the two ENSO phases.

The temperature difference results support the QBO amplitude results with larger QBO temperature modulations (dT) after 1990, but with smaller dT before 1982, during the time of La Niña. This might imply that the QBO has larger amplitude during El Niño than La Niña in the first time interval.

We then offer some hypotheses to explain the Taguchi (2010) ENSO-QBO relationship in the last part of chapter 2. Based on Geller et al. (2015) and Zhou et al. (2015), the period of the QBO is determined by the magnitude of the wave momentum flux driving the QBO, while the amplitude

of the QBO is determined by the magnitude of the wave phase speeds that comprise the gravity wave spectrum forcing the QBO. We hypothesize that the more widespread convection during El Niño results in a greater zonally averaged gravity wave momentum flux, which in turn, gives a shorter QBO period. The greater QBO amplitude during La Niña over the entire period is likely due to the more intense convection giving rise to a greater spread in the gravity wave phase speeds excited. The fact that the ENSO influence on the QBO amplitude is less stable than the ENSO influence on QBO period is likely due to different variations in the ENSO modulation of convection intensity during the early and later portions of this 60-year period. We then look into the tropical deep convection with OLR data for the two time intervals, and use the OLR results to support these hypotheses.

4.2 The QBO Influence on Tropical Convection

In chapter 3, we use a cloud resolving model to investigate the possible mechanisms for the QBO modulation of the tropical convection and precipitation. We run cases with both a three-dimensional isolated convection model framework and an idealized two-dimensional Walker circulation framework, and test the three possible mechanisms of how the QBO influences tropical convection. The three possible mechanisms are: the QBO modulation through the temperature and static stability anomaly near the tropopause; through the different zonal wind shear in the tropopause region; and through the

modulation of the large scale Walker circulation.

1. From our model results the only effect of the zonal wind shear is to increase the high cloud fraction, and there is no thermodynamic effect from the zonal wind shear.
2. In the isolated convection cases, the near tropopause temperature anomaly can modify the amount of the high cirrus cloud. The cirrus cloud fraction is larger when the CPT temperature is lower during the time of QBOE, and vise versa for the time of QBOW, but this effect can't be effectively transferred to lower levels. However, when the temperature (heating) anomaly is added to the idealized Walker circulation cases, which allows the large scale circulation development to react, the results show robust convection and precipitation differences between the QBOE and QBOW situations.
3. In an idealized Walker Circulation case with a QBO-like heating/cooling in the UTLS, there is a positive precipitation anomaly at the peak mean precipitation region, and negative precipitation anomalies at the flanks of the peak mean precipitation region in the QBOW case. The Walker Circulation diverges at a higher altitude in the QBOE phase. Using the MSE budget analyses for the rising branches of the Walker Circulation, we proposed a possible mechanism to explain the precipitation and Walker circulation responses.

With a cold temperature anomaly near the tropopause, the tropopause height and the vertical extension of the rising branch of the Walker circulation are both lifted upward. The peak of the vertical velocity profile is

moved upward also. The upward displacement of the peak in the vertical velocity profile increases the gross moist stability. Thus, in the rising branch of the Walker cell, when the input of the moist static energy is approximately unchanged, its precipitation will decrease, and the decrease precipitation is redistributed at the flanks of the Walker cell.

The sensitivities of the idealized Walker circulation model to the height of the near-tropopause temperature (heating) forcing, the SST perturbation amplitude and the horizontal domain size are tested in the final section of chapter 3.

Results show that the model responses to forced temperature changes are greater when the QBO signal penetrates further down or the tropical convection becomes stronger. The QBO modulation of the tropospheric convection and precipitation requires the QBO signal to get down low enough below the tropopause or the tropical convection to develop high enough. If there is no overlap between the QBO and tropical convection in altitude, the QBO modulation is not likely to be robust. We can also draw this conclusion from the rising branch vertical velocity difference between the QBOW (QBOE) phases. This conclusion agrees with the observational results that the QBO modulation is robust at the location where the convection is the strongest.

4.3 Implications and Future Works

Early research (Gray, 1984) found that both the phase of ENSO and the phase of the QBO affected the number of Atlantic hurricanes during a hurricane season, and these two factors were used in his early hurricane predictions. Later, however, the QBO was dropped as a factor in making their hurricane predictions (Klotzbach, 1987), leading some to believe that the QBO influence on Atlantic hurricanes was spurious. Recent work by Camargo and Sobel (2010), however, has determined that there was a statistically significant relation between QBO phase and Atlantic hurricane activity from the 1950s to the 1980s, but this relationship was no longer present after the 1980s.

In chapter 2 we have shown that for the entire period of the 1950s to the present time the larger QBO amplitudes and longer QBO periods during times of La Niña imply larger vertical shears of zonal winds in the vicinity of the tropopause and also larger QBO modulations of cold-point tropopause temperatures, both of which have been suggested to play a role in Atlantic hurricane formation (Gray et al.1984a, Emanuel 1988). Further investigation into the role of changing ENSO influences on the QBO before and after the 1980s might clarify the changing importance of the QBO on hurricane formation.

Zhou et al. (2004) showed that the winter dehydration region for air entering the stratosphere through the tropical tropopause is both largest in volume and coldest when the QBO is in its easterly phase under La

Niña conditions. Liang et al. (2011) have analyzed an AIRS/MLS troposphere/stratosphere data record for the period 2004-2010 and found that their values of the interannual variation of tropical mean stratospheric entry water vapor mixing ratios are very consistent with those suggested by Zhou et al. (2004). The CPT temperature can affect the entrance of the water vapor from the troposphere to stratosphere. In chapter 2 we have demonstrated that the influence of ENSO on the QBO significantly affects QBO modulations of tropical tropopause temperatures, and hence has impact on stratospheric entry water vapor mixing ratios. Stratospheric water vapor concentrations have been shown to have an appreciable effect on global warming (Solomon et al. 2010) and also on stratospheric ozone chemistry (Dvortsov and Solomon, 2001). Zhou et al. (2004) have pointed out that the interactions among the annual cycle, ENSO, and the QBO can give rise to complicated changes in the time behavior of water vapor mixing ratios of air entering the stratosphere, perhaps leading to an apparent trend. This is an area that needs further investigation.

The conclusions of this study may also be applied to temperature perturbations near the tropopause from other causes. One example is the lower-stratosphere temperature changes due to ozone changes (e.g. Sioris et al. 2014). The radiative forcing due to ozone changes can be viewed as an possible external forcing for changes in tropical deep convection. Another example is volcano eruptions, which can ejects large amount of aerosols into lower stratosphere. These aerosols heat the lower stratosphere by absorbing insolation and cools troposphere by reflecting sunlight. Within two years

after a strong volcano eruption, a temperature anomaly of several Kelvin is usually observed in the lower stratosphere (e.g. Free and Lanzante 2009). Although further studies are required, the results of this dissertation can be relevant in those events.

The current study uses a idealized radiation scheme for simplicity. Radiation processes may also play a role in contributing to the responses of the deep convection to the QBO. Of particular interest are the high cirrus clouds near the tropopause level. These cirrus clouds may exert large cloud radiative forcing due to their cold cloud-top temperature and long lifetime (Burkhardt and Kärcher, 2011). These high clouds are shown to be sensitive to the environmental conditions and very hard to capture in GCMs, even in coarse resolution CRMs. Future studies should take these cloud-radiation feedbacks into consideration of the QBO modulations on the tropical deep convection.

Almost all the previous observational studies are checking the composite of some troposphere phenomena according to their definition of QBO phase. There is no systematic result about the troposphere response. In fact, sometimes the results are not consistent with each other for different time intervals. For example, Camargo et al. (2010) showed that the Gray's (1984a,b) results of the QBO influence on North Atlantic tropical cyclone activity can be only seen from the the data before 1983, the relationship between the QBO and the North Atlantic TC activity can no longer be found afterward. Another example is the precipitation difference map be-

tween QBOE and QBOW in Liess and Geller (2012) paper, the precipitation difference in their figure 5 are represented as positive and negative patches on the map, both positive and negative patches exist in the equatorial band, there hasn't been good explanations to this situation.

Due to the complexity of the observational results, in this study, we intentionally start with a simple idealized equatorial modeling framework to disentangle the complicated processes in the real atmosphere. The conclusions of this study provide insights of and guidance to the problem. A future direction is to use GCMs, for example the super-parameterized GCMs, to investigate the region responses of the troposphere to the stratosphere QBO. Comparing with conventional convective parameterizations, GCM with super parameterization (Khairoutdinov et al. 2001, Grabowski et al. 2001) are able to better represent convection, and particularly the infrequent very strong convection (Li et al. 2011). Using a super parameterization GCM, one can examine the regional responses of deep convection to the QBO with a realistic climatology and compare the results with the observations (Liess and Geller 2012, Collimore et al. 2003, Camargo and Sobel, 2010), or even the QBO-ENSO interaction.

References

Andrews, D.G., J.R. Holton, and C.B. Leovy, 1987, Middle Atmosphere Dynamics. Academic Press, 489pp.

Arpe, K. and S. A. G. Leroy, 2009, Atlantic hurricanes-Testing impacts of local SSTs, ENSO, stratospheric QBO-Implications for global warming. Quaternary International, 195, 4-14.

Baldwin, M. P. et al., 2001, The quasi-biennial oscillation, Rev. Geophys., 39(2), 179-229.

Barnston, A. G. et al., 1997, Documentation of a highly ENSO-related SST region in the equatorial Pacific, Atmos.-Ocean, 35, 367-383.

Bell, S. W. and M. A. Geller, 2008, Tropopause inversion layer: Seasonal and latitudinal variations and representation in standard radiosonde data and global models. J. Geophys. Res.113: D05109.

Beres, J. H., 2004, Gravity wave generation by a three-dimensional thermal forcing. J. Atmos. Sci., 61, 1805-1815.

Bjerknes, J., 1969, Atmospheric teleconnections from the equatorial pacific. Journal of Physical Oceanography, 97(3), 163-172.

Bretherton, C. S., 2007, Challenges in numerical modeling of tropical circulations. The Global Circulation of the Atmosphere, T. Schneider and A. H. Sobel, Eds., Princeton University Press, 302-330.

Blossey, P. N., Z. Kuang and D. M. Romps, 2010., Isotopic composition of water in the tropical tropopause layer in cloud-resolving simulations of an idealized tropical circulation. J. Geophys. Res., 115, D24309.

Bretherton, C. S., P. N. Blossey, and M. E. Peters, 2006, Comparison of simple and cloud-resolving models of moist convection-radiation interaction with a mock-Walker circulation. Theor. Comp. Fluid. Dyn., doi:10.1007/s00162-006-0029-7.

Burkhardt, U. and B. Kärcher, 2011, Global radiative forcing from contrail cirrus, Nature Climate Change 1, 54-58 (2011) doi:10.1038/nclimate1068

Camargo, S. J. and A. H. Sobel, 2010, Revisiting the Influence of the Quasi-Biennial Oscillation on Tropical Cyclone Activity, Journal of Climate, vol. 23, pp. 5810-5825

Collimore, C. C., D. W. Martin, M. H. Hitchman, A. Huesmann, and D. E. Waliser, 2003, On the relationship between the QBO and Tropical deep

convection. J. Climate., 16, 2552-2568

Dai, A. and T. M. L. Wigley, 2000, Global patterns of ENSO induced precipitation. Geophys. Res. Lett., 27, 1283-1286.

Derbyshire, S. H., et al., 2004, Sensitivity of moist convection to environmental humidity. Quart. J. Roy. Met. Soc., 130, 3055-3079.

Durre I., S. V. Russell, and B. W. David, 2006, Overview of the Integrated Global Radiosonde Archive. J. Climate, 19, 53-68.

Dvortsov, V. L. and S. Solomon, 2001, Response of the stratospheric temperatures and ozone to past and future increases in stratospheric humidity. J. Geophys. Res., 106, doi: 10.1029/2000JD900637.

Emanuel, K. A., 1988, The maximum intensity of hurricanes. J. Atmos. Sci., 45, 1143-1155.

Emanuel, K. A., J. D. Neelin, and C.S. Bretherton, 1994, On large-scale circulations in convecting atmospheres. Quart. J. Roy. Met. Soc., 120, 1111-1143.

Liebmann B. and C. A. Smith, 1996, Description of a Complete (Interpolated) Outgoing Longwave Radiation Dataset. Bulletin of the American Meteorological Society, 77, 1275-1277.

Free M. and J. Lanzante, 2009, Effect of Volcanic Eruptions on the Vertical Temperature Profile in Radiosonde Data and Climate Models. J. Climate, 22, 2925-2939.

Garfinkel, C. I. and D. L. Hartmann, 2007, Effects of the El Niño-Southern Oscillation and the quasibiennial oscillation on polar temperatures in the stratosphere. J. Geophys. Res., 112: D19112.

Geller, M. A., W. Shen, M. Zhang, and W.-W. Tan, 1997, Calculations of the stratospheric quasi-biennial oscillation for time-varying wave forcing, J. Atmos. Sci., 54, 883-894.

Geller, M. A., T. Zhou, W. Yuan, 2015, The QBO, Gravity Waves Forced by Tropical Convection, and ENSO(in preparation)

Gettelman, A., M. L. Salby, and F. Sassi, 2002, Distribution and influence of convection in the tropical tropopause region, J. Geophys. Res., 107(D10), doi:10.1029/2001JD001048

Giorgetta, M. A., and L. Bengtsson,1999, Potential role of the quasi-biennial oscillation in the stratosphere-troposphere exchange as found in water vapor in general circulation model experiments, J. Geophys. Res., 104(D6), 6003-6019.

Gong J. and M. A. Geller., 2010, Vertical fluctuation energy in United States high vertical resolution radiosonde data as an indicator of convective gravity wave sources. J. Geophys. Res. 115: D11110, DOI: 10.1029/2009JD012265.

Grabowski, W. W., 2001, Coupling Cloud Processes with the Large-Scale Dynamics Using the Cloud-Resolving Convection Parameterization (CRCP), J. Atmos. Sci., 58, 978-997.

Gray, W. M., 1984a, Atlantic seasonal hurricane frequency. Part I: El Niño and 30-mb quasi-biennial oscillation influences. Mon. Wea. Rev., 112, 1649-1688.

Gray, W. M., 1984b, Atlantic seasonal hurricane frequency. Part II: Forecasting its variability. Mon. Wea. Rev., 112, 1669-1683.

Gray, W. M., J. D. Sheaffer, and J. Knaff, 1992a: A mechanism for the modulation of ENSO variability by the stratospheric QBO. J. Meteor. Soc. Japan, 70 (5), 975-994.

Gray, W. M., J. D. Sheaffer, and J. Knaff, 1992b, Hypothesized mechanism for stratospheric QBO influence on ENSO variability. Geophys. Res. Lett., 19, 107-110.

Hamilton, K., A. Hertzog, F. Vial, and G. Stenchikov, 2004, Longitudinal variation of the stratospheric quasi-biennial oscillation. J. Atmos. Sci., 61

(4), 383-402.

Ho, C.H., H. S. Kim, J. H. Jeong and S. W. Son, 2009, Influence of stratospheric quasi-biennial oscillation on Tropical cyclone tracks in western North Pacific. Geophys. Res. Lett., 36: L06702. doi:10.1029/2009GL037163

Holton, J. R., 2004, An Introduction to Dynamic Meteorology (4th edn). Elsevier Academic Press: Burlington, MA.

Khairoutdinov, M. F., and D.A. Randall, 2001, A cloud resolving model as a cloud parameterization in the NCAR Community Climate System Model: Preliminary Results. Geophys. Res. Lett., 28, 3617-3620.

Khairoutdinov, M. F., and D. A. Randall, 2003, Cloud resolving modeling of the ARM summer 1997 IOP: Model formulation, results, uncertainties, and sensitivities. J. Atmos. Sci., 60, 607-625.

Klotzbach, P. J., 2007, Recent developments in statistical prediction of seasonal Atlantic basin tropical cyclone activity. Tellus, 59A, 511-518.

Knaff, J. A., 1993, Evidence of a stratospheric QBO modulation of tropical convection. Colorado State University Tech. Rep.,Paper 520, 91 pp.

Kuang, Z., 2012, Weakly forced mock-Walker cells, J. Atmos. Sci., 69, 2759-2786.

Li F., D. Rosa, W. D. Collins, and M. F. Wehner, 2012, 'Super-parameterization': A better way to simulate regional extreme precipitation?, J. Adv. Model. Earth Syst., 4, M04002, doi:10.1029/2011MS000106.

Liang C. K., A. Eldering, A. Gettelman, B. Tian, S. Wong, E. J. Fetzer and K. N. Liou, 2011, Record of tropical interannual variability of temperature and water vapor from a combined AIRS-MLS data set. J. Geophys. Res., 116: D06103. doi:10.1029/2010JD014841

Liess, S. and M. A. Geller, 2012, On the Relationship Between QBO and Distribution of Tropical Deep Convection. J. Geophys. Res., 117: D03108. doi:10.1029/2011JD016317

Naujokat, B., 1986, An update of the observed quasi-biennial oscillation of the stratospheric winds over the tropics. J. Atmos. Sci., 43, 1873-1877.

Neelin, J. D., and I. M. Held, 1987, Modeling tropical convergence based on the moist static energy budget. Mon. Wea. Rev., 115, 3-12.

Pauluis, O., and S. T. Garner, 2006, Sensitivity of radiative-convective equilibrium simulations to horizontal resolution. J. Atmos Sci., 63, 1910-1923.

Phillip A. A. and B. N. Meisner, 1987, The Relationship between Large-Scale Convective Rainfall and Cold Cloud over the Western Hemisphere during

1982-84. Mon. Wea. Rev., 115, 51-74.

Plumb, R. A., 1982, The circulation of the middle atmosphere. Aust. Meteorol. Mag., 30, 107-121.

Plumb, R. A., and R.C. Bell, 1982, A model of the quasi-biennial oscillation on an equatorial beta-plane. Quart. J. Roy. Meteor. Soc., 108, 335-352.

Power, S. B., and I. N. Smith, 2007, Weakening of the Walker Circulation and apparent dominance of El Niño both reach record levels, but has ENSO really changed? Geophys. Res. Lett., 34, L18702, doi:10.1029/2007GL030854.

Randel, W. J., F. Wu, D. J. Gaffen, 2000, Interannual variability of the tropical tropopause derived from radiosonde data and NCEP reanalyses. J. Geophys. Res. 105: 15,509-15,524, DOI: 10.1029/2000JD900155.

Raymond, D. J., S. L. Sessions, A. H. Sobel, and Z. Fuchs, 2009, The Mechanics of Gross Moist Stability. J. Adv. Model. Earth Syst., 1, 9, doi:10.3894/JAMES.2009.1.9.

Reed, R. J., W. J. Campbell, L. A. Rasmussen, and D. G. Rogers, 1961, Evidence of downward-propagating annual wind reversal in the equatorial stratosphere. J. Geophys. Res., 66, 813-818.

Reid G. C, K. S. Gage, 1985, Interannual variations in the height of the tropi-

cal tropopause. J. Geophys. Res. 90: 5629-5635, DOI: 10.1029/JD090iD03p05629.

Seo, J., W. Choi, D. Youn, D. R. Park and J. Kim, 2013, Relationship between the stratospheric quasi-biennial oscillation and the spring rainfall in the western North Pacific, Journal: Geophysical Research Letters, DOI: 10.1002/2013GL058266

Schirber, S., 2015, Influence of ENSO on the QBO: Results from an ensemble of idealized simulations, J. Geophys. Res. Atmos., 120, 1109-1122, doi:10.1002/2014JD022460.

Sioris, C. E., C. A. McLinden, V. E. Fioletov, C. Adams, J. M. Zawodny, A. E. Bourassa, C. Z. Roth, and D. A. Degenstein, 2014, Trend and variability in ozone in the tropical lower stratosphere over 2.5 solar cycles observed by SAGE II and OSIRIS, Atmos. Chem. Phys., 14, 3479-3496.

Sobel, A., 2003, On the coexistence of an evaporation minimum and precipitation maximum in the warm pool. Journal of Climate, 16, 1003-1009.

Sobel, A., 2007, Simple models of ensemble-averaged precipitation and surface wind, given the SST. The Global Circulation of the Atmosphere, T. Schneider and A. H. Sobel, Eds., Princeton University Press.

Solomon, S., K. H. Rosenlof, R. W. Portmann, J. S. Daniel, S. M. Davis, T. J. Sanford, and G.-K. Plattner, 2010, Contributions of Stratospheric Water

Vapor to Decadal Changes in the Rate of Global Warming. Science, 327, 1219-1223

Taguchi, M., 2010, Observed connection of the stratospheric quasi-biennial oscillation with El Niño-Southern Oscillation in radiosonde data. J. Geophys. Res., 115: D18120. doi:10.1029/2010JD014325

Veryard, R. G., and R. A. Ebdon, 196, Fluctuations in tropical stratospheric winds. Meteor. Mag., 90, 125-143

Wallace, J. M., R. L. Panetta, and J. Estberg, 1993, Representation of the Equatorial Stratospheric Quasi-Biennial Oscillation in EOF Phase Space. J. Atmos. Sci., 50, 1751-1762

Wang, S., and A. H. Sobel, 2011, Response of convection to relative sea surface temperature: Cloud-resolving simulations in two and three dimensions, J. Geophys. Res., 116, D11119, doi:10.1029/2010JD015347

Xu, J., 1992, On the relationship between the stratospheric quasi-biennial oscillation and the tropospheric Southern Oscillation, J. Atmos. Sci., 49, 725-734

Yasunari, T., 1989, A possible link of the QBOs between the stratosphere, troposphere and sea surface temperature in the Tropics, J. Meteorol. Soc. Jpn., 67, 483-493

Yuan, W., M. A. Geller, and P. T Love, 2014: ENSO influence on QBO modulations of the tropical tropopause. Q. J. R. Meteorol. Soc., 140, 1670-1676. doi: 10.1002/qj.2247

Zhang, C., 1993: Large-scale variability of atmospheric deep convection in relation to sea surface temperature in the tropics. J. Climate, 6, 1898-1913.

Zhou, T., M. A. Geller, D.T. Shindell, R. Ruedy, I. Aleinov, L. Nazarenko, N.L. Tausnev, M. Kelley, S. Sun, Y. Cheng, R.D. Field, and G. Faluvegi, 2015, Modeling the QBO-Other Model Improvements Resulting from the Required Increased Vertical Resolution(in preparation)

Zhou, X., Geller, M.A. and Zhang, M., 2001, Tropical cold point tropopause characteristics derived from ECMWF reanalyses and soundings. J. Climate, 14: 1823-1838

Zhou, X. L., Geller, M.A. and Zhang, M., 2004. Temperature Fields in the Tropical Tropopause Transition Layer. J. Climate, 17: 2901-2908